BIOCHEMICAL AND BIOPHYSICAL ENGINEERING OF AN ARTIFICIAL BASEMENT MEMBRANE OF THE CORNEAL EPITHELIUM

by

Bernardo Yáñez Soto

A dissertation submitted in partial fulfillment of

the requirements for the degree of

Doctor of Philosophy

(Chemical Engineering)

at the

UNIVERSITY OF WISCONSIN-MADISON

2013

Date of final oral examination: 12/11/12

The dissertation is approved by the following members of the Final Oral Committee:

Paul F. Nealey, Professor, Chemical and Biological Engineering
David M. Lynn, Professor, Chemical and Biological Engineering
Sean P. Palecek, Professor, Chemical and Biological Engineering
Eric V. Shusta, Professor, Chemical and Biological Engineering
William L. Murphy, Professor, Biomedical Engineering

ABSTRACT

The insufficient supply of donor corneal tissue motivates the engineering of artificial corneas with a high degree of biointegration and significant rates of success. However, currently available artificial corneas suffer from problems, including epithelial downgrowth, infection and stromal melting. Most of the major problems, which eventually lead to rejection, could be greatly reduced or eliminated through the improved formation and maintenance of a healthy epithelium over the implant. We hypothesize that this epithelial formation may be enhanced through the incorporation of biomimetic chemical and physical cues found on the native basement membrane of the cornea onto the surface of the keratoprosthesis.

Hydrogels synthesized from poly (ethylene glycol) diacrylate (PEGDA) were investigated as a platform to simultaneously present human corneal epithelial cells (HCECs) *in vitro* with topography and adhesion peptides to mimic the native physical and chemical attributes of the basement membrane underlying the epithelium *in vivo*. PEGDA hydrogels prevented non-specific HCEC adhesion and were functionalized with the integrin-binding peptide Arg-Gly-Asp (RGD). Hydrogels molded with ridge and groove features with lateral dimensions from 200 nm to 2000 nm and 300 nm depth retained the topography after equilibrium swelling. The alignment of HCECs cultured on topographic surfaces functionalized with RGD showed substantially less dependence on the culture media than substrates promoting non-specific attachment. This demonstrates that the moldable RGD-functionalized hydrogels allow for decoupling of the cues from

surface chemistry, soluble factors, and topography that simultaneously impact HCEC behavior.

We also investigated the use of these non-fouling substrates in wound healing experiments, where we found that the rate of corneal epithelial wound healing was significantly increased by 50% in hydrogel surfaces containing topographic features, compared to flat surfaces with the same chemical characteristics. This increased healing is mainly due to the increased migration of the epithelial cells on the edge of the wound. These results show the potential benefit of restructuring and improving the surface of artificial corneas to enhance the coverage of the keratoprosthesis by epithelial cells and induce the formation of a functional epithelium.

ACKNOWLEDGEMENTS

I would like to thank the many people that influenced in my experience in graduate school. First of all, to my advisor, Prof. Paul Nealey, whose advice (both professional and personal) was always spot-on, steering me back on track whenever I was lost. Thanks to all past and present Nealey group members who help me go through this journey: Dr. Huimang Kang, Dr. Adam Welander, Dr. Karl Stuen, Dr. Sean Delcambre, Dr. Chin-Chu "Charlie" Liu, Dr. Gouliang Liu, Dr. Serdar Onses, Dr. Teresa Porri, Dr. Elizabeth Tocce, Dr. Michelle Wilson, Paulina Rincon, Marco Bedolla, Robert Seidel, Lance Williamson, Xuanxuan Chen and Justin Ren. All of them were wonderful labmates. Also thanks to Dr. Mike Efremov, Dr. Chris Thode and Ana Kiyanova, for all the technical help and fruitful discussion. I will miss my staring contests with Chris, my lengthy coffee talks with Marco and Paulina, and all the stories I shared with Michelle and Liz. Many thanks to all the undergraduates that provided me with a lot of support when I needed it: Natasha Kalkhof, Rachel Conti, Jessica Zeman, Jaimielyn Burke, Josseant Flores, Jose Sanchez and Erik Severson. I would also like to thank Dr. Chris Murphy and Dr. Paul Russell. Although our time together in Madison was short, your advice and friendship has always been valuable and I look forward to continue working for you.

Dr. Sara Liliensiek deserves her own paragraph. I would never be where I am without her. I'm not really sure what did I do to earn her friendship, but she helped me go through the best and the worst during graduate school. She took me under her wing,

offered me her advice and provided me of a family when I was away from mine. For all that I am eternally grateful. More than a co-worker, or a friend, she will always be my big sister in Madison.

This process has been a great adventure and I will always remember fondly my first year in Madison. It was like returning to my teenage years, thanks to Gordon Freeman, John Muller, Ben Tillotson, Elif Gurbuz, Laurie Hazeltine, Thomas Mallot, Adam Broderick and "the germans": Christian Gaertner, Thomas Monz and Konstanze Hahn.

I would like to thank all our friends in Wisconsin, who helped my family and I feel like home: Barbara Olivas, Alina Zea and Milli and Miguel Blanc. Also to my friends in Mexico, who always wait for us: Fabrizio, Gonzalo, Rafael, Gerardo and Ricardo.

During these years in Madison, I had the misfortune of losing both of my grandmothers. I know that they, along with my mother would be very proud of me. I owe a lot to my parents, Pepe and Cuca and my in-laws, Ramon and Ruth. I hope always to live up to their example. I would also like to thank all my family, especially my sisters, siblings in-law, aunts, uncles, nieces and nephews.

Lastly, I would like to thank to the four most important people in my life: my lovely wife Tania, who supported me through all the ordeal of graduate studies, sacrificing a lot during the process. She also deserves her own Ph. D., and her productivity can be proofed by our three extremely active "projects": Natalia, Estefania and Siena

TABLE OF CONTENTS

LIST OF FIGURES

CHAPTER 1: INTRODUCTION

1.1 Statement of the problem

The cornea is the transparent tissue situated at the front of the eye with high transmittance of visible radiation. It is an avascular and highly innervated tissue[1], essential for the production of images at the retina, the absorption of UV rays and the protection of the eye from the environment[2]. However, corneal functions are compromised with certain pathologies and injuries to the eye, such as erosion, chemical burns, herpetic infections, autoimmune diseases, or stromal ulcerations[3], making corneal disorders one of the leading causes of blindness worldwide[4]. The traditional therapy to treat these conditions is to perform transplantations of human donor corneal grafts. These allografts have a high rate of tissue tolerance and visual performance; but for certain ailments, such as the presence of scarring, alkali burns, high vascularization or severe dry eye, the success rate of corneal transplants drops dramatically. Furthermore, since the demand of corneas exceeds the amount of corneal donors[5], and the risk of rejection and transmission of diseases (HIV, hepatitis) related with organ donation is always present, the design and use of high-performance keratoprostheses or artificial corneas is essential for improved patient outcome[6,7].

The materials used in keratoprostheses have evolved from glass and hard polymers, to hydrogels able to incorporate biological or organic materials[1,6-8]. However, keratoprosthesis in current use suffer from problems related to the biointegration of the device, such as extrusion, infection, epithelial downgrowth and the formation of

retroprostethic membranes[6]. Several attempts to solve these problems have included the use of porous skirts that allow the infiltration of fibroblasts, and the use of softer materials, to reduce the mechanical stresses that can lead to perforation[2,6,9]. Another approach to reduce the formation of membranes and epithelial downgrowth include the use of materials that inhibit the adsorption of proteins[10]. However, to completely address those problems, maintain a normal pre-corneal tear film, ensure a good optical surface and provide a barrier against infection, it has been suggested that an ideal keratoprosthesis must promote the growth, stratification and maintenance of a healthy epithelial layer over the device[6-8,11].

1.2 Corneal structure

Currently used keratoprostheses address the biointegration of the device to the donor exclusively through the stromal component of the cornea. However, the cornea is a complex and structured tissue, approximately 0.5-0.6 mm in thickness, which contains three important layers[2,3,12] (Figure 1.1): 1) Epithelium, which accounts for 10% of the total thickness. This tissue is characterized as a nonkeratinizing stratified squamous epithelium containing corneal epithelial cells (CECs) which provide the self renewal properties of the tissue. The corneal basal cells adhere to the underlying basement membrane (BM), an acellular layer made mostly of collagen, which possesses a rich topography (Figure 1.2)[13,14]. The corneal BM is a specialized extracellular matrix (ECM), with components produced by epithelial cells and stromal keratocytes[12]. 2) Stroma, which represents about 90% of the total thickness. It is composed of quiescent

keratocytes and collagen fibers with a parallel orientation, forming lamellae. The fibers in each lamella have a uniform diameter and are perpendicular to the adjacent lamella, giving the cornea its transparency. 3) Endothelium, a single layer of non-proliferating cells adhered to the Descemet's membrane. It regulates the normal hydration of the stroma by exchanging fluids from the stroma to the anterior chamber.

1.3 The corneal epithelium and its basement membrane

The corneal epithelium is a highly specialized tissue made of 5-7 layers of regularly arranged differentiating epithelial cells[15]. It provides a smooth refractive surface for the passage of light and forms a barrier that prevents hydration of the stroma and penetration of pathogens[16]. The corneal epithelium is in constant restoration, completely renewing every 7 to 10 days[17]. This renewal rate is supported by the stem cells in the limbus (the transitional zone between the cornea and the conjunctiva), that undergo cell division and migrate towards the central part of the cornea, differentiating into basal epithelial cells. Epithelial cells in the basal layer are transient amplifying cells and experience a few cell divisions before migrating to the suprabasal layers, where they terminally-differentiate[15,18,19], expressing keratin 12[20], and α6β4 integrin, which participates in the formation of desmosomes and hemidesmosomes[21]. The cells migrate into the wing layers, and then into the superficial layers, where cells flatten and form tight junctions. These superficial cells present microvilli on their anterior surface to facilitate the transport of metabolites and reinforce the retention of tear film. The cells are eventually shed, continuing the renewal cycle[15,18,19].

The basal cells are tightly adhered to the underlying BM, a laminar structure with a thickness of 50 nm, composed mainly of collagen IV, laminin, heparin, and proteoglycans[12]. The BM has an anterior structure (lamina lucida) that provides hemidesmosomal attachments, and a posterior portion (lamina densa) which is anchored to the Bowman's membrane[18]. In addition to its structural roles in supporting attached cells, the BM serves as a reservoir for cytoactive compounds such as growth factors. The BM has been shown to affect cell shape, migration, differentiation and proliferation trough cell substrate RGD-integrin interactions[22-25].

1.4 Corneal epithelial wound healing

To understand the necessary parameters for the epithelialization of a corneal prosthetic, knowledge of the epithelial wound healing process is essential. Epithelial wound healing occurs in four steps: 1) lag phase, where cells reorganize their attachments to adjacent cells and BM; 2) migration phase, where the leading edge of wound becomes thin and the epithelial sheet migrates toward the center of the defect at a speed of 20-50 μm/h; 3) Differentiation phase, where epithelial cells proliferate and stratify to reestablish normal thickness, and 4) Maintenance phase, where BM components are synthesized, assembled and remodeled[12]. These steps are promoted by the flow of ions from surrounding tissue[26], growth factors (GF), cytokines and ECM proteins[12]. Wound healing is complete when the epithelium is firmly anchored to the BM, thus wound healing is dependent on the adhesion mediators of cells, or integrins[16]. Once healed, the renewal of the epithelium depends on the synchronization of the proliferation and differentiation of

the transiently amplifying cells[16]. Since the corneal BM is the microenvironment providing cues to the epithelial cells, in order to have a healthy epithelium, it is fundamental to have a surface that supports cell adhesion, is permeable to nutrients and metabolites, and presents other chemical and topographical cues[1].

1.5 Influence of ECM on cell behavior

The behavior of cells and tissues in an organism is highly dependent on the numerous chemical and mechanical cues presented by the substrate and surrounding cells. Within an organism, most cells are in contact with the ECM, a flexible, protein-base material composed mainly of collagen, elastin, hyaluronic acid, proteoglycans, fibronectin (FN) and laminin (LN)[27]. Far from being a mere inert scaffold, the ECM is a dynamic entity that is continuously produced, degraded and reshaped by cells. Its components have been shown to influence adhesion[28,29], migration[30-32], proliferation[33,34], morphology of cell[35,36], cytoskeletal arrangement[37,38], stratification[39], gene expression[40,41], cell differentiation[42,43] and apoptosis[44].

The ECM can be present as an interstitial matrix in connective tissue or as a specialized form such as the basement membrane (BM) in epithelial and endothelial tissues[45]. It has been shown for many cell-types that the ECM influences cell behavior at three different levels[46]:

1. Biochemically. Cells can interact with elements of the ECM trough specific bonds[28,30,33,35,47].
2. Mechanically. Cells can sense the stiffness of the matrix and the forces

applied to it and respond by modifying the cytoskeletal elements[37,40,42,48].

3. Topographically. The ECM has a complex 3-D topography in the micro and nanoscale which is known to affect cell behavior[29,31,32,34,36,38,39,41,43,44,46,49-70].

1.6 Regulation of cell behavior by topographic cues

Topographical cues are among the most important signals received by the cells from the ECM. During the past 15 years, the influence of topography on cell behavior has been intensively investigated. There have been studies on many types of features, such as pits, steps, waves, nodes, pores or general roughness[46]. Although shape[46,50] and regularity[51] of the topography appear to produce different responses, most of the work on topographic cues has been done on grooves/ridges anisotropic arrays due to the higher control over its geometry, and the simplicity in the definition of measurable endpoints (Figure 1.3).

Some observed behaviors in studies about the response of cells to the ECM are:

a) Elongation and alignment.

The most obvious behavior observed in cells cultured on micro and nanotopographies is the elongation and alignment of cells to anisotropic features, a phenomena called "contact guidance" (Figure 1.4), which has been studied extensively in our laboratories[29,36,38,55,56,66-68] and others[43,65,70-72]. Most cell-types align to grooves, but there is no alignment in some cells-types, including macrophages or neurophils[46]. Alignment has been proven to also depend on the depth of the features. For example, epithelial cells do not align on features less

than 300 nm deep[56]. Within aligned cells the spatial organization of the microtubules and microfilaments of cells cultured on patterned surfaces also align with the features[38]. The upper limit where CECs can distinguish the underlying topography (contact acuity) is close to 4 μm[68], and the lower limit is in the range of 60-100 nm[56,71,73]. It has been demonstrated that elongation and alignment of cells is constant for variable widths[67], but the major promoter of alignment is the depth of the features[56,67,72]. In general, for our cell-type of interest, human CECs (HCECs), the smaller the features, the more elongated the cells along the axis of the features become[68]. Some recent studies showed that on substrates presenting non-specific interactions with the cells, the orientation of HCECs to the smaller sizes of patterns varied from parallel to perpendicular when cultured on serum-free media[36]. However, this behavior disappeared on studies conducted on substrates allowing for the specific interaction of the cells through integrin-adhesion[74,75].

There are very few studies regarding the influence of topographical vs. chemical cues. Britland et. al. investigated this hierarchical effect overlaying cell adhesive chemical strips orthogonally to groove topographies, where they found that baby hamster kidney cells aligned preferentially along the chemical tracks[76]. However, Charest et. al. stamped fibronectin lanes orthogonally on lithographically produced grooves, and osteoblasts displayed a topography-dependent contact guidance[77]. This highlights the need to develop systems to

distinguish the relative influence of chemical and topographical cues on the regulation of the different cell-types.

b) Adhesion

One of the required conditions for the design of biomimetic systems is to reproduce the adhesion of the HCECs to their substrate environment. Previous reports have shown that patterning a substrate increases the formation of adhesive structures[53], and a 2-fold increase in adhesion of HCECs cultured on the smallest features of patterned scaffolds was measured by Karuri, et. al. when subjected to shear stress[29]. Adhesion of cells is dependent on two mechanisms: 1) adsorption of proteins and 2) direct interaction with receptors[78]. The former mechanism has been used to chemically increase adhesion of cells, like the plasma treatment of materials[6,78], the use of adhesive synthetic polymers[79,80], amine-functionalization of surfaces[81], or other physical modifications to the materials[6]. However, since the adhesion mediated through integrin receptors activates many cellular pathways[82], the use of these biomolecules to modulate adhesion is the most advantageous method to reproduce the cellular environment.

Integrins are heterodimeric receptors that link the ECM with the cytoskeleton of cells. These receptors are known to regulate other aspects of cell behavior in addition to adhesion, including cell survival, proliferation, motility and differentiation[82]. There are many integrin-binding motifs, but the sequence Arg-Gly-Asp (RGD), discovered by Pierschbacher and Ruoslahti in 1984[83] is ubiquitous and recognized by at least 12 integrin dimers[84]. It was first shown to

be recognized in fibronectin, but later found in many other ECM proteins; although not all proteins containing RGD mediate cell adhesion, suggesting that RGD has to be available for the receptors. Studies using cyclic motifs improve cell adhesion, indicating that affinity also depends on conformation of the aminoacids[84]. The RGD sequence has been extensively used as an adhesion promoter[28,33,85-99]. A summary of some studies using RGD as an adhesion promoter is shown in Table 1.I[86-89,91,94,95,97,99-104].

c) Migration

Topography can also affect the migration of cells[54]. Velocity of migration is dependent on the size of the topography[32], and HCECs tend to migrate preferentially along the direction of the patterns[32,36,52,54,61,70]. If subjected to electric fields perpendicular to the topography, Rajnicek et. al. showed that CECs tend to migrate in the direction of the field[72]. Diehl et. al. observed a higher rate of migration for HCEC on 1600 nm compared to other feature sizes[52]. Cell migration also depends on the strength of the cell adhesion: if cell adhesion is low, cells cannot develop enough traction to migrate, if cell adhesion is too high, the receptors cannot dissociate and migration is also impaired[105]. Immobilizing specific growth factors (GF), including Fibroblast GF (FGF)[30] and Epidermal GF (EGF)[106] has been shown to promote adhesion towards the GF gradient.

d) Proliferation

Protein adsorption on different Self Assembled Monolayers (SAMs) has been shown to modulate proliferation of HCECs[34]. The immobilization of collagen,

fibronectin and RGDS promoted the adhesion and proliferation of corneal epithelial cells[33]. On nanostructured polystyrene cells showed increased adhesion and proliferation compared with flat surfaces[65]. Proliferation of SV40 and CECs was found to decrease with nanoscale topographies below the 1600 nm pitch[107].

e) Gene expression

Expression and genomic studies related to the response of fibroblasts and osteoblasts to topography show changes in the expression of several proteins such as: tyrosine kinases (enzymes that phosphorylate proteins and stimulate proliferation and differentiation); GF; G proteins, such as Ras, Rab, and Rho (regulators of the cytoskeletal conformation, formation of filopodia and lamellipodia and proliferation of cells); matrix metalloproteases and collagen matrix (which stimulates the rearrangement of the ECM)[41,58]. Our laboratory investigated the influence of topography on human umbilical vein endothelial cell (HUVEC) gene expression, using gene arrays[108]. Of the 47,000 targeted transcripts, 3171 genes showed significant differences between HUVECs plated on planar surfaces and cells plated on 400 nm pitch substrates. Genes that presented the most significant increases on topographic features were those involved in protein modification and maintenance, while the most significant decreases were on cell cycle proteins. Several ECM proteins, including integrins, collagens and laminins were uniformly downregulated for the topographic substrates vs. the flat surfaces[108].

In the majority of the studies performed in the past, the behavior of the cells exposed to micro and nanotopography can be attributed to two distinct factors: reaction of the cells to the topography itself, or reaction of the cells to local differences in chemistry, imparted by the nano-imprinting techniques[50], allowing for confusion in the interpretation of the results. To avoid this controversy and differentiate the chemical effects from the topography, it is important to have control of the surface chemistry of the substrates. Cell proliferation rates can be greatly influenced depending on the surface chemistry as has been shown by Franco, et. al.[34] Furthermore, the proteins adsorbed on surfaces have a major effect on the cellular response, and the hydrophobic/hydrophilic character of the materials can influence the adsorbed protein layer[34,35]. It has also been found that the charge density on the surfaces influences cell adhesion and proliferation for SV-40 transformed Human CECs (SV40-HCECs)[34] and bovine endothelial cells[79]. Therefore, the use of substrates that inhibit the adsorption of proteins, but allow the incorporation of bio-ligands specific to cellular receptors may untangle these effects.

1.7 Use of Poly (ethylene glycol) hydrogels as non-fouling, functionalizable substrates for corneal epithelial cells

Hydrogels are hydrophilic water-insoluble polymer networks with the property of swelling to an equilibrium volume, retaining their original shape. The hydrophilic character of these materials is due to the nature of the dispersing forces due to the chemical residues in the backbone or lateral chains (usually -OH, -COOH, -CONH-, -$CONH_2$, -SO_3H); and their insolubility depends on the cohesive forces in the formation of

a three-dimensional network[109]. These cohesive forces can be generated by chemically crosslinking the polymers using radical polymerization, addition reactions, condensation reactions, etc. (in chemical or irreversible hydrogels); or by physically crosslinking with cooperative and associative forces, such as ionic interactions, hydrogen bonds, protein interactions, antigen-antibody interaction, etc. (in physical or reversible hydrogels)[110]. These different crosslinking methods give hydrogels their versatility for use as drug delivery agents, biosensors or scaffolds in tissue engineering applications[111-113].

Because of their high water content, tissue-like properties, biocompatibility, good mass transfer[114,115], protein adsorption resistance, ability to be engineered to promote environmental responsiveness by the functionalization with bioligands[116] or modified crosslinking techniques[110,117], and the possibility to tailor their mechanical properties to match those of many soft tissues[118]. Hydrogels are excellent materials for biomedical applications[109,113], such as diagnostics, therapeutic devices[119], implants[1,120], drug delivery systems[121] or use as a synthetic basement membrane[1,109,111-113].

Hydrogels for biomedical applications can be made from natural polymers, like collagen, hyaluronate, fibrin, alginate, agarose or chitosan; or from synthetic polymers such as poly(acrylic acid) (PAA), poly(ethylene glycol) (PEG) or poly(vinyl alcohol) (PVA), and their copolymers[122]. Among the synthetic hydrogels, PEG is particularly appealing. It is soluble in water, transparent, nontoxic, FDA approved for internal consumption, hospitable to biological materials, non-immunogenic, prevents protein adsorption, can be coupled to biomolecules[122,123], and it is permeable to glucose and other metabolites[124]. It can be tailored using different crosslinking methods[110], and it can be

copolymerized with degradable polymers (PLA, LGA)[110,125]. Peptides can be incorporated to promote cell adhesion or enzymatic degradation[111,126-128]. PEG hydrogels has been extensively studied because of these desirable properties[28,87,89,98,99,106,123,125-127,129-135].

An important method to crosslink PEG hydrogels is through photopolymerization. The use of photopolymerizable materials allows for both spatial and temporal control of polymerization, versatility of formulations and the possibility of premixing and storing the precursor solution under appropriate conditions until use. Shapes are retained upon photopolymerization, allowing the possibility of molding. Porosity can be added by introducing salts that will be leached out after hydration[136]. Photopolymerizable systems normally have a monomer with a polymerizable residue; a photoinitiator and a source of light, depending on the transparency of the non-polymerized mixture and the extinction coefficient of the photoinitiator to a particular wavelength[118,136,137]. Bryant, et. al.[138] and Williams et. al.[139] compared the cytocompatibility between different photoinitiators for different cell lines. Both studies concluded that one of the most tolerated photoinitiators is 2-hydroxy-1-[4-(hydroxyetoxy)phenyl]-2-methyl-1-propanone (Irgacure 2959).

Several techniques have been proposed and tested to impart hydrogels a defined topography, such as photonic crystals and inverse colloids[140-145]; direct writing techniques[146,147], or photolithography[124,129,134]; however, these techniques are usually complicated and expensive. A more simple approach, explored by the Langer research group at the Massachusetts Institute of Technology, is the use of soft lithography

techniques[131,135,148]. They were able to determine the right conditions to obtain negative replicas of the stamps[122], and mold features as small as 50 nm[131].

There are different methods to covalently bind biomolecules to PEG hydrogels[96], including: 1) Activation. In these methods, the surface of the pre-formed hydrogel is derivatised with a functional group reactive to peptides. Among them, we can find the use of N-Hydroxysuccinimide (NHS) and its derivatives[102] or the use of Tresyl chloride[95] (Figure 1.5A); although this approach has the inconvenient of being unselective[149]. 2) Incorporation. The biomolecule is reacted directly to the primary solution (Figure 1.5B). An example of this technique is the use of Michael-type reactions[101]. 3) Polymerization. A biomolecule is coupled to the compound with a reactive end and is incorporated into the hydrogel during crosslinking[91] (Figure 1.5C).

1.8 Objectives

The scope of this work involves the design of a biomaterial based on the use of hydrogels to mimic the microenvironment and instructional cues of the corneal epithelial basement membrane. This will be achieved by examining the following specific aims:

1. Incorporation of biochemical cues into PEG hydrogel substrates to promote integrin-specific human corneal epithelial cell attachment and proliferation.
2. Fabrication of biochemically and topographically engineered PEG hydrogels with non-fouling characteristics to isolate the effect of the topographic cues from the biochemistry of the substrate, and to decouple the confounding influence of non-specific protein adsorption from soluble factors within the media.

3. Use of the above materials with controlled topography and chemistry to design tissue-engineered corneal epithelial basement membranes that promote corneal epithelial wound healing.

1.9 Results

In the work presented here we investigated the use of poly(ethylene glycol) diacrylate (PEGDA) hydrogels to mimic native biophysical biochemical cues from the human cornea. Although we observed that the non-fouling characteristics of PEGDA hydrogels are dependent on the molecular weight of the pre-polymer, the cell attachment of human corneal epithelial cells (HCECs) was limited or absent on PEGDA MW 3400 hydrogels and this specific material was used as a platform for further studies. PEGDA MW 3400 hydrogels were functionalized with the integrin-binding RGD peptide, a short sequence found in multiple extracellular matrix proteins that are known to impact HCEC behavior. Upon incorporation of increasing levels of RGD peptide into the PEGDA gel, we observed a direct correlation with the number of cells attached. In addition, variations in the percentage of cells attached between primary HCEC and two HCEC cell lines suggest this attachment might be cell-type specific. The use of scrambled sequences and competitive assays using soluble RGD demonstrate the integrin-specific attachment to RGD through the absence of HCEC cell attachment. Proliferation of HCECs on RGD-functionalized substrates appeared to be independent of the RGD content of the substrate. These results demonstrate the plausibility of providing HCECs with specific biochemical cues to direct cellular behavior.

Next, we incorporated topography to our PEGDA substrates functionalized with adhesion peptides to mimic the native physical and chemical attributes of the basement membrane underlying the epithelium *in vivo*. We observed that the swelling of hydrogels impacted negatively on the retention of the topography, but hydrogels synthesized from aqueous solutions of 20% PEGDA (MW of 3400 g/mol) swelled minimally after curing and were molded with ridge and groove features with lateral dimensions from 200 nm to 2000 nm and 300 nm depth. HCECs were cultured on topographic surfaces functionalized with RGD and compared to control unfunctionalized topographic substrates. HCEC alignment, either parallel or perpendicular to ridges, was influenced by the culture media on substrates promoting non-specific attachment. In contrast, the alignment of HCECs cultured on RGD hydrogels showed substantially less dependence on the culture media. In the latter case, the moldable RGD-functionalized hydrogels allowed for decoupling the cues from surface chemistry, soluble factors, and topography that simultaneously impact HCEC behavior.

We developed an *in vitro* wound healing assay to test the influence of our substrates with controlled chemistry and topography, and demonstrated that the rate of corneal epithelial wound healing is increased by 50% in hydrogel surfaces containing topographic features, compared to flat surfaces. This increased healing is not due to increased proliferation or increased spreading of the epithelial cells, but to the increased migration of cells in the border of the wound. These results show the potential benefit of resurfacing the surface of artificial corneas to enhance the formation of a functional epithelium.

1.10 Figures

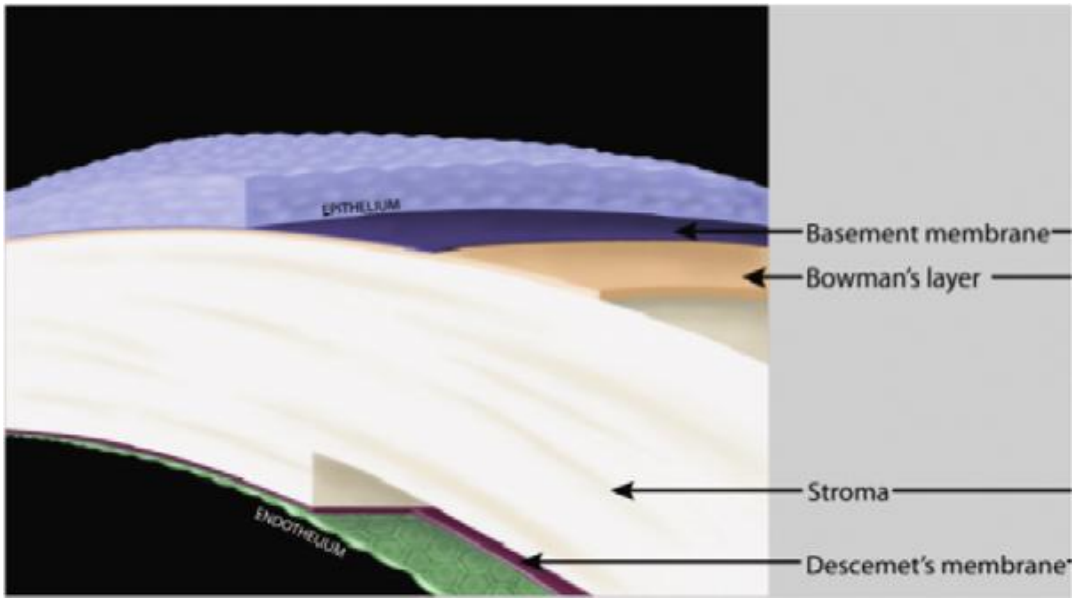

Figure 1.1.- Scheme showing the layers of the human cornea

Epithelium, stroma and endothelium, and the structures supporting them: basement membrane, Bowman's layer and Descemet's membrane. From Last, JA, et. al. (2009) *Journal of Structural Biology* 167, 19-24 (Reference 150)

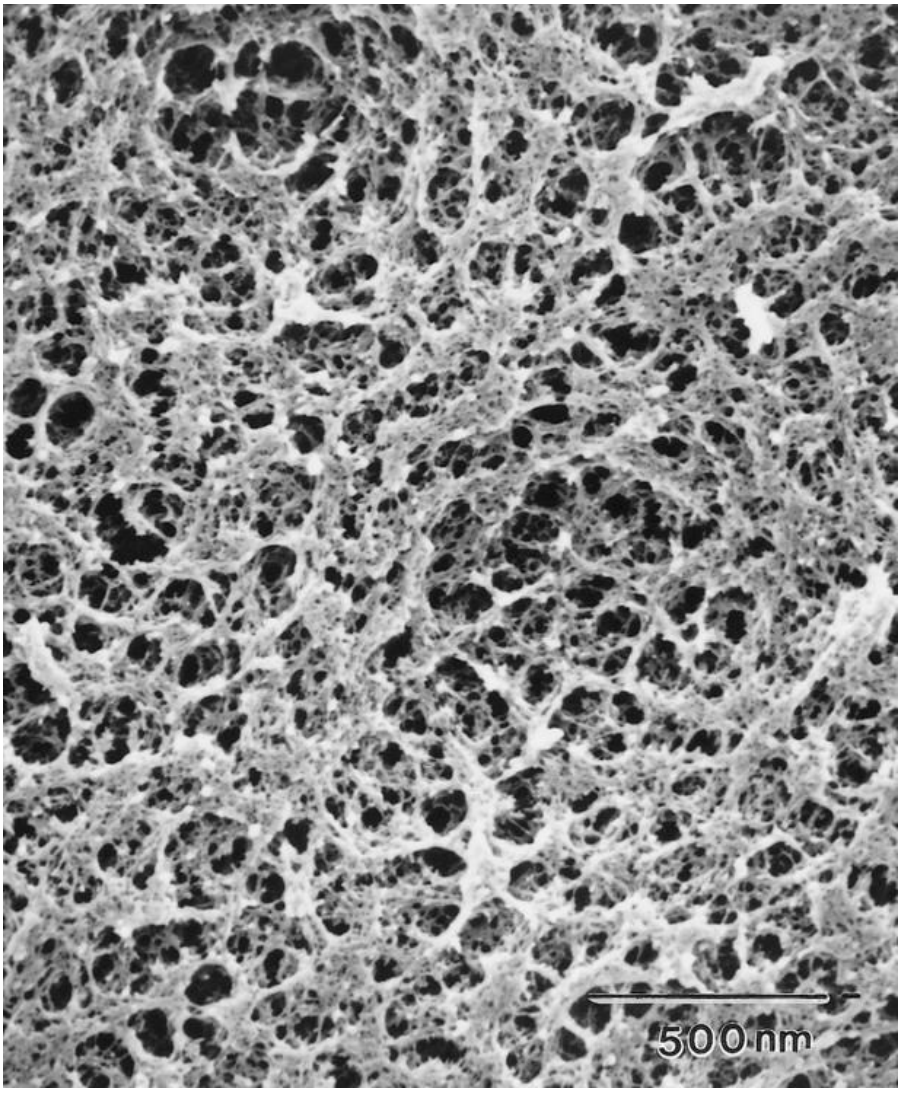

Figure 1.2.- Scanning electron micrograph of the epithelial basement membrane of the human cornea

showing the topography consisting of fibers and pores. From Abrams, GA et. al., (2000) *Cornea* 19(1), 57-64 (reference 13)

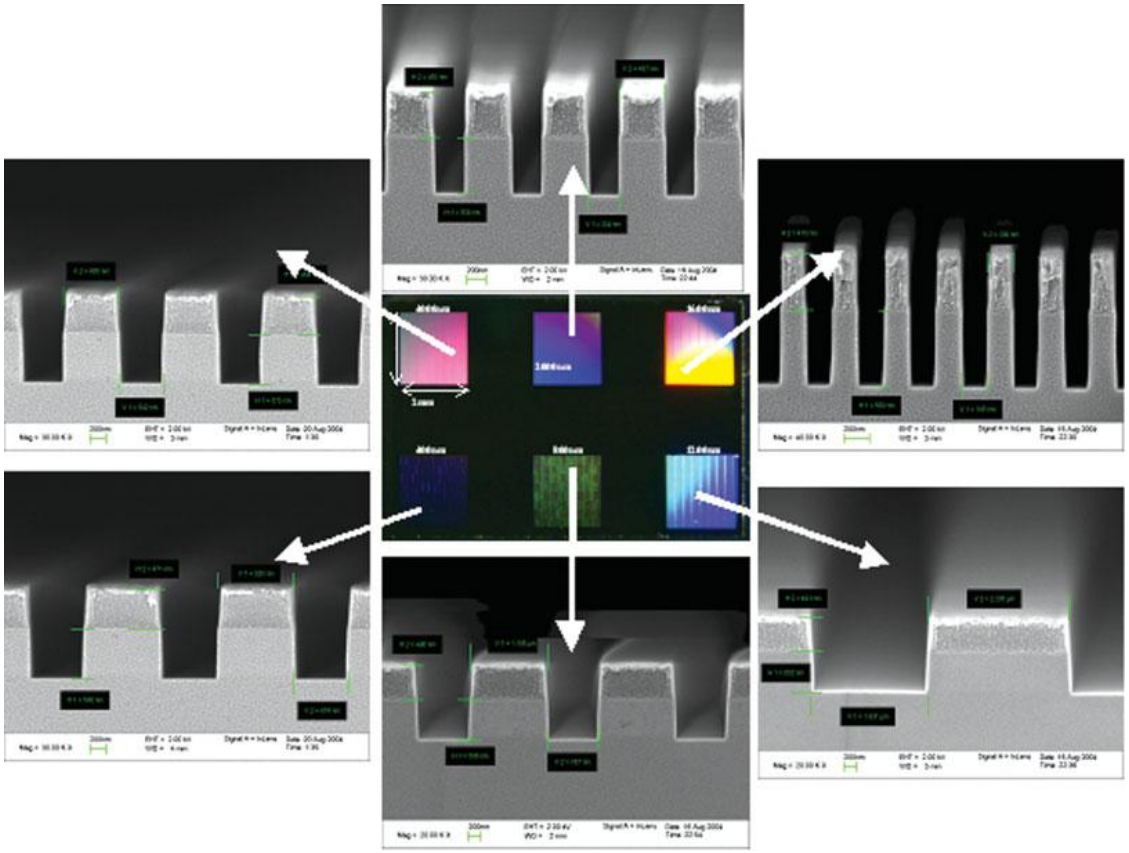

Figure 1.3.- Scanning electron micrographs of a chip patterned with six different topographies.

From the right bottom, clockwise: 4000 nm, 2000 nm, 1600 nm, 1200 nm, 800 nm and 400 nm pitch. From Fraser, SA et. al., (2008) *J Biomed Mat Res A* 86(3), 725-735 (reference 56)

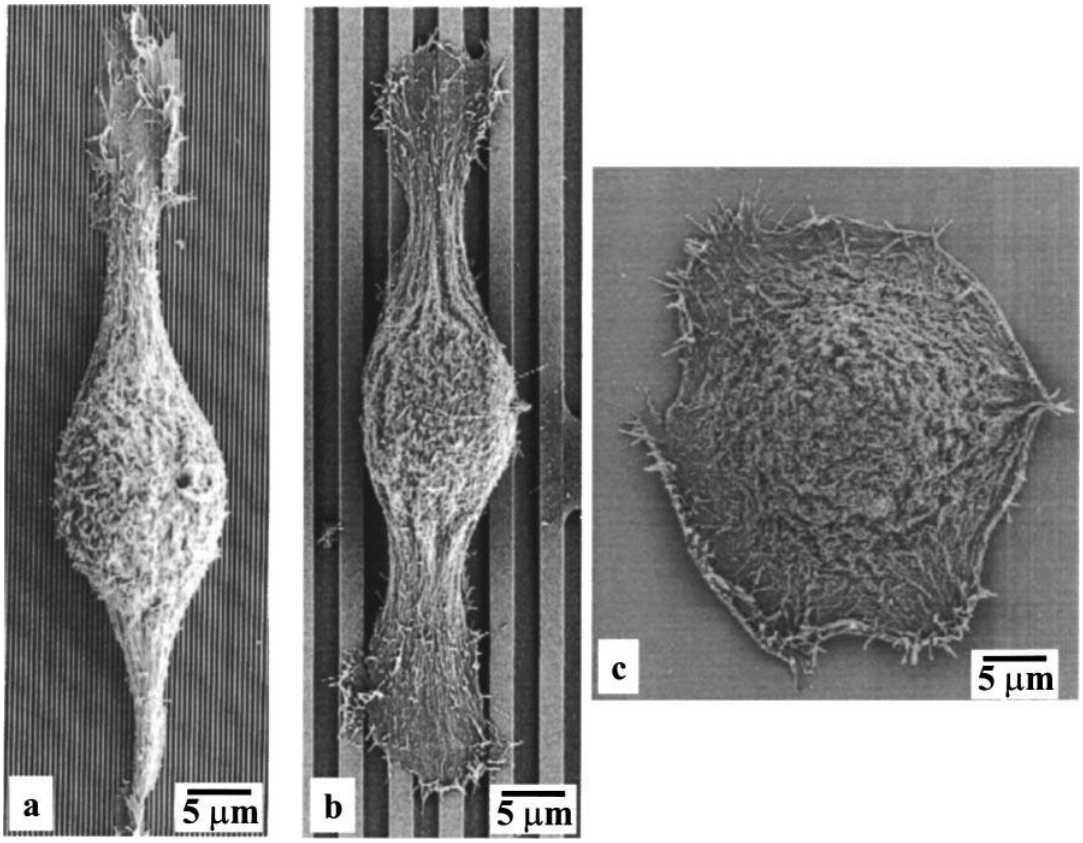

Figure 1.4.- HCECs elongate and align along grooves and ridges.

a) HCEC aligned on 400 nm pitch. b) HCEC aligned on 4000 nm pitch. c) HCEC on smooth substrate. From Teixeira AI, et. al. (2003) *J Vac Sci Technol B* 21(2), 683-687 (Reference 68)

Macromer used	Concentration	Crosslinking	Peptide	Tethering method	Reported amount	Surface density	Cellular type	Cellular response	Reference
-	-	-	G**RGD**Y and G**YIGSR**Y	tresyl chloride to link to glass	12.1 pmol/cm2	12.1 pmol/cm2	HFFs	Cells spread better on RGD than YIGSR	(94)
-	-	-	G**RGD**Y	tresyl chloride to link to glass	0.001/0.01/0.1/1.0/10/ 100/1000 fmol/cm2	0.001/0.01/0.1/1.0/10/100/1 000 fmol/cm2	HFFs	Maximal cell spreading at 1 fmol/cms. Focal contacts at 10 fmol/cm2	(104)
PEGDA 8 kDa	10% and 23% (w/v)	Photopolymerization with 2,2-dimethyl-2-phenyl-acetophenone in N-vinylpyrrolidone 365 nm, 10 mW/cm2, 90 s	Y**RGD**S	Acryloyl-PEG-NHS 3.4 kDa and Acryloyl-NHS	0.001/0.01/0.1/1.0 pmol/cm2	0.001/0.01/0.1/1.0 pmol/cm2	HFFs	Spreading proportinoal to peptide presentation.	(91)
p(Aam-co-EG/AA) IPN with PEG 1000	-	Photopolymerized wutg D,L-camphorquinone 470 nm, 3 min	Ac-CGGNGEP**RGD**TYRAY-NH2	Acryloyl-PEG-NH2 3.4 kDa + SMCC	Not reported	-	RCO	Cell adhesion and mineralization of ECM were RGD dependent	(100)
-	-	-	Ac-CGGNGEP**RGD**TYRAY-NH2	Linked covalently to quartz surfaces	0.01/0.62/3.8 pmol/cm2	0.01/0.62/3.8 pmol/cm2	RCO	Increased cell adhesion and calcification >0.62 pmol/cm2	(97)
PEGDA 8 kDa and PEG-diacrylmide 3.4 kDa	23% (w/v)	Photopolymerization with N-vinylpyrrolidone 50-75 mW/cm2 for 1-2 min	Ac-GCGYG**RGD**SPG-NH2	Michael-type reaction	0.368/1.18/3.68 pmol/cm2	0.368/1.18/3.68 pmol/cm2	Fibroblasts and HUVECs	Cell spreading after 4 hours was proportional to RGD presentation	(101)
HEMA	70% (w/w)	Benzoyl peroxide	**RGD**S and YIGSR	Tresyl-chloride	Not reported	-	Immortalized HCECs and HVECs	Good adhesion with YIGSR, less adhesion with RGDS	(95)
PEGDA 10 kDa	10% (w/v)	Photopolymerization with 2,2-dimethyl-2-phenyl-acetophenone in N-vinylpyrrolidone 365 nm, 10 mW/cm2, 30 s	**RGD**S, TMKIIPFNRLTIGG and YIGSR	Acryloyl-PEG-NHS 3.4 kDa	2.6/5.2/6.5 umol/mL RGDS 2.0-4.9 umol/mL TMKIIPFNRLTIGG 2.8 umol/mL YIGSR	2.6/5.2/6.5 pmol/cm2 RGDS 2.0-4.9 pmol/cm2 TMKIIPFNRLTIGG 2.8 pmol/cm2 YIGSR	Neutrophils	Adhesion proportional to peptide presentation. Spreading RGDS+TMKIIPFNRLTIG>RGDS+YIGSR> RGDS	(89)
8-arm PEG-acrylate 20 kDa	25% (w/v)	PEG dithiol 3.4 kDa	GCGGG**RGD**SPG, GCGGGV**PHSRN**G and GCGGG**YIGSR**G	Michael-type reaction	0.08/.32/1.24/3.9 pmol/cm2	0.08/.32/1.24/3.9 pmol/cm2	HMVEC and HVSMC	Adhesion RGD>PHSRN>YIGSR Best YIGSR+RGD Migration is best with YIGSR+RGD	(88)
PEGDA, Mw not mentioned	15% (w/v)	Photopolymerization with Irgacure D2959 365 nm, 4 mW/cm2 5 min	Y**RGD**S	Acryloyl-PEG-NHS 3.4 kDa	0.05/1.25/2.5 mM	0.05/1.25/2.5 pmol/cm2	MSCs	Proliferation not modified. Osteogenesis increased with peptide presentation	(99)
MVG Alginate 250 kDa	2% (w/v)	Ionic crosslinking with calcium sulfate	GGGG**RGD**SP	NHS	36/58/78/100 nm spacing	0.30/0.11/0.04 pmol/cm2	MC3T3-E1 and D1	Proliferation increased with peptide presentation. Differentiation was increased with peptide presentation	(102)
p(HEMA-co-MAA)	95% HEMA 5% MAA 0.78% EDGMA	Photopolymerized with Darocur 1173 254 nm	WQPPRARI and **RGD**S	Acryloyl-PEG-NHS 3.4 kDa	Not reported	-	Rabbit CECs	RGD inhibited CEC growth	(103)
4-arm PEG-VS 20 kDa	10% (w/v)	With bicysteine degradable crosslinker	Ac-G**RGD**SPC-NH2	Michael-type reaction	0.01/0.1/1.0 mM	0.01/0.1/1.0 pmol/cm2	MDCK	Cell spreading after 30h	(86)
p(IPAAm-co-CIPAAm)	Monolayer	Graft polymerization to TCPM	RGD, **RGD**S, G**RGD**S	EDC/NHS	0.2/0.6/1.0/2.0 nmol/cm2	0.2/0.6/1.0/2.0 nmol/cm2	BAECs	Spreading GRGDS>RGDS>RGD Spreading proportional to peptide presentation	(87)

NOTES: HFF-human foreskin fibroblast; RCO-rat calvaria osteoblast-like; HUVEC-human umbilical vein endothelial cell; HCEC-human corneal epithelial cell; HVEC-human vascular endothelial cell HMVEC-human microvascular endothelial cell; HVSMC-human vescular

Table 1.I.- Summary of studies using RGD as an adhesion promoter.

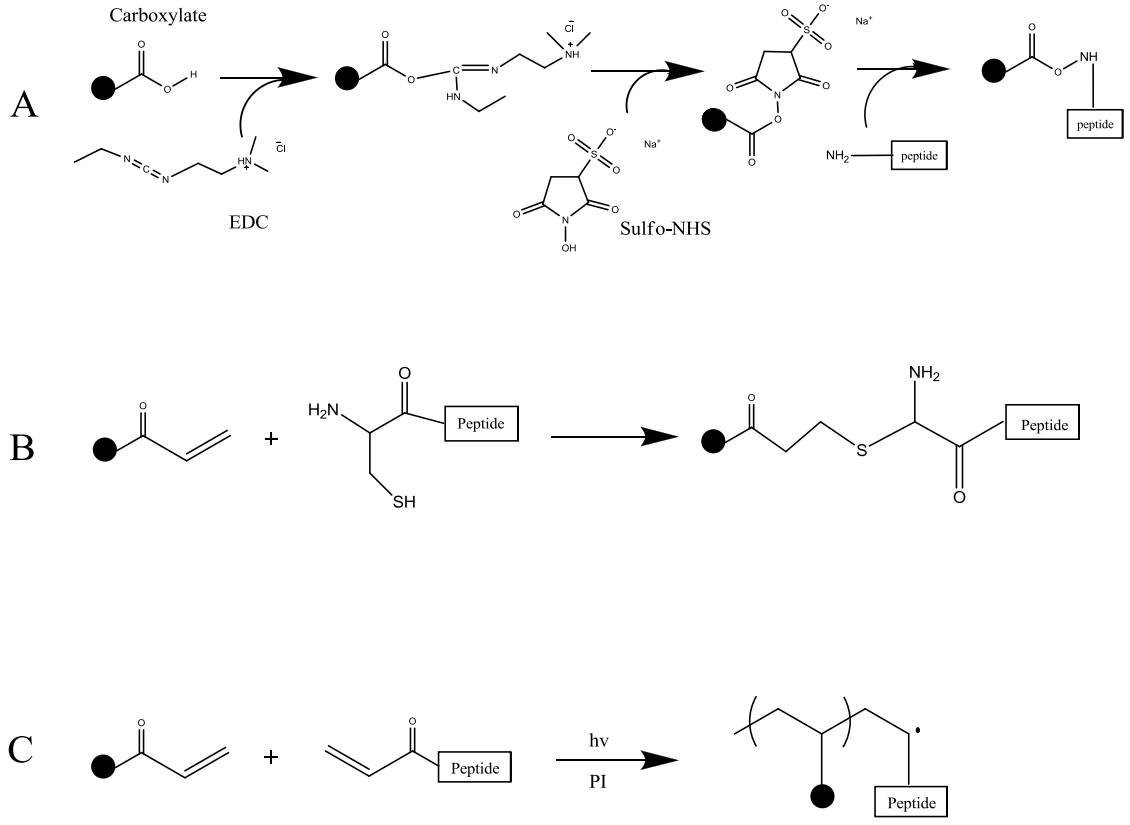

Figure 1.5.- Methods to covalently bind biomolecules to PEG hydrogels.

A) Activation. B) Incorporation. C) Polymerization.

1.11 References

1. Myung D, Duhamel PE, Cochran JR, Noolandi J, Ta CN, Frank CW. Development of Hydrogel-Based Keratoprostheses: A Materials Perspective. Biotechnology progress 2008;24(3):735-741.

2. Chirila TV, Hicks CR, Dalton PD, Vijayasekaran S, Lou X, Hong Y, Clayton AB, Ziegelaar BW, Fitton JH, Platten S. Artificial cornea. Progress in polymer science 1998;23(3):447-473.

3. Germain L, Carrier P, Auger FA, Salesse C, GuÃ©rin SL. Can we produce a human corneal equivalent by tissue engineering? Progress in retinal and eye research 2000;19(5):497-527.

4. Whitcher JP, Srinivasan M, Upadhyay MP. Corneal blindness: a global perspective. Bulletin of the World Health Organization 2001;79:214-221.

5. Aiken-O'Neill P, Mannis MJ. Summary of corneal transplant activity: Eye Bank Association of America. Cornea 2002;21(1):1.

6. Hicks CR, Fitton JH, Chirila TV, Crawford GJ, Constable IJ. Keratoprostheses: advancing toward a true artificial cornea. Survey of ophthalmology 1997;42(2):175-189.

7. Ilhan-Sarac O, Akpek EK. Current concepts and techniques in keratoprosthesis. Current Opinion in Ophthalmology 2005;16(4):246.

8. Lai JY, Hsiue GH. Functional biomedical polymers for corneal regenerative medicine. Reactive and Functional Polymers 2007;67(11):1284-1291.

9. Chirila TV. An overview of the development of artificial corneas with porous skirts and the use of PHEMA for such an application. Biomaterials 2001;22(24):3311-3317.

10. Myung D, Farooqui N, Zheng LL, Koh W, Gupta S, Bakri A, Noolandi J, Cochran JR, Frank CW, Ta CN. Bioactive interpenetrating polymer network hydrogels that support corneal epithelial wound healing. Journal of Biomedical Materials Research Part A 2009;90(1):70-81.

11. Aquavella JV, Qian Y, McCormick GJ, Palakuru JR. Keratoprosthesis: current techniques. Cornea 2006;25(6):656.

12. Bentley E, Murphy CJ. Topical therapeutic agents that modulate corneal wound healing. VETERINARY CLINICS OF NORTH AMERICA SMALL ANIMAL PRACTICE 2004:623-638.

13. Abrams GA, Schaus SS, Goodman SL, Nealey PF, Murphy CJ. Nanoscale topography of the corneal epithelial basement membrane and Descemet's membrane of the human. Cornea 2000;19(1):57.

14. Abrams GA, Goodman SL, Nealey PF, Franco M, Murphy CJ. Nanoscale topography of the basement membrane underlying the corneal epithelium of the rhesus macaque. Cell and Tissue Research 2000;299(1):39-46.

15. Kenyon K. Anatomy and pathology of the ocular surface. International Ophtalmology Clinics 1979;19:3-35.

16. Lu L, Reinach PS, Kao WWY. Corneal epithelial wound healing. Experimental Biology and Medicine 2001;226(7):653-664.

17. Dua HS, Gomes JA, Singh A. Corneal epithelial wound healing. British journal of ophthalmology 1994;78(5):401-408.

18. Arffa RC. Clinical applications of corneal topographic analysis. 1991. Informa UK Ltd UK. p 122-132.

19. Maudgal PC, Missotten L. Superficial keratitis. Bulletin de la Societa belge d'ophtalmologie 1980;187(1):1.

20. Sun TT, Eichner R, Nelson WG, Tseng SCG, Weiss RA, Jarvinen M, Woodcock-Mitchell J. Keratin classes: molecular markers for different types of epithelial differentiation. Journal of Investigative Dermatology 1983;81:109s-115s.

21. Stepp MA, Zhu L, Cranfill R. Changes in beta 4 integrin expression and localization in vivo in response to corneal epithelial injury. Investigative ophthalmology & visual science 1996;37(8):1593-1601.

22. Blake DA, Yu H, Young DL, Caldwell DR. Matrix stimulates the proliferation of human corneal endothelial cells in culture. Investigative ophthalmology & visual science 1997;38(6):1119-1129.

23. Ekblom P, Timplt R. Cell-to-cell contact and extracellular matrix A multifaceted approach emerging Editorial overview. Current opinion in cell biology 1996;8:599-601.

24. Streuli CH, Bissell MJ. Expression of extracellular matrix components is regulated by substratum. The Journal of cell biology 1990;110(4):1405-1415.

25. Trinkaus-Randall V, Newton AW, Franzblau C. The synthesis and role of integrin in corneal epithelial cells in culture. Investigative ophthalmology & visual science 1990;31(3):440-447.

26. Reid B, Song B, McCaig CD, Zhao M. Wound healing in rat cornea: the role of electric currents. The FASEB journal 2005;19(3):379-386.

27. Karp G. Cell and Molecular Biology: J. Wiley; 2002.

28. Halstenberg S, Panitch A, Rizzi S, Hall H, Hubbell JA. Biologically engineered protein-graft-poly (ethylene glycol) hydrogels: a cell adhesive and plasmin-degradable biosynthetic material for tissue repair. Biomacromolecules 2002;3(4):710-723.

29. Karuri NW, Liliensiek S, Teixeira AI, Abrams G, Campbell S, Nealey PF, Murphy CJ. Biological length scale topography enhances cell-substratum adhesion of human corneal epithelial cells. Journal of cell science 2004;117(Pt 15):3153.

30. DeLong SA, Moon JJ, West JL. Covalently immobilized gradients of bFGF on hydrogel scaffolds for directed cell migration. Biomaterials 2005;26(16):3227-3234.

31. Dalton B, McFarland GA, Steele JG. Stimulation of epithelial tissue migration by certain porous topographies is independent of fluid flux. Journal of biomedical materials research 2001;56(1):83-92.

32. Dalton B, Walboomers XF, Dziegielewski M, Evans MDM, Taylor S, Jansen JA, Steele JG. Modulation of epithelial tissue and cell migration by microgrooves. Journal of biomedical materials research 2001;56(2):195-207.

33. Kobayashi H, Ikacia Y. Corneal cell adhesion and proliferation on hydrogel sheets bound with cell-adhesive proteins. Current eye research 1991;10(10):899-908.

34. Franco M, Nealey PF, Campbell S, Teixeira AI, Murphy CJ. Adhesion and proliferation of corneal epithelial cells on self-assembled monolayers. Journal of biomedical materials research 2000;52(2):261-269.

35. Allen LT, Tosetto M, Miller IS, Oâ€™Connor DP, Penney SC, Lynch I, Keenan AK, Pennington SR, Dawson KA, Gallagher WM. Surface-induced changes in protein adsorption and implications for cellular phenotypic responses to surface interaction. Biomaterials 2006;27(16):3096-3108.

36. Teixeira AI, McKie GA, Foley JD, Bertics PJ, Nealey PF, Murphy CJ. The effect of environmental factors on the response of human corneal epithelial cells to nanoscale substrate topography. Biomaterials 2006;27(21):3945-3954.

37. Chen CS, Tan J, Tien J. Mechanotransduction at cell-matrix and cell-cell contacts. Annu. Rev. Biomed. Eng. 2004;6:275-302.

38. Karuri NW, Nealey PF, Murphy CJ, Albrecht RM. Structural organization of the cytoskeleton in SV40 human corneal epithelial cells cultured on nanoâ€ • and microscale grooves. Scanning 2008;30(5):405-413.

39. Dalton BA, Evans MDM, McFarland GA, Steele JG. Modulation of corneal epithelial stratification by polymer surface topography. Journal of biomedical materials research 1999;45(4):384-394.

40. Dalby MJ, Riehle MO, Sutherland DS, Agheli H, Curtis ASG. Use of nanotopography to study mechanotransduction in fibroblastsâ€“methods and perspectives. European journal of cell biology 2004;83(4):159-169.

41. Dalby MJ, Yarwood SJ, Johnstone HJH, Affrossman S, Riehle MO. Fibroblast signaling events in response to nanotopography: a gene array study. NanoBioscience, IEEE Transactions on 2002;1(1):12-17.

42. Discher DE, Janmey P, Wang Y. Tissue cells feel and respond to the stiffness of their substrate. Science 2005;310(5751):1139.

43. Charest JL, GarcÃ-a AJ, King WP. Myoblast alignment and differentiation on cell culture substrates with microscale topography and model chemistries. Biomaterials 2007;28(13):2202-2210.

44. Chen CS, Mrksich M, Huang S, Whitesides GM, Ingber DE. Geometric control of cell life and death. Science 1997;276(5317):1425.

45. Alberts B, Bray D, Lewis J, Raff M, Roberts K, Watson JD. Molecular biology of the cell. Garland, New York 2002.

46. Flemming RG, Murphy CJ, Abrams GA, Goodman SL, Nealey PF. Effects of synthetic micro-and nano-structured surfaces on cell behavior. Biomaterials 1999;20(6):573-588.

47. Wilson CJ, Clegg RE, Leavesley DI, Pearcy MJ. Mediation of biomaterial-cell interactions by adsorbed proteins: a review. Tissue engineering 2005;11(1-2):1-18.

48. Ingber DE. Tensegrity: the architectural basis of cellular mechanotransduction. Annual review of physiology 1997;59(1):575-599.

49. Curtis A. Tutorial on the biology of nanotopography. NanoBioscience, IEEE Transactions on 2004;3(4):293-295.

50. Curtis A, Wilkinson C. Topographical control of cells. Biomaterials 1997;18(24):1573-1583.

51. Curtis ASG, Casey B, Gallagher JO, Pasqui D, Wood MA, Wilkinson CDW. Substratum nanotopography and the adhesion of biological cells. Are symmetry or regularity of nanotopography important? Biophysical chemistry 2001;94(3):275-283.

52. Diehl KA, Foley JD, Nealey PF, Murphy CJ. Nanoscale topography modulates corneal epithelial cell migration. Journal of Biomedical Materials Research Part A 2005;75(3):603-611.

53. Evans MDM, Dalton B, Steele JG. Persistent adhesion of epithelial tissue is sensitive to polymer topography. Journal of biomedical materials research 1999;46(4):485-493.

54. Fitton JH, Dalton BA, Beumer G, Johnson G, Griesser HJ, Steele JG. Surface topography can interfere with epithelial tissue migration. Journal of biomedical materials research 1998;42(2):245-257.

55. Foley JD, Grunwald EW, Nealey PF, Murphy CJ. Cooperative modulation of neuritogenesis by PC12 cells by topography and nerve growth factor. Biomaterials 2005;26(17):3639-3644.

56. Fraser SA, Ting YH, Mallon KS, Wendt AE, Murphy CJ, Nealey PF. Sub micron and nanoscale feature depth modulates alignment of stromal fibroblasts and corneal epithelial cells in serum rich and serum free media. Journal of Biomedical Materials Research Part A 2008;86(3):725-735.

57. Hahn MS, Miller JS, West JL. Three-Dimensional Biochemical and Biomechanical Patterning of Hydrogels for Guiding Cell Behavior. Advanced Materials 2006;18(20):2679-2684.

58. Hamilton DW, Brunette DM. The effect of substratum topography on osteoblast adhesion mediated signal transduction and phosphorylation. Biomaterials 2007;28(10):1806-1819.

59. Hamilton DW, Riehle MO, Monaghan W, Curtis ASG. Articular chondrocyte passage number: influence on adhesion, migration, cytoskeletal organisation and phenotype in response to nano-and micro-metric topography. Cell biology international 2005;29(6):408-421.

60. Hategan A, Sengupta K, Kahn S, Sackmann E, Discher DE. Topographical pattern dynamics in passive adhesion of cell membranes. Biophysical journal 2004;87(5):3547-3560.

61. Kaiser JP, Reinmann A, Bruinink A. The effect of topographic characteristics on cell migration velocity. Biomaterials 2006;27(30):5230-5241.

62. Karuri NW, Porri TJ, Albrecht RM, Murphy CJ, Nealey PF. Nano-and Microscale Holes Modulate Cell-Substrate Adhesion, Cytoskeletal Organization, and< formula formulatype=. NanoBioscience, IEEE Transactions on 2006;5(4):273-280.

63. Li WJ, Tuli R, Huang X, Laquerriere P, Tuan RS. Multilineage differentiation of human mesenchymal stem cells in a three-dimensional nanofibrous scaffold. Biomaterials 2005;26(25):5158-5166.

64. Lim JY, Dreiss AD, Zhou Z, Hansen JC, Siedlecki CA, Hengstebeck RW, Cheng J, Winograd N, Donahue HJ. The regulation of integrin-mediated osteoblast focal adhesion and focal adhesion kinase expression by nanoscale topography. Biomaterials 2007;28(10):1787-1797.

65. Rebollar E, Frischauf I, Olbrich M, Peterbauer T, Hering S, Preiner J, Hinterdorfer P, Romanin C, Heitz J. Proliferation of aligned mammalian cells on laser-nanostructured polystyrene. Biomaterials 2008;29(12):1796-1806.

66. Russell P, Gasiorowski JZ, Nealy PF, Murphy CJ. Response of human trabecular meshwork cells to topographic cues on the nanoscale level. Investigative ophthalmology & visual science 2008;49(2):629-635.

67. Teixeira AI, Abrams GA, Bertics PJ, Murphy CJ, Nealey PF. Epithelial contact guidance on well-defined micro- and nanostructured substrates. Journal of Cell Science 2003;116(Pt 10):1881-1892.

68. Teixeira AI, Abrams GA, Murphy CJ, Nealey PF. Cell behavior on lithographically defined nanostructured substrates. Journal of Vacuum Science & Technology B: Microelectronics and Nanometer Structures 2003;21:683.

69. Tobasnick G, Curtis ASG. Chloride channels and the reactions of cells to topography. Eur Cell Mater, in press. von Euler A, Roomans GM (1992) Ion transport in colon cancer cell cultures studied by X-ray microanalysis. Cell Biol Int Rep 2001;16:293-306.

70. Wang X, Ohlin CA, Lu Q, Hu J. Cell directional migration and oriented division on three-dimensional laser-induced periodic surface structures on polystyrene. Biomaterials 2008;29(13):2049-2059.

71. Eliason MT, Charest JL, Simmons BA, GarcÃ-a AJ, King WP. Nanoimprint fabrication of polymer cell substrates with combined microscale and nanoscale topography. Journal of Vacuum Science & Technology B: Microelectronics and Nanometer Structures 2007;25(4):L31-L34.

72. Rajnicek AM, Foubister LE, McCaig CD. Alignment of corneal and lens epithelial cells by co-operative effects of substratum topography and DC electric fields. Biomaterials 2008;29(13):2082-2095.

73. Tocce EJ, Smirnov VK, Kibalov DS, Liliensiek SJ, Murphy CJ, Nealey PF. The ability of corneal epithelial cells to recognize high aspect ratio nanostructures. Biomaterials 2010;31(14):4064-4072.

74. Tocce EJ, Liliensiek SJ, Broderick AH, Jiang Y, Murphy KC, Murphy CJ, Lynn DM, Nealey PF. The influence of biomimetic topographic features and the extracellular matrix peptide RGD on human corneal epithelial contact guidance. Acta Biomaterialia 2012.

75. Yanez-Soto B, Liliensiek SJ, Murphy CJ, Nealey PF. Biochemically and topographically engineered poly(ethylene glycol) diacrylate hydrogels with biomimetic characteristics as substrates for human corneal epithelial cells. Journal of Biomedical Materials Research Part A 2012.

76. Britland S, Morgan H, Wojiak-Stodart B, Riehle M, Curtis A, Wilkinson C. Synergistic and hierarchical adhesive and topographic guidance of BHK cells. Experimental cell research 1996;228(2):313-325.

77. Charest JL, Eliason MT, Garcia AJ, King WP. Combined microscale mechanical topography and chemical patterns on polymer cell culture substrates. Biomaterials 2006;27(11):2487-2494.

78. Rafat M, Griffith M, Hakim M, Muzakare L, Li F, Khulbe KC, Matsuura T. Plasma surface modification and characterization of collagen-based artificial cornea for enhanced epithelialization. Journal of Applied Polymer Science 2007;106(3):2056-2064.

79. Chen YM, Shiraishi N, Satokawa H, Kakugo A, Narita T, Gong JP, Osada Y, Yamamoto K, Ando J. Cultivation of endothelial cells on adhesive protein-free synthetic polymer gels. Biomaterials 2005;26(22):4588-4596.

80. Schneider GB, English A, Abraham M, Zaharias R, Stanford C, Keller J. The effect of hydrogel charge density on cell attachment. Biomaterials 2004;25(15):3023-3028.

81. Rimmer S, Johnson C, Zhao B, Collier J, Gilmore L, Sabnis S, Wyman P, Sammon C, Fullwood NJ, MacNeil S. Epithelialization of hydrogels achieved by amine functionalization and co-culture with stromal cells. Biomaterials 2007;28(35):5319-5331.

82. Miranti CK, Brugge JS. Sensing the environment: a historical perspective on integrin signal transduction. Nature Cell Biology 2002;4(4):83-90.

83. Pierschbacher MD, Ruoslahti E. Cell attachment activity of fibronectin can be duplicated by small synthetic fragments of the molecule. Nature 1984;309(5963):30.

84. Ruoslahti E. RGD and other recognition sequences for integrins. Annual review of cell and developmental biology 1996;12(1):697-715.

85. Cavalcanti-Adam EA, Micoulet A, BlÃ¼mmel J, Auernheimer J, Kessler H, Spatz JP. Lateral spacing of integrin ligands influences cell spreading and focal adhesion assembly. European journal of cell biology 2006;85(3):219-224.

86. Chung IM, Enemchukwu NO, Khaja SD, Murthy N, Mantalaris A, García AJ. Bioadhesive hydrogel microenvironments to modulate epithelial morphogenesis. Biomaterials 2008;29(17):2637-2645.

87. Ebara M, Yamato M, Aoyagi T, Kikuchi A, Sakai K, Okano T. The effect of extensible PEG tethers on shielding between grafted thermo-responsive polymer chains and integrin-RGD binding. Biomaterials 2008;29(27):3650-3655.

88. Fittkau MH, Zilla P, Bezuidenhout D, Lutolf MP, Human P, Hubbell JA, Davies N. The selective modulation of endothelial cell mobility on RGD peptide containing surfaces by YIGSR peptides. Biomaterials 2005;26(2):167-174.

89. Gonzalez AL, Gobin AS, West JL, McIntire LV, Smith CW. Integrin interactions with immobilized peptides in polyethylene glycol diacrylate hydrogels. Tissue engineering 2004;10(11-12):1775-1786.

90. Harbers GM, Gamble LJ, Irwin EF, Castner DG, Healy KE. Development and characterization of a high-throughput system for assessing cell-surface receptor-ligand engagement. Langmuir 2005;21(18):8374-8384.

91. Hern DL, Hubbell JA. Incorporation of adhesion peptides into nonadhesive hydrogels useful for tissue resurfacing. Journal of Biomedical Materials Research Part A 1998;39(2):266-276.

92. Hersel U, Dahmen C, Kessler H. RGD modified polymers: biomaterials for stimulated cell adhesion and beyond. Biomaterials 2003;24(24):4385-4415.

93. Mardilovich A, Craig JA, McCammon MQ, Garg A, Kokkoli E. Design of a novel fibronectin-mimetic peptide-amphiphile for functionalized biomaterials. Langmuir 2006;22(7):3259-3264.

94. Massia SP, Hubbell JA. Convalent surface immobilization of Arg-Gly-Asp-and Tyr-Ile-Gly-Ser-Arg-containing peptides to obtain well-defined cell-adhesive substrates. Analytical biochemistry 1990;187(2):292-301.

95. Merrett K, Griffith CM, Deslandes Y, Pleizier G, Sheardown H. Adhesion of corneal epithelial cells to cell adhesion peptide modified pHEMA surfaces. Journal of Biomaterials Science, Polymer Edition 2001;12(6):647-671.

96. Perlin L, MacNeil S, Rimmer S. Production and performance of biomaterials containing RGD peptides. Soft Matter 2008;4(12):2331-2349.

97. Rezania A, Healy KE. The effect of peptide surface density on mineralization of a matrix deposited by osteogenic cells. Journal of biomedical materials research 2000;52(4):595-600.

98. Wacker BK, Alford SK, Scott EA, Das Thakur M, Longmore GD, Elbert DL. Endothelial cell migration on RGD-peptide-containing PEG hydrogels in the presence of sphingosine 1-phosphate. Biophysical journal 2008;94(1):273-285.

99. Yang F, Williams CG, Wang D, Lee H, Manson PN, Elisseeff J. The effect of incorporating RGD adhesive peptide in polyethylene glycol diacrylate hydrogel on osteogenesis of bone marrow stromal cells. Biomaterials 2005;26(30):5991-5998.

100. Bearinger JP, Castner DG, Healy KE. Biomolecular modification of p (AAm-co-EG/AA) IPNs supports osteoblast adhesion and phenotypic expression. Journal of Biomaterials Science, Polymer Edition 1998;9(7):629-652.

101. Elbert DL, Hubbell JA. Conjugate addition reactions combined with free-radical cross-linking for the design of materials for tissue engineering. Biomacromolecules 2001;2(2):430-441.

102. Hsiong S, Lee K, Alsberg E, Mooney D. Nanoscale RGD peptide organization regulates cell proliferation and differentiation. 2005.

103. Jacob JT, Rochefort JR, Bi J, Gebhardt BM. Corneal epithelial cell growth over tethered protein/peptide surface modified hydrogels. Journal of Biomedical Materials Research Part B: Applied Biomaterials 2005;72B(1):198-205.

104. Massia SP, Hubbell JA. An RGD spacing of 440 nm is sufficient for integrin alpha V beta 3-mediated fibroblast spreading and 140 nm for focal contact and stress fiber formation. Journal of Cell Biology 1991;114(5):1089.

105. Palecek SP, Loftus JC, Ginsberg MH, Lauffenburger DA, Horwitz AF. Integrin-ligand binding properties govern cell migration speed through cell-substratum adhesiveness. Nature 1997;385(6616):537-540.

106. Klenkler BJ, Chen H, Chen Y, Brook MA, Sheardown H. A high-density PEG interfacial layer alters the response to an EGF tethered polydimethylsiloxane surface. Journal of Biomaterials Science, Polymer Edition 2008;19(11):1411-1424.

107. Liliensiek SJ, Campbell S, Nealey PF, Murphy CJ. The scale of substratum topographic features modulates proliferation of corneal epithelial cells and corneal fibroblasts. Journal of Biomedical Materials Research Part A 2006;79(1):185-192.

108. Gasiorowski JZ, Liliensiek SJ, Russell P, Stephan DA, Nealey PF, Murphy CJ. Alterations in gene expression of human vascular endothelial cells associated with nanotopographic cues. Biomaterials 2010;31(34):8882-8888.

109. Baroli B. Hydrogels for tissue engineering and delivery of tissue-inducing substances. Journal of pharmaceutical sciences 2007;96(9):2197-2223.

110. Hennink WE, Van Nostrum CF. Novel crosslinking methods to design hydrogels. Advanced Drug Delivery Reviews 2002;54(1):13-36.

111. Brandl F, Sommer F, Goepferich A. Rational design of hydrogels for tissue engineering: impact of physical factors on cell behavior. Biomaterials 2007;28(2):134-146.

112. Drury JL, Mooney DJ. Hydrogels for tissue engineering: scaffold design variables and applications. Biomaterials 2003;24(24):4337-4351.

113. Hoffman AS. Hydrogels for biomedical applications. Advanced drug delivery reviews 2002.

114. Amsden B. Solute diffusion within hydrogels. Mechanisms and models. Macromolecules 1998;31(23):8382-8395.

115. Cruise GM, Scharp DS, Hubbell JA. Characterization of permeability and network structure of interfacially photopolymerized poly (ethylene glycol) diacrylate hydrogels. Biomaterials 1998;19(14):1287-1294.

116. Ehrick JD, Deo SK, Browning TW, Bachas LG, Madou MJ, Daunert S. Genetically engineered protein in hydrogels tailors stimuli-responsive characteristics. Nature materials 2005;4(4):298-302.

117. Ehrbar M, Rizzi SC, Hlushchuk R, Djonov V, Zisch AH, Hubbell JA, Weber FE, Lutolf MP. Enzymatic formation of modular cell-instructive fibrin analogs for tissue engineering. Biomaterials 2007;28(26):3856-3866.

118. Nguyen KT, West JL. Photopolymerizable hydrogels for tissue engineering applications. Biomaterials 2002;23(22):4307-4314.

119. Pratoomsoot C, Tanioka H, Hori K, Kawasaki S, Kinoshita S, Tighe PJ, Dua H, Shakesheff KM, Rose FRAJ. A thermoreversible hydrogel as a biosynthetic bandage for corneal wound repair. Biomaterials 2008;29(3):272-281.

120. Cruise GM, Hegre OD, Scharp DS, Hubbell JA. A sensitivity study of the key parameters in the interfacial photopolymerization of poly (ethylene glycol) diacrylate upon porcine islets. Biotechnology and bioengineering 2000;57(6):655-665.

121. Tauro JR, Gemeinhart RA. Matrix metalloprotease triggered delivery of cancer chemotherapeutics from hydrogel matrixes. Bioconjugate chemistry 2005;16(5):1133-1139.

122. Lee KY, Mooney DJ. Hydrogels for tissue engineering. Chem. Rev 2001;101(7):1869-1880.

123. Harris JM. Poly (ethylene glycol) chemistry: biotechnical and biomedical applications. New York: Springer; 1992.

124. Myung D, Koh W, Bakri A, Zhang F, Marshall A, Ko J, Noolandi J, Carrasco M, Cochran JR, Frank CW. Design and fabrication of an artificial cornea based on a photolithographically patterned hydrogel construct. Biomedical microdevices 2007;9(6):911-922.

125. Bryant SJ, Anseth KS. Hydrogel properties influence ECM production by chondrocytes photoencapsulated in poly (ethylene glycol) hydrogels. Journal of biomedical materials research 2001;59(1):63-72.

126. AdelÃ¶w C, Segura T, Hubbell JA, Frey P. The effect of enzymatically degradable poly (ethylene glycol) hydrogels on smooth muscle cell phenotype. Biomaterials 2008;29(3):314-326.

127. Raeber GP, Lutolf MP, Hubbell JA. Molecularly engineered PEG hydrogels: a novel model system for proteolytically mediated cell migration. Biophysical journal 2005;89(2):1374-1388.

128. West JL, Hubbell JA. Polymeric biomaterials with degradation sites for proteases involved in cell migration. Macromolecules 1999;32(1):241-244.

129. Hahn MS, Taite LJ, Moon JJ, Rowland MC, Ruffino KA, West JL. Photolithographic patterning of polyethylene glycol hydrogels. Biomaterials 2006;27(12):2519-2524.

130. Kim J, Lee KW, Hefferan TE, Currier BL, Lu L, Yaszemski MJ. Biodegradable and Photopolymerizable Hydrogels for Tissue Engineering Based on Poly (ethylene glycol) and Sebacic acid. http://www.nt.ntnu.no/users/skoge/prost/proceedings/aiche-2006/data/papers/P49534.pdf; Accessed on November 27, 2012.

131. Kim P, Kim DH, Kim B, Choi SK, Lee SH, Khademhosseini A, Langer R, Suh KY. Fabrication of nanostructures of polyethylene glycol for applications to protein adsorption and cell adhesion. Nanotechnology 2005;16(10):2420.

132. Lee HJ, Lee JS, Chansakul T, Yu C, Elisseeff JH, Yu SM. Collagen mimetic peptide-conjugated photopolymerizable PEG hydrogel. Biomaterials 2006;27(30):5268-5276.

133. Pfister PM, Wendlandt M, Neuenschwander P, Suter UW. Surface-textured PEG-based hydrogels with adjustable elasticity: Synthesis and characterization. Biomaterials 2007;28(4):567-575.

134. Revzin A, Russell RJ, Yadavalli VK, Koh WG, Deister C, Hile DD, Mellott MB, Pishko MV. Fabrication of poly (ethylene glycol) hydrogel microstructures using photolithography. Langmuir 2001;17(18):5440-5447.

135. Suh KY, Seong J, Khademhosseini A, Laibinis PE, Langer R. A simple soft lithographic route to fabrication of poly (ethylene glycol) microstructures for protein and cell patterning. Biomaterials 2004;25(3):557-563.

136. Baroli B. Photopolymerization of biomaterials: issues and potentialities in drug delivery, tissue engineering, and cell encapsulation applications. Journal of Chemical Technology and Biotechnology 2006;81(4):491-499.

137. Fouassier JP, Allonas X, Burget D. Photopolymerization reactions under visible lights: principle, mechanisms and examples of applications. Progress in organic coatings 2003;47(1):16-36.

138. Bryant SJ, Nuttelman CR, Anseth KS. Cytocompatibility of UV and visible light photoinitiating systems on cultured NIH/3T3 fibroblasts in vitro. Journal of Biomaterials Science, Polymer Edition 2000;11(5):439-457.

139. Williams CG, Malik AN, Kim TK, Manson PN, Elisseeff JH. Variable cytocompatibility of six cell lines with photoinitiators used for polymerizing hydrogels and cell encapsulation. Biomaterials 2005;26(11):1211-1218.

140. Braun PV, Wiltzius P. Microporous materials: Electrochemically grown photonic crystals. Nature 1999;402(6762):603-604.

141. Gratson GM, García-Santamaría F, Lousse V, Xu M, Fan S, Lewis JA, Braun PV. Direct-Write Assembly of Three-Dimensional Photonic Crystals: Conversion of Polymer Scaffolds to Silicon Hollow-Woodpile Structures. Advanced Materials 2006;18(4):461-465.

142. Kotov NA, Liu Y, Wang S, Cumming C, Eghtedari M, Vargas G, Motamedi M, Nichols J, Cortiella J. Inverted colloidal crystals as three-dimensional cell scaffolds. Langmuir 2004;20(19):7887-7892.

143. Lee J, Shanbhag S, Kotov NA. Inverted colloidal crystals as three-dimensional microenvironments for cellular co-cultures. J. Mater. Chem. 2006;16(35):3558-3564.

144. Liu Y, Wang S, Krouse J, Kotov NA, Eghtedari M, Vargas G, Motamedi M. Rapid aqueous photo-polymerization route to polymer and polymer-composite hydrogel 3D inverted colloidal crystal scaffolds. Journal of Biomedical Materials Research Part A 2007;83(1):1-9.

145. Wood MA. Colloidal lithography and current fabrication techniques producing in-plane nanotopography for biological applications. Journal of The Royal Society Interface 2007;4(12):1-17.

146. Lewis JA. Direct ink writing of 3D functional materials. Advanced Functional Materials 2006;16(17):2193-2204.

147. Lewis JA, Gratson GM. Direct writing in three dimensions. Materials today 2004;7(7):32-39.

148. Suh KY, Langer R. Microstructures of poly (ethylene glycol) by molding and dewetting. Applied physics letters 2003;83(8):1668-1670.

149. Lutolf MP, Tirelli N, Cerritelli S, Cavalli L, Hubbell JA. Systematic modulation of Michael-type reactivity of thiols through the use of charged amino acids. Bioconjugate chemistry 2001;12(6):1051-1056.

150. Last JA, Liliensiek SJ, Nealey PF, Murphy CJ. Determining the mechanical properties of human corneal basement membranes with atomic force microscopy. Journal of structural biology 2009;167(1):19-24.

CHAPTER 2: INCORPORATION OF BIOCHEMICAL CUES INTO A POLY(ETHYLENE GLYCOL) DIACRYLATE HYDROGEL SUBSTRATE TO PROMOTE HUMAN CORNEAL EPITHELIAL CELL ATTACHMENT AND PROLIFERATION.

2.1 Introduction

The behavior of cells and tissues in an organism is highly dependent on the numerous chemical and mechanical cues presented by the media, the neighboring cells and the extracellular matrix (ECM)[1]. The ECM-cell interactions can be further divided onto biochemical cues, mechanical cues and topographical cues[2]. The impact of those signals on cell behavior has been extensively studied[3-8]. The incorporation of the necessary information for the cell to promote certain behaviors onto biomaterials is important for biomedical fields such as tissue engineering, the design of artificial organs and cell culture.

Artificial corneas are an important therapy that involves the design of biomaterials as an artificial ECM with biomimetic characteristics. Several corneal prosthetics have been developed although they are limited by problems such as extrusion, infection, epithelial down-growth and the formation of opaque retroprosthetic membranes[9]. The coverage of the device with an epithelial layer has been proposed as a solution for those issues[9]. To achieve the formation and maintenance of a healthy corneal epithelium, the design of corneal prosthetics requires the use of biomaterials that include all the relevant cues found within the native corneal epithelial environment, and more specifically, the

basement membrane (BM), a thin and highly specialized ECM component that supports the corneal epithelium[10]. We believe that incorporation of these native extracellular cues onto the external surface of prosthetics will improve the device design through the formation and maintenance of a healthy corneal epithelium.

To ensure the isolation of the specific cell substrate receptors and the downstream signaling pathways responsible for the behavior of human corneal epithelial cells (HCECs), the substrates used must be engineered to inhibit the non-specific protein adsorption and, at the same time, allow for their functionalization with specific ECM ligands. Hydrogels synthesized with poly(ethylene glycol) (PEG) are suitable biomaterials for the incorporation of biophysical and biochemical cues found in the corneal BM. This material has already been used extensively in other FDA approved medical applications including nonfouling coatings[11] and artificial ECM [12]. In addition, they possess many desirable qualities including resistance to protein adsorption and lack of toxicity both *in vitro* and *in vivo*[13-15]. PEG hydrogel substrates can be fabricated using several different established methods that allow the incorporation of different ligands[16], including crosslinking via radical polymerization or chemical reaction and subsequent co-polymerization with biodegradable materials, such as poly(lactic acid)[17] or biodegradable peptides[12]. In summary, PEG hydrogels allow for a flexible platform to investigate the impact of biophysical and biochemical cues on HCEC behavior.

The objective of our particular study involves the fabrication of polymeric PEGDA substrates that allow for incorporation of specific ECM peptides from the corneal BM to investigate the impact of biochemical cues on several HCEC behaviors including

attachment, cell area and proliferation. The peptide RGD (Arg-Gly-Asp) is a rational first choice as the bioactive ligand to be incorporated into PEG hydrogels to provide specific and relevant adhesion moieties to the HCECs because this sequence is involved in binding to cell substrate adhesion receptors including several integrins[18]. In addition, we chose to include commonly used HCEC cell lines SV40-HCEC and hTCEpi immortalized cell lines as well as primary HCEC cells to provide a thorough characterization of HCEC behavior. These studies have fundamental relevance to our understanding of HCEC interaction with the underlying substrate. They will aid in the development of better cell culture systems and improved corneal prosthetics.

2.2 Materials and methods

2.2.1 Synthesis of ECM peptides

RGD peptide (Cys-Gly-Gly-Arg-Gly-Asp-Ser-Pro) and scrambled peptide RDG (Cys-Gly-Gly-Arg-Asp-Gly-Ser-Pro) were synthesized by solid phase peptide synthesis on Fmoc-Rink Amide MBHA resin with Fmoc-protected α-amino groups using a peptide synthesizer (CS Bio, Menlo Park, CA). 2,2,5,7,8-pentamethyl-chroman-6-sulfonyl was used as side-chain protecting group for Arg. The resulting peptide molecules were cleaved from the resin for four hours using a TFA:TIS:water (95:2.5:2.5) solution, filtered to remove resin and precipitated in diethyl ether. Peptides were analyzed by matrix-assisted laser desorption/ionization time of flight (MALDI-TOF) mass

spectrometry (Bruker Reflex II time-of-flight mass spectrometer) and used without further purification.

2.2.2 Fabrication of PEGDA hydrogels

Precursor solutions of 20% (w/v) poly(ethylene glycol) diacrylate (PEGDA) were prepared by dissolving either PEGDA 3400 MW (Glycosan Biosystems, UT), or PEGDA 700 MW (Sigma-Aldrich, Japan) in 10 mM 4-(2-hydroxyethyl)-1-piperazineethanesulfonic acid (HEPES) buffer at pH 8.0. 0.05% 1-propanone, 2-hydroxy-1-[4-(hydoxyethoxy)phenyl]-2-methyl-1-propanone (Irgacure 2959, Ciba AG) was used as the photoinitiator. Variable amounts of RGD or RDG peptide containing a cysteine residue were added to the precursor solutions to reach final concentrations of 0, 1, 5, 10 or 20 mM. All hydrogel substrates were prepared within a 100% nitrogen atmosphere to eliminate potential inhibition of free radical polymerization by oxygen. A 20 μL drop of the precursor solution was placed on top of a degassed poly(dimethyl siloxane) (PDMS, Sylgard® 184, Dow Corning, MI) flat stamp with 0.5 mm PDMS spacers. The precursor solution was then covered by a glass cover slip previously treated with 3-(trichlorosilyl) propyl methacrylate (TPM, Sigma-Aldrich, UK) to ensure adhesion of the gels to the surface. The construct was polymerized under UV-light (364 nm for 900 s at 7.0 mW/cm^2) and sterilized for 24 hours by soaking in 5% Isopropylic alcohol (IPA) in 1X phosphate buffered saline (PBS, pH 7.2). Hydrogel substrates were rinsed and soaked for 24 hours in 1X PBS and pre-incubated for 2 hours in the appropriate cell culture media for full equilibration.

2.2.3 Cell culture

Primary cell strains of pooled HCEC and two different human corneal epithelial cell lines were used to test the hydrogel substrates. Primary human corneal epithelial cells (HCEC) were harvested from human cadaver corneas graciously donated by the Lions Eye Bank of Wisconsin, Madison or the Missouri Lions Eye Bank (Columbia, MO) as previously reported[19]. Following disaggregation of HCEC with dispase solution (1.2 units/ml at 37 °C for 4 h, Boehringer Mannheim, Germany), cells from 2 to 4 corneas were centrifuged and re-suspended in epithelial medium. Epithelial medium consist of a 3:2 ratio of Ham's F12:Dulbelco's Modified Eagles medium (DMEM) (Invitrogen, CA), supplemented with 2.5% (v/v) fetal bovine serum (FBS), 0.4 μg/mL hydrocortisone, 8.4 ng/mL cholera toxin, 5 μg/mL insulin, 24 μg/mL adenine, 10 ng/mL epidermal growth factor, 100 units penicillin, and 100 μg/mL streptomycin[20,21]. Both the primary HCECs and and the immortalized human corneal epithelial cell line hTCEpi (courtesy of Dr. James Jester, UC-Irvine)[22] were maintained in culture in 100 mm tissue culture plates containing a mitomycin-c treated Swiss 3T3 fibroblast layer. Cells were incubated at 37 °C and 5% CO_2 until they reached approximately 70% confluence. HCEC were used between passages 1 and 4 and hTCEpi cells were used between passages 40 and 50.

SV40-HCECs (from Dr Kaoru Araki-Sasaki, Kiniki Central Hospital, Hyogo, Japan[23]) were grown in 100 mm tissue culture plates at 37 °C with 5% CO_2 in a modified, Supplemented Hormonal Epithelial Medium (SHEM; Sigma-Aldrich, Co., St Louis, MO, USA). SHEM, which is made up of Dulbecco's modified Eagle's medium (DMEM),

Ham's F-12 and 10% fetal bovine serum (FBS; Sigma-Aldrich, Co.). Passages 19-25 of the SV40-HCECs were used for our experiments.

2.2.4 Analysis of Cell Attachment and Proliferation

An experimental set consisted of 3 replicates of each hydrogel substrate plated at a density of 10,000; three replicates of each hydrogel substrate plated at a density of 20,000; and three replicates of each hydrogel substrate plated at a density of 30,000 cells per cm^2. All cells were incubated for 24 h after plating to allow for attachment and spreading. For the initial cell attachment experiments, the number of adherent HCECs were counted after 24 hours in culture. Hydrogel samples with HCECs were imaged using a Zeiss Axiovert 100M fluorescence microscope (Zeiss, Germany). Phase images of cells on each of the surfaces were obtained using a 10X objective lens. At least four images, which encompassed the majority of the PEGDA surface, were taken for each substrate as well as control tissue culture polystyrene (TCPS). Each experimental set contained at least three replicates per substrate per plating density, and was repeated in triplicate.

For calculation of cell proliferation, cells numbers were also analyzed after 120 hours to calculate the percent increase. The rate of proliferation was calculated as percentage increase = 100 X (N-No)/No, where N is the number of cells at 120 hours and No is the number of cells at the 24 hour timepoint[24].

2.2.5 Immunocytochemistry

Cells were stained for actin-filaments using actin-phalloidin which provides an outline of the cell for measurement of cell area and DAPI for measurement of cell number as previously described[25]. Briefly, following incubation, cells were fixed with 1% paraformaldehyde–PBS (Electron Microscopy Sciences, PA) at room temperature for 20 min. Cells were then permeabilized with 0.1% Triton X-100 (Sigma–Aldrich, MO) in 1X PBS for 7 min, and then exposed to 1% (w/w) bovine serum albumin (Sigma–Aldrich, MO) in 1X PBS for 20 min to block non-specific binding. Cells were then incubated with 5 μg/mL of TRITC–phalloidin (Sigma–Aldrich, MO) containing 0.1 μg/mL 4',6-Diamidino-2- phenylindole (DAPI) (Invitrogen, CA) in 1X PBS for 40 min, to label both filamentous actin (red), and the nucleus (blue).

2.2.6 Soluble RGD peptide competitive assay

Soluble RGD peptide (Gly-Gly-Gly-Arg-Gly-Asp-Ser-Pro) or soluble, control RDG peptide (Gly-Gly-Gly-Arg-Asp-Gly-Ser-Pro) were dissolved in the cell-appropriate media to reach concentrations of 10 μM, 100 μM and 1000 μM. Hydrogel substrates functionalized with 10 mM RGD were pre-incubated with the corresponding peptide-containing media prior to plating. After two hours of pre-incubation, cells were plated onto substrates in the presence of either soluble RGD or RDG peptide, incubated for 24 hours, and adherent cells were counted as previously described.

2.2.7 Statistics

Experiments were analyzed using analysis of variance (ANOVA). When variability was determined to be significant ($P < 0.05$), the Tukey's multiple comparison test was used to determine significance between groups. Significance was further divided into "statistically significant" ($0.01 \leq P \leq 0.05$), "very significant" ($0.001 \leq P < 0.01$), and "extremely significant" ($P < 0.001$).

2.3 Results

2.3.1 PEGDA MW 3400 inhibits non-specific HCEC attachment.

The inhibition of non-specific HCEC attachment is dependent on the molecular weight of the PEGDA pre-polymer. In order to select the molecular weight of PEGDA pre-polymer that inhibits non-specific HCEC attachment; we tested two different molecular weights, including PEGDA MW 700 and PEGDA MW 3400. We included primary HCECs and two immortalized HCEC lines to determine if non-specific cell attachment is cell-type specific. The three cell-types studied were cultured on the surface of hydrogels for 24 hours, and adherent cells were quantified. All the corneal cell types cultured on PEGDA MW 700 hydrogels showed an extremely significant increase ($P < 0.001$) in the number of cells adherent to the substrate compared to cells cultured on PEGDA MW 3400 hydrogels (figure 2.1). More specifically, SV40-HCECs cultured on PEGDA MW 700 presented a 365-fold increase with respect to cells cultured on PEGDA MW 3400, while hTCEpi cells had an 8.7-fold increase and primary hCECs showed a

4.7-fold increase in cell number. Based on our results, the best non-fouling properties were found on hydrogels made with PEGDA MW 3400. Therefore it was used for subsequent experiments involving functionalization of the hydrogel substrate with specific peptides.

2.3.2 HCECs exhibit specific RGD-dependent attachment on flat functionalized PEG surfaces

Peptides were covalently incorporated to the acrylate groups of the PEGDA macromer via a Michael-type addition reaction[26], where candidate peptides containing thiol groups react with the acrylate groups present in PEGDA to form stable covalent linkages (scheme 2.1). To validate HCEC attachment specificity through integrin binding, variable amounts of the peptide RGD or control "scrambled" RDG were added to precursor solutions of 20% PEGDA MW 3400 to reach the final peptide concentrations of 1, 5, 10 or 20 mM in the solution. Flat hydrogels were synthesized by applying 30 μL onto a flat PDMS and covering with a previously TPM-treated glass coverslip in a nitrogen atmosphere. The hydrogels were UV-crosslikned, sterilized and rinsed and soaked in culture medium until equilibration. HCECs were cultured and stained and imaged for the level of cell attachment. As expected, unfunctionalized hydrogels synthesized with PEGDA MW 3400 or substrates functionalized with the scrambled peptide RDG showed no significant attachment of HCECs for any of the scrambled peptide concentrations (1-20mM) (images not shown). Images in figure 2.2 demonstrate a monotonically increasing number of attached HCECs with increasing

concentration of RGD in the hydrogels. The cell number of HCECs on 5mM RGD substrates increased 33-fold compared to the control unfunctionalized hydrogel and 22-fold compared to the 5 mM scrambled peptide. On 10 mM RGD substrates, the HCEC number increased 49-fold compared to the control unfunctionalized hydrogel and 5-fold compared to the hydrogels functionalized with10 mM scrambled peptide. HCECs on 20 mM RGD substrates exhibited an extremely significant increase of 60-fold compared to the control unfunctionalized hydrogels and 120-fold increase compared with the 20 mM scrambled peptide (figure 2.3). These results demonstrate that our substrates are non-fouling and possess a controlled biochemistry that allows for specific RGD-integrin attachment.

To further test the specificity of the HCEC attachment to the RGD peptide, each of the three corneal cell-types was plated onto 5 mM RGD substrates, in the presence of media containing a range of concentrations of either soluble RGD or RDG peptides (0-1000 μM). HCECs cultured in media with the control soluble scrambled RDG peptide demonstrated no negative effect on the cells ability to adhere and a significant increase in the number of cells attached with respect to cells cultured in media with no peptide. However, cells cultured in soluble RGD peptide-containing media showed a competitive effect in cell binding to the substrate resulting in a decreased number of cells attached with increasing RGD concentration, and no cells attached when the concentration reached 1000 μM RGD (figure 2.4).

2.3.3 Increased RGD concentration influences the cell area of SV40-HCECs

In addition to initial cell attachment to the peptide-modified hydrogel substrates, we also investigated potential changes in cell spreading through quantification of the total projected cell area. After 120 h in culture, primary HCEC and hTCEpi cells demonstrated no significant difference in the projected area of cells cultured on substrates functionalized with our range of RGD concentrations. hTCEpi cells had an average area of 1690 μm^2 and primary HCECs had an average area of 1585 μm^2 (figure 2.5). However, SV40-HCECs cultured on 10 mM RGD and 20 mM RGD hydrogels showed a significant increase in cell area with respect to cells cultured on 5 mM RGD hydrogels ($P < 0.05$ and $P < 0.001$ respectively). SV40-HCECs averaged 431 μm^2 in the 5 mM RGD gels, 627 μm^2 in the 10 mM RGD gels and 736 μm^2 in the 20 mM RGD gels (figure 2.5).

2.3.4 HCEC proliferation showed no significant differences with a range of RGD concentrations.

We further investigated the impact of increasing RGD and control RDG concentration on the proliferation rate of HCEC's. In order to account for variations in plating efficiency due to the different RGD concentrations, cells were plated at the proper density to achieve an initial number of 8,000-18,000 cells/cm^2. Total cell counts were obtained at 24 and 120 hour time points. After 5 days in culture, results indicate no significant difference in proliferation rates between concentrations of RGD in the hydrogel (figure 2.6).

2.4 Discussion

In our investigation of specific effects on HCEC behavior from a particular ECM peptide, our first goal was the identification of a material that inhibits protein adsorption and allows for controlled interaction of HCEC cells with specific ligands. As mentioned previously, PEGDA hydrogels are resistant to protein adsorption; however, studies from Park, et. al.[27], Du, et. al.[28] and Nolan, et. al.[29] have indicated potential issues with non-specific binding of several different cell-types to low molecular weight PEGDA hydrogels. For this purpose, we investigated two different molecular weights of PEGDA hydrogels. Our results were in accord with these previous studies as all three corneal epithelial cell-types attached non-specifically to PEGDA MW 700, but not to PEGDA MW 3400. The non-specific cell attachment most likely occurs via the generation of multifunctional poly(acrylate) (PA) regions during cross-linking of the materials through free-radical polymerization[30,31]. In the formed hydrogels, the ratio of PA domains to PEG domains increases with decreasing molecular weight. PEGDA 700 has a PA:PEG ratio of 15%, while the PA:PEG ratio in PEGDA 3400 is 3%, thereby potentially increasing the level of non-specific binding for the low molecular weight PEGDA[31-33]. In summary, hydrogels made with low molecular weight of PEGDA were dismissed as feasible substrates because of their tendency to allow for non-specific interactions with HCECs. Interestingly, the immortalized SV40-HCEC line appeared to be the least affected by the absence of specific peptides and had a significant ability to bind to unfunctionalized PEGDA compared to the primary HCECs and hTCEpi cells. The SV40-HCEC line has been widely used as a model system for corneal epithelial cells and

the significant increase in cell attachment as compared to primary HCEC cells on PEGDA 700 indicate this cell line may not be an ideal model in which to study specific peptide interactions[34]. In summary, all three HCEC cell types plated onto PEGDA 3400 demonstrated little to no attachment and this molecular weight was selected as the hydrogel platform to incorporate our ECM peptide of interest, RGD for HCEC behavioral studies.

Although there are several alternative methods to tether ECM-like peptides to our hydrogel substrates, we have selected a conjugate addition reaction (Michael-type)[26]. Briefly, candidate peptides containing a thiol group trough a cysteine residue react with the acrylate groups present in the PEGDA precursor solution. We utilized this system specifically for its ability to incorporate biological molecules into acrylated polymers with rapid reaction times and no undesirable formation of by-products.

As a model to test the impact of biochemical cues presented by functionalized PEGDA hydrogels to corneal epithelial cells, we selected the adhesive peptide RGD. The RGD peptide sequence is present within many relevant ECM and basement membrane proteins including collagen, fibronectin and laminin[35], and is involved in binding to cell substrate adhesion receptors including integrins, such as $\alpha_5\beta_1$, $\alpha_V\beta_1$, $\alpha_V\beta_3$ and $\alpha_V\beta_5$[18]. RGD has been extensively shown to promote adhesion in various cells types, such as fibroblasts[36], endothelial cells[37], neutrophils[38] and corneal epithelial cells[39]. Several studies have demonstrated the role of the RGD-binding $\alpha_5\beta_1$ integrin in the homeostasis[40] and healing[41] of the corneal epithelium. Furthermore, it has been recently demonstrated that the functionalization of PEG-based hydrogels with RGD peptides

reduces the observed immune response *in vivo* compared with non-functionalized PEG when hydrogels were implanted subcutaneously in wild-type mice[42]. These reasons highlight the relevance of using RGD as an adhesive peptide for HCECs.

Results from our cell attachment studies demonstrate the direct correlation between the increased number of cells attached and the increased concentration of RGD peptide. While a small, but insignificant number of cells adhered to the unfunctionalized substrates, we observed that the number of cells attached to RGD-tethered hydrogels increased monotonically with increasing RGD concentration, demonstrating the ability of incorporating peptide into PEGDA hydrogels to control our substrates biochemically. Our study defined a concentration of RGD between 1 and 5 mM RGD where cell attachment increased greatly up to a threshold concentration of 10 mM, where the number of cells attached reaches a plateau for all the HCEC types studied. The attachment was solely mediated by the RGD sequence, as can be noted by the absence of significant attachment when scrambled peptide was used. The determined threshold concentration of peptide that promotes adhesion correlates well with other epithelial cell studies. In Mertz, et. al. a hyaluronic acid scaffold functionalized with 4 mg/mL (2 mM) of RGD induced faster epithelial outgrowth than control surfaces and surfaces with 2 mg/mL peptide (1 mM)[43]. In addition, Epithelial cells demonstrated enhanced spreading when the RGD density was increased from 0.01 mM to 1 mM on PEG hydrogels[44]. Although the cell affinity for RGD peptides is greatly increased by the use of cyclic RGD[45], the focus on this work was to test our ability to incorporate biochemical

molecules to topographic substrates, therefore a short sequence that has demonstrated specific HCEC attachment was used[46].

Our system also indicates the specific interaction of the HCEC cells with the RGD peptide through our soluble RGD studies which compete for cell adhesion binding sites and interfere with the ability of the cell to adhere. When cells were exposed to increased concentration of soluble RGD, we observed a decrease in the number of cells attached. In summary, we demonstrate HCEC attachment that is RGD peptide-specific and dependent on the concentration.

In the course of our studies, we observed no significant difference in cell area after 120 h in culture with the range of concentrations of peptide used in our hydrogel substrates for the primary HCEC and the hTCEpi cell line, suggesting that for those cell types the available number of surface signals on our substrates is greater than the number of cell receptors[47]. However, for the case of the SV40-HCEC type, a small but significant increase of projected cell area was observed with increasing RGD concentration, which, along with the increased number of attached cells to all surfaces, points out the different behavior for this immortalized cell type vs primary HCECs and hTCEpi cells.

We also investigated the impact of RGD functionalized PEGDA hydrogel substrates on the abilility of HCEC cells to proliferate. Upon first examination, proliferation was observed to be dependent on initial cell number, where cells with insufficient cell-cell interaction do not proliferate well[48]. Therefore, in order to get consistent proliferation measurements we selected surfaces where the initial cell density at 24 hours was between

8,000 and 20,000 per cm^2. Under those conditions, no significant difference between concentrations was observed. This observation is supported by studies such as Yang, et. al. where they observed that the concentration of RGD does not change the proliferation of bone marrow stromal cells[49], or Jacob, et. Al, where RGD tethered surfaces did not increase the proliferation of rabbit corneal epithelial cells[50]. However, some groups have reported differences in proliferation with RGD concentration, suggesting this behavior is cell-type dependent. Smooth muscle cells show a negative correlation of proliferation with RGD concentration[51], human dermal fibroblasts show a positive correlation[48], and pre-osteoblasts show a maximum proliferation at intermediate RGD concentration[52]. Lee, et. al. investigated the influence of RGD on osteoblasts, and concluded that proliferation is more dependent on the clustering of RGD than the overall RGD concentration[53].

In summary, we achieved the fabrication of non-fouling materials that can be incorporated with specific biochemical motifs to promote HCEC attachment. These materials can provide controlled biochemical cues to HCECs to form an epithelial layer and improve corneal prosthetics, and can be used to investigate the behavior of cells. Other peptides found in fibronectin or laminin can be incorporated to promote the binding and signaling of other receptors, such as syndecans or the $\alpha_6\beta_4$ integrin, which have been established as key components in the corneal epithelium wound healing[54,55]. Furthermore, for future studies, we can incorporate physical cues, such as topography, onto UV-polymerizable hydrogels using techniques as soft lithography[56], colloidal lithography[57] or photolithography[58].

2.5 Conclusions

In order to investigate the biochemical effects of ECM cues on the adherence of HCECs, we fabricated non-fouling substrates made of PEGDA hydrogels and functionalize them with variable amounts of the adhesive peptide RGD. Our results indicate that the number of HCECs adhered on our substrates increased in a dose-dependent manner with increasing concentration of RGD. The lack of attachment on substrates functionalized with scrambled RDG peptide and on substrates where the media was supplemented with soluble RGD indicates that the adhesion is specific to certain integrin receptors. In this study we also investigated the proliferation of HCECs on such substrates, and we observed that proliferation is independent of RGD concentration. These results will aid in the design of materials for the fabrication of artificial corneas, by allowing the biochemical control of the epithelial cell behavior trough specific cell receptors.

2.6 Figures

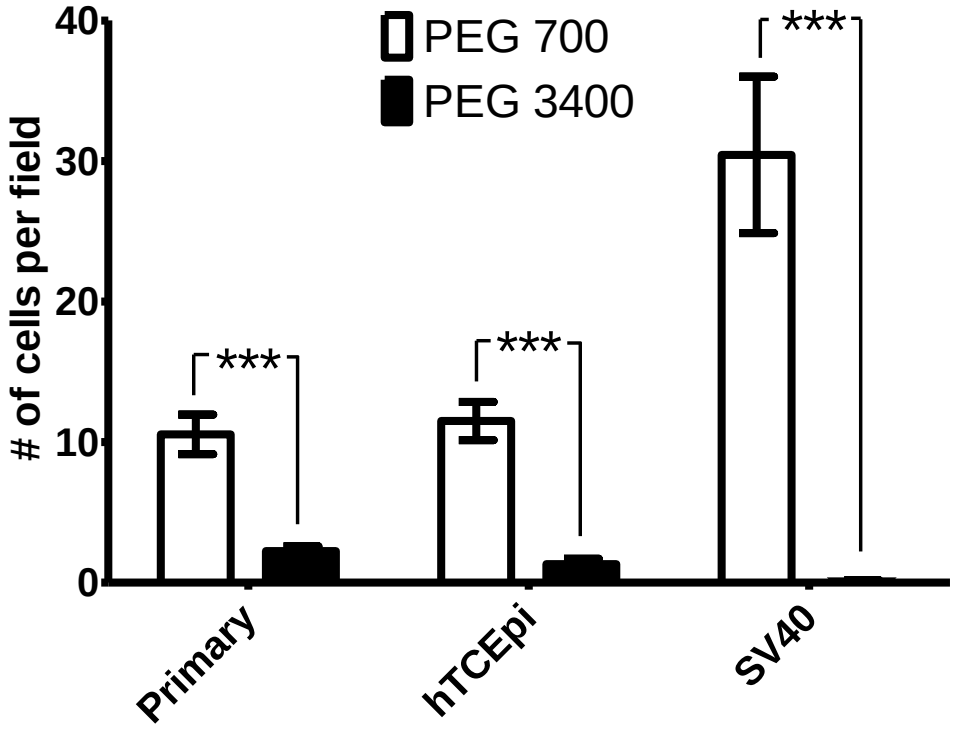

Figure 2.1.- Inhibition of cell attachment is molecular weight dependent.

Hydrogels made with PEGDA MW 700 precursor allowed non-specific cell binding and attachment, whereas hydrogels made with PEGDA MW 3400 showed no significant cell attachment in all cell-types tested. Results demonstrated a 4.7-fold difference in primary cells, a 8.7-fold difference in hTCEpi and a 365-fold difference in SV40 ($P < 0.001$).

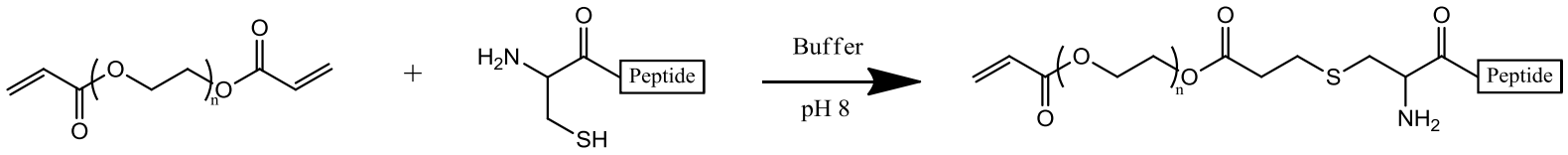

Scheme 2.1.- Michael-type addition reaction between a cysteine-containing peptide and PEGDA

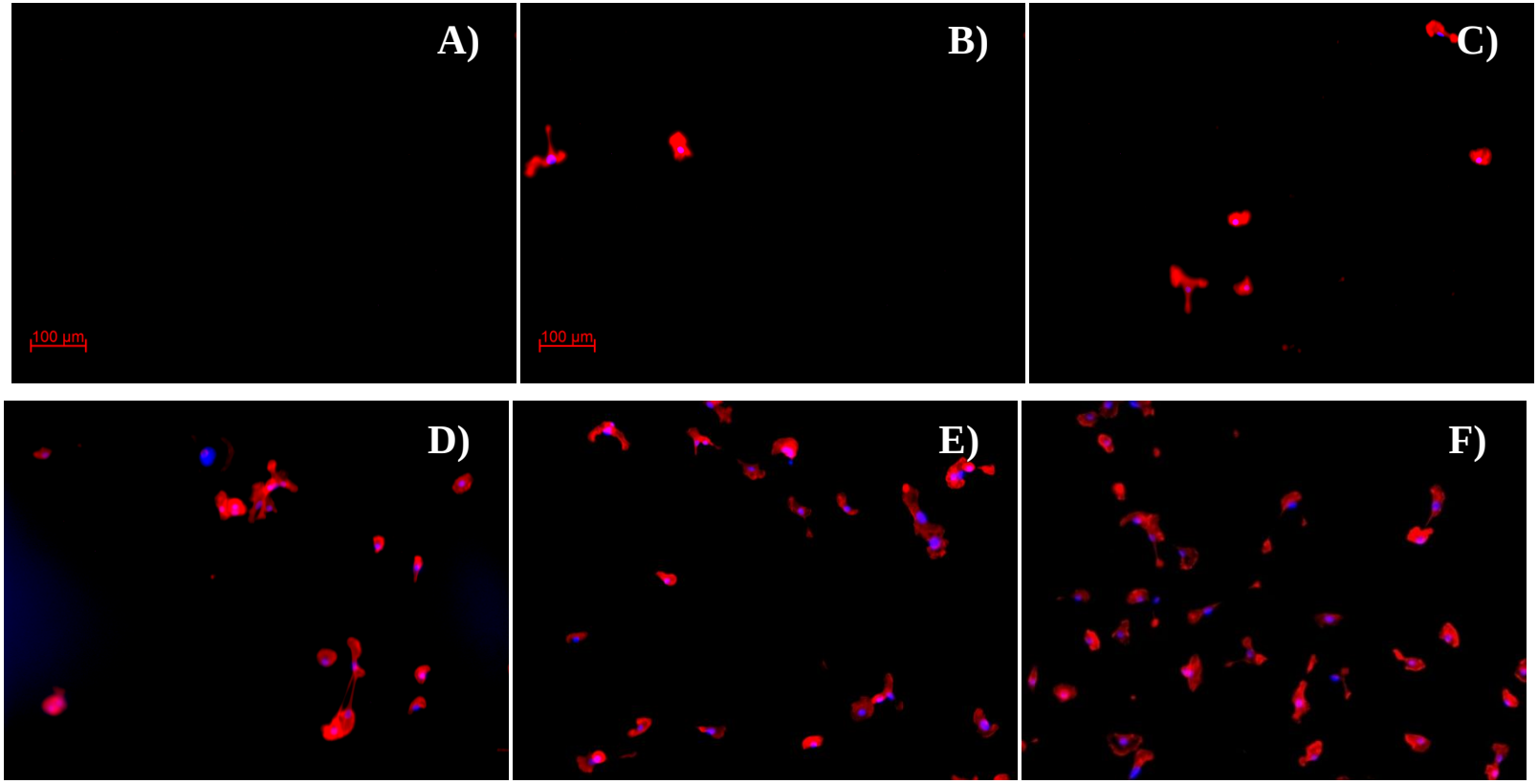

Figure 2.2.- Increasing levels of RGD peptide promote cell attachment on PEGDA MW 3400 hydrogels.

Cells were plated for 24 hours, followed by fixation, staining and analysis of cell attachment. Red: TRITC-Phalloidine. Blue: DAPI. A) Unfunctionalized PEG hydrogel. B) PEG hydrogel functionalized with 1 mM RGD. C) PEG hydrogel functionalized with 5 mM RGD. D) PEG hydrogel functionalized with 10 mM RGD. E) PEG hydrogel functionalized with 20 mM RGD. F) TCPS.

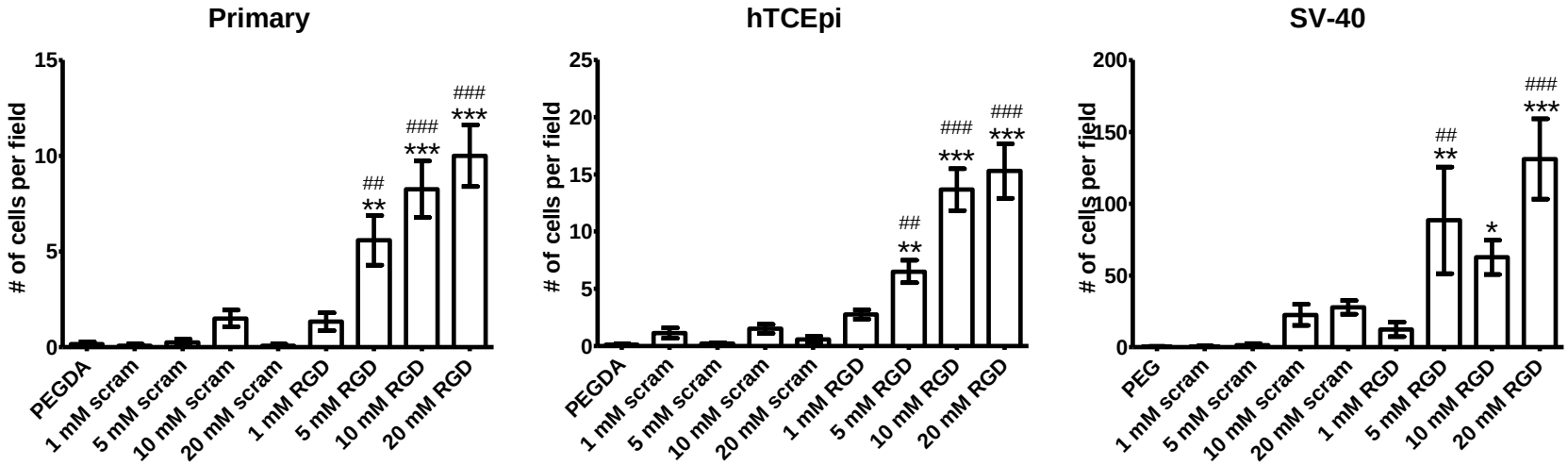

Figure 2.3.- Cell attachment is RGD concentration dependent.

Non-functionalized PEGDA MW 3400 hydrogels and hydrogels prepared with scrambled peptide *RDG* showed no non-specific binding for all cell types studied. Hydrogels functionalized with increasing RGD concentration show increasing number of cells attached in 24-hour adhesion assay.

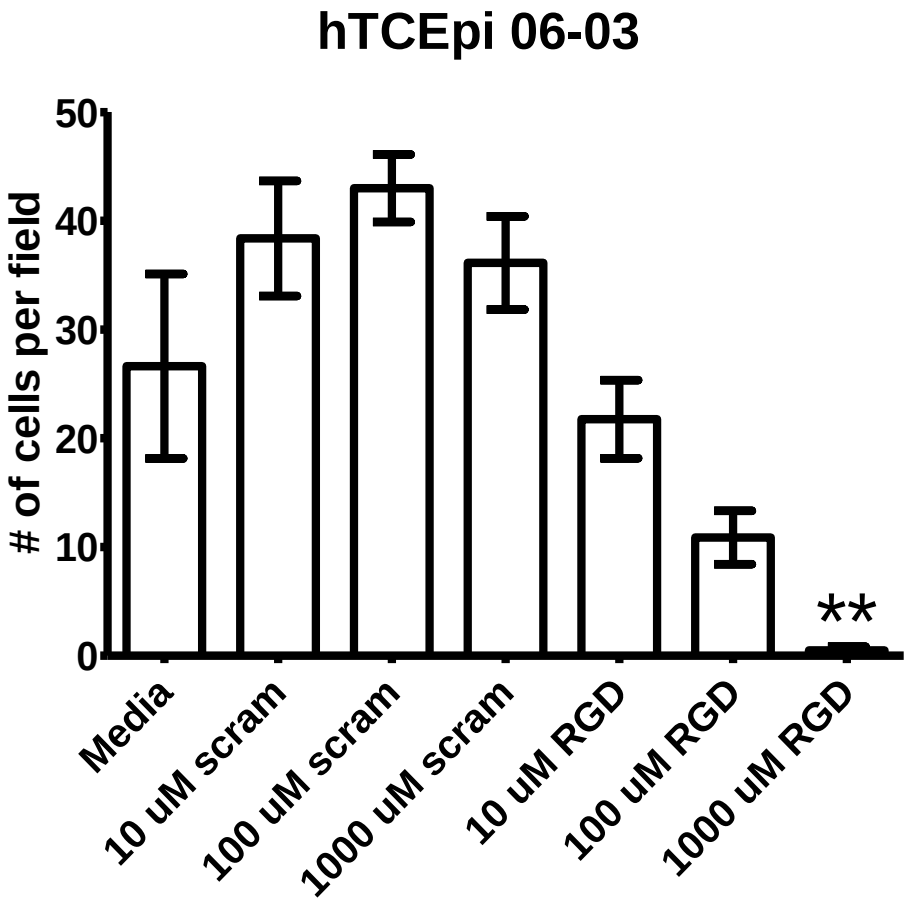

Figure 2.4.- Soluble RGD assay demonstrates specificity of RGD-cell interaction. hTCEpi cultured on PEGDA MW 3400 hydrogels, functionalized with 10 mM RGD showed normal attachment when cultured on media supplemented with soluble scrambled RDG peptide. A significant decrease in the number of cells attached was observed in the 1000 μM RGD concentration compared to media with no soluble RGD. Error Bars: SEM. (**= $0.001 < P < 0.01$)

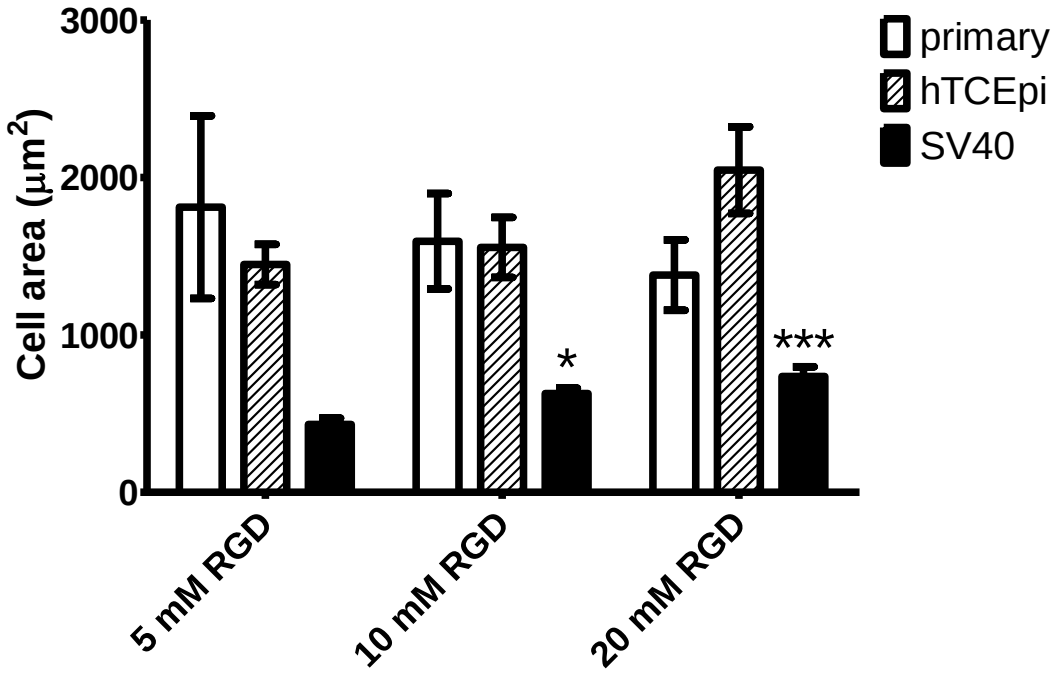

Figure 2.5.- On day 5, SV40 cells plated on hydrogels with increasing RGD concentration showed significant increase of projected cell area,

where cells cultured on 5 mM RGD gels had an average area of 431 μm^2, cells cultured on 10 mM RGD gels had an average area of 627 μm^2 and cells cultured on 20 mM RGD gels had an average area of 736 μm^2. hTCEpi and primary hCEC had no significant difference in projected area, where hTCEpi cells had an average area of 1690 μm^2 and primary cells had an average area of 1585 μm^2 (*= $0.01 < P < 0.05$, ***= $P < 0.001$)

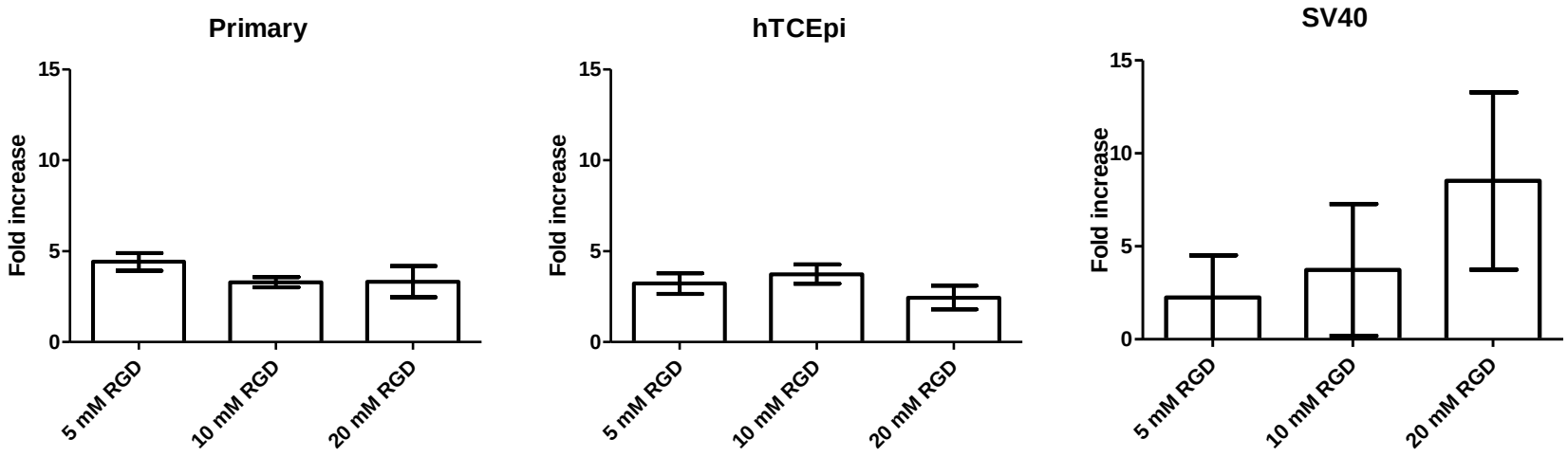

Figure 2.6.- Cell proliferation as fold increase.

Not significant differences of proliferation due to concentration were observed for any cell type, although SV40-HCECs showed a higher proliferative state than primary-HCECs or hTCEpi cell type.

2.7 References

1. Lutolf MP, Hubbell JA. Synthetic biomaterials as instructive extracellular microenvironments for morphogenesis in tissue engineering. Nature biotechnology 2005;23(1):47-55.

2. Flemming RG, Murphy CJ, Abrams GA, Goodman SL, Nealey PF. Effects of synthetic micro-and nano-structured surfaces on cell behavior. Biomaterials 1999;20(6):573-588.

3. Halstenberg S, Panitch A, Rizzi S, Hall H, Hubbell JA. Biologically engineered protein-graft-poly (ethylene glycol) hydrogels: a cell adhesive and plasmin-degradable biosynthetic material for tissue repair. Biomacromolecules 2002;3(4):710-723.

4. DeLong SA, Moon JJ, West JL. Covalently immobilized gradients of bFGF on hydrogel scaffolds for directed cell migration. Biomaterials 2005;26(16):3227-3234.

5. Chen CS, Tan J, Tien J. Mechanotransduction at cell-matrix and cell-cell contacts. Annu. Rev. Biomed. Eng. 2004;6:275-302.

6. Discher DE, Janmey P, Wang Y. Tissue cells feel and respond to the stiffness of their substrate. Science 2005;310(5751):1139.

7. Teixeira AI, McKie GA, Foley JD, Bertics PJ, Nealey PF, Murphy CJ. The effect of environmental factors on the response of human corneal epithelial cells to nanoscale substrate topography. Biomaterials 2006;27(21):3945-3954.

8. Chen CS, Mrksich M, Huang S, Whitesides GM, Ingber DE. Geometric control of cell life and death. Science 1997;276(5317):1425.

9. Hicks CR, Fitton JH, Chirila TV, Crawford GJ, Constable IJ. Keratoprostheses: advancing toward a true artificial cornea. Survey of ophthalmology 1997;42(2):175-189.

10. Flemming RG, Murphy CJ, Abrams GA, Goodman SL, Nealey PF. Effects of synthetic micro- and nano-structured surfaces on cell behavior. Biomaterials 1999;20(6):573-588.

11. Leckband D, Sheth S, Halperin A. Grafted poly (ethylene oxide) brushes as nonfouling surface coatings. Journal of Biomaterials Science, Polymer Edition 1999;10(10):1125-1147.

12. Mann BK, Gobin AS, Tsai AT, Schmedlen RH, West JL. Smooth muscle cell growth in photopolymerized hydrogels with cell adhesive and proteolytically degradable domains: synthetic ECM analogs for tissue engineering. Biomaterials 2001;22(22):3045-3051.

13. Lee KY, Mooney DJ. Hydrogels for tissue engineering. Chem. Rev 2001;101(7):1869-1880.

14. Drury JL, Mooney DJ. Hydrogels for tissue engineering: scaffold design variables and applications. Biomaterials 2003;24(24):4337-4351.

15. Hahn MS, Taite LJ, Moon JJ, Rowland MC, Ruffino KA, West JL. Photolithographic patterning of polyethylene glycol hydrogels. Biomaterials 2006;27(12):2519-2524.

16. Perlin L, MacNeil S, Rimmer S. Production and performance of biomaterials containing RGD peptides. Soft Matter 2008;4(12):2331-2349.

17. Metters AT, Anseth KS, Bowman CN. Fundamental studies of a novel, biodegradable PEG-b-PLA hydrogel. Polymer 2000;41(11):3993-4004.

18. Ruoslahti E. RGD and other recognition sequences for integrins. Annual review of cell and developmental biology 1996;12(1):697-715.

19. Teixeira AI, Abrams GA, Bertics PJ, Murphy CJ, Nealey PF. Epithelial contact guidance on well-defined micro- and nanostructured substrates. Journal of Cell Science 2003;116(Pt 10):1881-1892.

20. Allen-Hoffmann BL, Rheinwald JG. Polycyclic aromatic hydrocarbon mutagenesis of human epidermal keratinocytes in culture. Proceedings of the National Academy of Sciences of the United States of America 1984;81:7802-7806.

21. Sabatini LM, Allen-Hoffmann BL, Warner TF, Azen EA. Serial Cultivation of Epithelial Cells from Human and Macaque Salivary Glands. In Vitro Cellular & Developmental Biology 1991;27A(12):939-948.

22. Robertson DM, Li L, Fisher S, Pearce VP, Shay JW, Wright WE, Cavanagh HD, Jester JV. Characterization of growth and differentiation in a telomerase-immortalized human corneal epithelial cell line. Investigative ophthalmology & visual science 2005;46(2):470.

23. Araki-Sasaki K, Ohashi Y, Sasabe T, Hayashi K, Watanabe H, Tano Y, Handa H. An SV40-immortalized human corneal epithelial cell line and its characterization. Investigative ophthalmology & visual science 1995;36(3):614.

24. Liliensiek SJ, Campbell S, Nealey PF, Murphy CJ. The scale of substratum topographic features modulates proliferation of corneal epithelial cells and corneal fibroblasts. Journal of Biomedical Materials Research Part A 2006;79(1):185-192.

25. Tocce EJ, Smirnov VK, Kibalov DS, Liliensiek SJ, Murphy CJ, Nealey PF. The ability of corneal epithelial cells to recognize high aspect ratio nanostructures. Biomaterials 2010;31(14):4064-4072.

26. Elbert DL, Hubbell JA. Conjugate addition reactions combined with free-radical cross-linking for the design of materials for tissue engineering. Biomacromolecules 2001;2(2):430-441.

27. Park JH, Bae YH. Hydrogels based on poly (ethylene oxide) and poly (tetramethylene oxide) or poly (dimethyl siloxane): synthesis, characterization, in vitro protein adsorption and platelet adhesion. Biomaterials 2002;23(8):1797-1808.

28. Du H, Chandaroy P, Hui SW. Grafted poly-(ethylene glycol) on lipid surfaces inhibits protein adsorption and cell adhesion. Biochimica et Biophysica Acta (BBA)-Biomembranes 1997;1326(2):236-248.

29. Nolan CM, Reyes CD, Debord JD, García AJ, Lyon LA. Phase transition behavior, protein adsorption, and cell adhesion resistance of poly (ethylene glycol) cross-linked microgel particles. Biomacromolecules 2005;6(4):2032-2039.

30. Lin-Gibson S, Jones RL, Washburn NR, Horkay F. Structure- Property Relationships of Photopolymerizable Poly (ethylene glycol) Dimethacrylate Hydrogels. Macromolecules 2005;38(7):2897-2902.

31. Beamish JA, Zhu J, Kottke-Marchant K, Marchant RE. The effects of monoacrylated poly (ethylene glycol) on the properties of poly (ethylene glycol) diacrylate hydrogels used for tissue engineering. Journal of Biomedical Materials Research Part A;92(2):441-450.

32. Kingshott P, Thissen H, Griesser HJ. Effects of cloud-point grafting, chain length, and density of PEG layers on competitive adsorption of ocular proteins. Biomaterials 2002;23(9):2043-2056.

33. Gombotz WR, Guanghui W, Horbett TA, Hoffman AS. Protein adsorption to poly (ethylene oxide) surfaces. Journal of biomedical materials research 1991;25(12):1547-1562.

34. Castro-Muñozledo F. Corneal epithelial cell cultures as a tool for research, drug screening and testing. Experimental eye research 2008;86(3):459-469.

35. Tuori A, Uusitalo H, Burgeson RE, Terttunen J, Virtanen I. The immunohistochemical composition of the human corneal basement membrane. Cornea 1996;15(3):286.

36. Hern DL, Hubbell JA. Incorporation of adhesion peptides into nonadhesive hydrogels useful for tissue resurfacing. Journal of Biomedical Materials Research Part A 1998;39(2):266-276.

37. Fittkau MH, Zilla P, Bezuidenhout D, Lutolf MP, Human P, Hubbell JA, Davies N. The selective modulation of endothelial cell mobility on RGD peptide containing surfaces by YIGSR peptides. Biomaterials 2005;26(2):167-174.

38. Gonzalez AL, Gobin AS, West JL, McIntire LV, Smith CW. Integrin interactions with immobilized peptides in polyethylene glycol diacrylate hydrogels. Tissue engineering 2004;10(11-12):1775-1786.

39. Kobayashi H, Ikacia Y. Corneal cell adhesion and proliferation on hydrogel sheets bound with cell-adhesive proteins. Current eye research 1991;10(10):899-908.

40. Lauweryns B vdOJ, Volpes R, Foets B, Missotten, L. Distribution of very late activation integrins in the human cornea. Investigative ophthalmology & visual science 1991;32:2079-2085.

41. Jain S, Azar DT. Extracellular matrix and growth factors in corneal wound healing. Current Opinion in Ophthalmology 1994;5(4):3.

42. Lynn AD, Kyriakides TR, Bryant SJ. Characterization of the in vitro macrophage response and in vivo host response to poly (ethylene glycol)-based hydrogels. Journal of Biomedical Materials Research Part A 2009;93(3):941-953.

43. Mertz PM, Davis SC, Franzen L, Uchima FD, Pickett MP, Pierschbacher MD, Polarek JW. Effects of an arginine-glycine-aspartic acid peptide-containing artificial matrix on epithelial migration in vitro and experimental second-degree burn wound healing in vivo. Journal of Burn Care & Research 1996;17(3):199.

44. Chung IM, Enemchukwu NO, Khaja SD, Murthy N, Mantalaris A, García AJ. Bioadhesive hydrogel microenvironments to modulate epithelial morphogenesis. Biomaterials 2008;29(17):2637-2645.

45. Von Der Mark K, Park J, Bauer S, Schmuki P. Nanoscale engineering of biomimetic surfaces: cues from the extracellular matrix. Cell and tissue research;339(1):131-153.

46. Wilson M, Liliensiek, SJ., Murphy, CJ., Murphy, WL., Nealey, PF. Hydrogels with well-defined peptide-hydrogel spacing and concentration: impact on epithelial cell behavior. Soft Matter 2012;8(2):390-398.

47. VandeVondele S, Vörös J, Hubbell JA. RGD grafted poly l lysine graft (polyethylene glycol) copolymers block non specific protein adsorption while promoting cell adhesion. Biotechnology and bioengineering 2003;82(7):784-790.

48. Liu SQ, Rachel Ee PL, Ke CY, Hedrick JL, Yang YY. Biodegradable poly (ethylene glycol)-peptide hydrogels with well-defined structure and properties for cell delivery. Biomaterials 2009;30(8):1453-1461.

49. Yang F, Williams CG, Wang D, Lee H, Manson PN, Elisseeff J. The effect of incorporating RGD adhesive peptide in polyethylene glycol diacrylate hydrogel on osteogenesis of bone marrow stromal cells. Biomaterials 2005;26(30):5991-5998.

50. Jacob JT, Rochefort JR, Bi J, Gebhardt BM. Corneal epithelial cell growth over tethered protein/peptide surface modified hydrogels. Journal of Biomedical Materials Research Part B: Applied Biomaterials 2005;72B(1):198-205.

51. Mann BK, West JL. Cell adhesion peptides alter smooth muscle cell adhesion, proliferation, migration, and matrix protein synthesis on modified surfaces and in polymer scaffolds. Journal of biomedical materials research 2002;60(1):86-93.

52. Comisar WA, Kazmers NH, Mooney DJ, Linderman JJ. Engineering RGD nanopatterned hydrogels to control preosteoblast behavior: a combined computational and experimental approach. Biomaterials 2007;28(30):4409-4417.

53. Lee KY, Alsberg E, Hsiong S, Comisar W, Linderman J, Ziff R, Mooney D. Nanoscale adhesion ligand organization regulates osteoblast proliferation and differentiation. Nano Letters 2004;4(8):1501-1506.

54. Stepp MA, Gibson HE, Gala PH, StaIglesia DD, Pajoohesh-Ganji A, Pal-Ghosh S, Brown M, Aquino C, Schwartz AM, Goldberger O. Defects in keratinocyte activation during wound healing in the syndecan-1-deficient mouse. Journal of cell science 2002;115(23):4517-4532.

55. Jones JCR. The 3 laminin subunit, 6 4 and 3 1 integrin coordinately regulate wound healing in cultured epithelial cells and in the skin. Journal of Cell Science 1999;112:2615-2629.

56. Suh KY, Seong J, Khademhosseini A, Laibinis PE, Langer R. A simple soft lithographic route to fabrication of poly (ethylene glycol) microstructures for protein and cell patterning. Biomaterials 2004;25(3):557-563.

57. Stachowiak AN, Bershteyn A, Tzatzalos E, Irvine DJ. Bioactive hydrogels with an ordered cellular structure combine interconnected macroporosity and robust mechanical properties. Advanced Materials 2005;17(4):399-403.

58. Revzin A, Russell RJ, Yadavalli VK, Koh WG, Deister C, Hile DD, Mellott MB, Pishko MV. Fabrication of poly (ethylene glycol) hydrogel microstructures using photolithography. Langmuir 2001;17(18):5440-5447.

CHAPTER 3: BIOCHEMICALLY AND TOPOGRAPHICALLY ENGINEERED POLY(ETHYLENE GLYCOL) DIACRYLATE HYDROGELS WITH BIOMIMETIC CHARACTERISTICS AS SUBSTRATES FOR HUMAN CORNEAL EPITHELIAL CELLS.

3.1 Introduction

Transplantation with human donor corneal grafts is the primary treatment for the majority of corneal disorders that cause visual impairment[1]. However, demand for grafts far exceeds the amount of donor tissue available and the success rate of corneal transplantation with human donor tissue is reduced in patients with certain pathologies[2], emphasizing the need for artificial prostheses[3]. We hypothesize that the incorporation of both biochemical (molecules interacting with the cell) and biophysical (topography and compliance) cues[4] derived from the corneal basement membrane (BM), into the surface of artificial corneas may promote human corneal epithelial cell (HCEC) behaviors that support re-epithelialization and tissue regeneration, minimizing complications such as extrusion, infection and epithelial down-growth[2,5] of current corneal prostheses.

Previous research from our laboratory has quantified the topography of the corneal BM[6], and demonstrated that the scale of the topography modulates adhesion[7], contact guidance[8,9], migration[10] and proliferation[11] in HCECs. In addition, HCECs cultured in serum-free media exhibited alterations in the response to topographic cues when the features transitioned between the nano and micron scale, such as cells aligning parallel to microscale ridges, but perpendicular to nanoscale ridges[8,12-14]. These results demonstrate that topographic cues of relevant nano and submicron size should be considered and incorporated in the design criterion for a synthetic BM, and suggest the synergistic

influence of several factors including topographic cues, the adsorbed protein layer, and soluble factors. However, the nonspecific adsorption of proteins on the rigid substrates utilized in these experiments precludes specific knowledge of the surface chemistry, thereby complicating the potential isolation of the specific cell substrate receptors involved in the response to biophysical cues and the identification of downstream signaling pathways responsible for the differential cell behaviors observed. A major objective of our study is the development of soft substrates with controlled surface chemistry that allow for the inhibition of non-specific protein adsorption, the provision of well-defined cell-substrate adhesion motifs, and the simulation of the *in vivo* range of topography[15].

Poly(ethylene glycol) (PEG) hydrogels are excellent candidates as biomaterials because of their potential for incorporating both biophysical and biochemical cues and their prevention of non-specific protein adsorption, biocompatibility and FDA approval for use in humans[16,17]. PEG hydrogels can be synthesized using a variety of established methods that allow for integration of ligands[18] or co-polymerization with biodegradable materials[19,20]. In addition, topographic micron-scale features have been incorporated into UV-polymerizable hydrogels using soft lithography[21] and photolithography[22].

The adhesive peptide RGD (Arg-Gly-Asp) was used as the bioactive ligand to be incorporated into PEG hydrogels. This sequence constitutes an important ligand for the $\alpha_5\beta_1$ integrin[23], which is a relevant receptor for the corneal epithelial cell adhesion to the BM[24] and the wound healing of the corneal epithelium[25-27]. This supports the use of

RGD as a peptide to elicit specific adhesion responses in HCECs and decouple the influence of surface biochemistry and topography on HCEC response.

Herein, we report the fabrication of PEGDA substrates that allow for the simultaneous presentation of uniform biochemistry and biotopography to HCECs. The purpose is to investigate whether the scale of topography on substrates with controlled mechanisms of cell attachment differentially modulates cell behavior in the presence or absence of other cues, including external soluble factors from the media. The results from this study are important to our understanding of HCEC behavior in the presence of multiple cues and will aid in the development of more biologically and clinically relevant materials and systems.

3.2 Materials and methods

3.2.1 Synthesis of PEG diacrylate (PEGDA)

PEGDA pre-polymers of molecular weight 3400 g/mol (PEGDA 3400) and 8000 g/mol (PEGDA 8000) were synthesized according to previously published methods[28]. Briefly, PEGDA was synthesized by combining 3 grams of vacuum-dried OH-terminated PEG (Hampton Research, NJ) into 50 mL of anhydrous toluene (Acros Organics, NJ) with 2X molar excess acryloyl chloride (Sigma-Aldrich, MD) and 2X molar excess triethylamine (Sigma-Aldrich, NJ) with respect to the oligomer end-groups. The mixture was incubated for four hours at 70° C in nitrogen. The resulting insoluble triethlyamine salts in the solution were filtered and the PEGDA was precipitated in cold diethyl ether

and dried for 48 hours. PEGDA was dialyzed using dialysis tubing for four hours with three changes of Milli-Q H_2O (Millipore). The lyophilized product was verified with ^1H NMR spectrometry using a Bruker AC-300 instrument and matrix-assisted laser desorption/ ionization time-of-flight (MALDI-TOF) mass spectrometry with a Bruker Reflex II instrument.

3.2.2 Measurement of the swelling ratio in unbound PEGDA hydrogels

Precursor solutions of various mass fractions (Table 3.I) were prepared by dissolving either PEGDA 8000, PEGDA 3400 or PEGDA of molecular weight 700 g/mol (PEGDA 700) (Sigma-Aldrich, Japan) in 10 mM 4-(2-hydroxyethyl)-1-piperazineethanesulfonic acid (HEPES) buffer at pH 8.0. 0.067% mass concentration (w/v) of Lithium phenyl-2,4,6-trimethylbenzoylphosphinate (LAP) was used as the photoinitiator. A 30 μL drop of the precursor solution was placed on top of a degassed poly(dimethyl siloxane) (PDMS, Sylgard® 184, Dow Corning, MI) surface using a 1 mm spacer in nitrogen atmosphere. The precursor solution was then covered with another PDMS surface. The hydrogels were polymerized under long wavelength UV light (364 nm for 900 s at 7.0 mW/cm^2) and their weight was measured immediately (W_R, relaxed gel weight). Gels were then soaked in DI water for 72 hour and their equilibrium swollen weight (W_s) was measured after removing excess water by carefully wicking with a spatula. Gels were frozen and lyophilized and their dry weight was measured (W_D). The relaxed swelling ratio (Q_R) (volume of swollen gel/volume of relaxed gel) was approximated as

$Q_R=[W_S\rho_{pol}+W_D(\rho_w-\rho_{pol})]/[W_R\rho_{pol}+W_D(\rho_w-\rho_{pol})]$; where ρ_{pol} is the density of PEG (1.1192 g/mL) and ρ_w is the density of water (0.9982 g/mL) at 20° C.

3.2.3 Synthesis of ECM peptides

RGD peptide (Cys-Gly-Gly-Arg-Gly-Asp-Ser-Pro) synthesis was conducted in solid phase on Fmoc-Rink Amide MBHA resin with Fmoc-protected α-amino groups using a peptide synthesizer (CS Bio, Menlo Park, CA). To protect the Arg side chain, 2,2,5,7,8-pentamethyl-chroman-6-sulfonyl was used. The resulting peptide molecules were cleaved from the resin for four hours using a solution of TFA:TIS:water (95:2.5:2.5), filtered and precipitated in diethyl ether. Each batch was analyzed by matrix-assisted laser desorption/ionization time of flight (MALDI-TOF) mass spectrometry (Bruker Reflex II time-of-flight mass spectrometer) and used without further purification.

3.2.4 Fabrication of substrates with topographic features

Precursor solutions of 20% (w/w) PEGDA were prepared by dissolving PEGDA 8000, PEGDA 3400 or PEGDA 700 in 10 mM HEPES buffer at pH 8.0. LAP with a concentration of 0.067% (w/v) was used as the photoinitiator. RGD peptide was added to the precursor solutions to reach a final concentrations of 10 mM. Topography was incorporated into the hydrogel substrates using a replica-molding technique (Figure 3.1)[29]. In a nitrogen atmosphere, a 30μL drop of the precursor solution was placed on top of a degassed PDMS stamp containing the desired topography with 0.5 mm PDMS spacers. The precursor solution was then covered by a glass coverslip previously treated

with 3-(trichlorosilyl) propyl methacrylate (TPM, Sigma-Aldrich, UK) to ensure adhesion of the gels to the surface. The construct was polymerized under UV-light (364 nm for 900 s at 7.0 mW/cm^2) and the PDMS stamps were peeled off, transferring the pattern to the surface of the hydrogel. Hydrogel substrates were sterilized for 24 hours by soaking in 5% isopropyl alcohol (IPA) in 1X phosphate buffered saline (PBS, pH 7.2), rinsed for 24 hours in 1X PBS and pre-incubated for two hours in the appropriate cell culture media for full equilibration.

For control substrates allowing non-specific protein adsorption, we molded a photocrosslinkable mercapto-ester, Norland Optical Adhesive 81 (NOA-81, Norland Products Inc, NJ) as described previously[11]. The substrates were sterilized for 24 hours in 5% IPA in 1X PBS (pH 7.2), rinsed for 24 hours in 1X PBS and pre-incubated for two hours in the appropriate cell culture media.

3.2.5 AFM imaging of molded hydrogels

Molded hydrogels containing topographic features were imaged by atomic force microscopy (AFM), using a Nanoscope IIIa Multimode scanning probe microscope (Veeco Instruments Inc., CA). After hydration in PBS for at least 48 h at room temperature, samples were scanned in a fluid cell in contact mode using a SNL-10 silicon nitride cantilever with a silicon tip (Veeco Probes, CA).

3.2.6 HCEC culture

HCECs were harvested from human cadaver corneas graciously provided by the Lions Eye Bank of Wisconsin, Madison or the Missouri Lions Eye Bank (Columbia, MO) as previously reported[8]. Cells from two to four corneas were centrifuged and re-suspended in either epithelial medium (EP medium)[30,31] or in Epilife® medium (Invitrogen, CA) with a proprietary growth supplement (Epilife® Defined Growth Supplement)[12]. All HCECs were incubated at 37 °C and 5% CO_2 until they reached approximately 70% confluence. HCECs were used between passages 1 and 4.

3.2.7 Immunocytochemistry

Cells were stained for actin-filaments and the nucleus for the measurement of cell number as previously described[14]. Briefly, following incubation, cells were fixed with a 1% paraformaldehyde solution in PBS (Electron Microscopy Sciences, PA) at room temperature for 20 minutes. Cells were then permeabilized with 0.1% (w/v) Triton X-100 (Sigma–Aldrich, MO) in 1X PBS for 7 minutes, and then exposed to 1% (w/v) bovine serum albumin (Sigma–Aldrich, MO) in 1X PBS for 20 min to block non-specific binding. Cells were then incubated with 5 μg/mL of TRITC–phalloidin (Sigma–Aldrich, MO) containing 0.1 μg/mL 4’,6-Diamidino-2- phenylindole (DAPI) (Invitrogen, CA) in 1X PBS for 40 minutes, to label both filamentous actin (red), and the nucleus (blue).

3.2.8 Analysis of cell elongation and alignment

Each experimental set consisted of groups encompassing three types of substrates: substrates made with 10 mM RGD-hydrogel, substrates made with 10 mM scrambled RDG-hydrogel as a negative control, and substrates made with NOA-81 as a fouling control. Each group contained 3-5 samples. The substrates were molded with topographic features containing six separate areas with different ridge/groove widths (400, 800, 1200, 1600, 2000, 4000 nm pitch) and intervening planar control areas[13]. HCECs were plated at a density of 10,000 cells/cm^2 in either EP medium or Epilife®, cultured for 24 hours, fixed and stained. Images of fluorescently labelled cells on each substrate were obtained using a 10X objective lens. On each topographic substrate at least four images were taken of each pitch size and flat control areas present between patterned areas. Image analysis was performed using AxioVision software (Zeiss, NY). The cell elongation and angle of alignment were collected from the images and sorted using parameters previously described by our group[8,32]. Cells were deemed elongated with elongation factors greater than 1.3 and calculated as previously described.[9], A cell was considered aligned parallel if the angle was less than 10° and perpendicular if the angle was between 80° and 90°. Results represent the arithmetic mean percentage of the aligned cells with respect to the total population. Each experiment was repeated in triplicate.

3.2.9 Statistics

Experimental data were analyzed using analysis of variance (ANOVA). When variability was determined to be significant (α=0.05) the Bonferroni multiple comparison test was used to determine significance between flat surfaces and topographic surfaces. Significant results were further divided into "statistically significant" ($0.01 \leq P \leq 0.05$, *), "very significant" ($0.001 \leq P < 0.01$, **), and "extremely significant" ($P < 0.001$, ***).

3.3 Results

3.3.1 Hydrogels synthesized with 20% (w/w) PEGDA 3400 prevent non-specific cell adhesion and retain nanoscale topography.

Hydrogels were synthesized through the free radical polymerization of PEGDA using photoinitiators (Scheme 3.1). The general technique used to mold topographic features into PEGDA hydrogels is depicted in Figure 3.1. A PDMS substrate containing the topography (Figure 3.1A) is covered with a spacer and a drop of the precursor solution is placed on top (Figure 3.1B). The precursor solution is covered with a glass coverslip previously treated with TPM to ensure attachment of the gel to the glass surface (Figure 3.1C). The hydrogel is UV-photopolymerized and the PDMS stamp is removed (Figure 3.1D). The hydrogel is then soaked in the proper media (Figure 3.1F).

To evaluate the ability of the hydrogels to incorporate topographic features after swelling, we first characterized the swelling behavior of hydrogels as a function of molecular weight and concentration, using different precursor solutions (Table 3.I). Free

floating hydrogels were synthesized, using the technique depicted in Figure 3.1. The glass coverslip was substituted with a flat PDMS surface to ensure detachment of the hydrogels. These unbound hydrogels were immediately weighed, soaked in distilled water until equilibration, and subsequently weighed in the fully swollen state. The relaxed swelling ratio (Q_R), defined as the ratio of the volume at equilibrium swelling to the volume at the relaxed state (after crosslinking, but before swelling), was calculated as described in the methods section. Figure 3.2A shows Q_R as a function of the concentration and molecular weight of precursors. Hydrogels synthesized using PEGDA 8000 exhibited the highest Q_R, ranging from 1.6 in P-8000/10 to 2.4 in P-8000/25. Hydrogels made with PEGDA 3400 had a Q_R ranging from 1 in P-3400/10 to 1.4 in P-3400/25. PEGDA 700 hydrogels demonstrated low levels of swelling over the range of concentrations tested. In summary: 1) swelling increased monotonically with increasing molecular weight of PEGDA, and 2) swelling increased with increasing concentration of the pre-polymer in the mixture.

To test the retention of topographic features after equilibrium swelling, hydrogels containing 4000 nm pitch groove-and-ridges topography were synthesized following the general technique shown in Figure 1. In spite of the low level of swelling obtained with low polymer concentrations, hydrogels made with less than 20% (w/w) polymer failed to replicate the topographic features (results not shown). Therefore, we selected the 20% (w/w) hydrogels to image using atomic force microscopy (AFM). The distortion of topographic features after swelling increased with increasing molecular weight. The features on hydrogels molded using P-8000/20 no longer exhibit sharp edges and have a

rounded appearance (see insert in Figure 3.2). Due to the large distortion of the topography, PEGDA 8000 was not used in cell culture studies. In the same figure, hydrogels P-700/20 and P-3400/20 can be appreciated to retain the molded features, thus meeting the design objective criteria.

As mentioned in the previous chapter, the inhibition of non-specific HCEC attachment was also dependent on the molecular weight of the PEGDA pre-polymer. Hydrogels made with P-3400/20 provided the best balance of non-fouling properties and retention of topographic features and were selected for the experiments using topographic hydrogels functionalized with specific peptides.

3.3.2 Controlled chemical and topographic cues impact HCEC area, elongation ratio and contact guidance differentially in serum-containing and serum-free media.

To test the influence of topography on the hydrogels, P-3400/20 hydrogels functionalized with 10 mM RGD were synthesized and molded for cell culture experiments. The topographic molds contained six separate areas with different ridge/groove widths (400, 800, 1200, 1600, 2000 and 4000 nm pitch), and intervening planar control areas[13]. HCECs were plated onto these substrates, as well as rigid control surfaces made with NOA-81 that allows non-specific cell-surface interactions. HCECs were cultured in EP medium or serum-free Epilife®. The choice of media was motivated by previous work from our group, where different media compositions have induced alterations in the HCECs response to topographic cues[12,13]. After 24 hours, cells were fixed, stained and imaged. As an example of the differences in orientation, elongation

and cell area that can be distinguished in HCECs on different substrates and media compositions, we have included images of HCECs on the 4000 nm pitch topography in Figure 3.3.

We analyzed and compared the area of the HCECs as a function of topographic feature pitch and media type for each type of substrate (NOA-81, RGD or RDG). HCECs plated onto topographically patterned NOA-81 and cultured in Epilife®, had decreased average area, between 57% and 86% compared to the area of cells plated on flat surfaces (Figure 3.4A). Although there were no significant differences in cell area between flat surfaces and 400 nm topography when cultured on RGD hydrogels in Epilife®, HCECs on 800 nm pitch topographies were 61% smaller than cells on flat surfaces, while cells plated on large-pitch topographies were 120% (1600 nm pitch) and 126% (2000-4000 nm pitch) larger than cells on flat surfaces (Figure 3.4B). Cells cultured in EP medium did not show a significant difference in area between the flat substrates and the topographic surfaces, regardless of the topographic dimensions or substrate composition (Figure 3.4C and 3.4D). In summary, cells in Epilife® showed more sensitivity to the underlying topographic features with regards to changes in cell area than cells cultured on EP media for both substrate types.

The average elongation ratio was also compared as a function of topography and media type for each substrate. In Epilife®, the average elongation ratio of cells cultured on 1200-4000 nm pitch substrates increased 20% with respect to the elongation ratio of cells on flat surfaces for both NOA-81 surfaces and hydrogels functionalized with RGD (Fig 3.5A and 3.5B). In EP medium, cells cultured on small pitches (400-800 nm) on

NOA-81 were significantly more elongated than HCECs on flat surfaces, however, the elongation ratio of cells on topographies larger than 1200 nm was not significantly different when compared to planar surfaces (Figure 3.5C). On RGD hydrogels in EP medium, HCECs on topographic surfaces exhibited no difference in elongation compared to cells cultured on flat surfaces (Figure 3.5D). In general, the spreading of HCECs depended on the topographic feature size in Epilife®, but demonstrated a less pronounced dependency on topography when cultured in EP media.

HCEC orientation and alignment with the underlying nano and micron scale topography demonstrated the most noticeable difference in behavior between the two medias used. HCECs presented a bimodal distribution, where cells align either parallel or perpendicular to the topographic features. The proportion of cells in each population varied with substrate and media type. Cells in Epilife® presented a significant and preferential perpendicular alignment for both nano and micron-scale topographies on the NOA-81 substrates (Figure 3.6A). In contrast, when EP medium was used with the NOA-81 substrates, HCECs exhibited an obvious change in the response to the topographic cues. Cells aligned preferentially parallel to the topography for both nano-sized (400-800 nm) and micron-sized (4000 nm), while the distribution was more uniform on the features transitioning from the nano to the micron-scale (1200-1600 nm). On these substrates we can distinguish a “U” shape in the alignment profile (Figure 3.6C). HCECs cultured in either EP medium or Epilife® on RGD-hydrogel substrates displayed a parallel alignment profile matching the aforementioned “U” shape (Figures

3.6B and 3.6D). In conclusion, contact guidance was dependent on both the substrate type and soluble factors within the culture media.

3.4 Discussion

Non-fouling PEGDA hydrogel substrates were developed to simultaneously present biologically relevant biochemical and topographical cues to cells in a soft material. One important aim of this work was to identify a soft moldable material that allows for the retention of topographic features in the nano and micron-scale, and provides controlled interactions of HCECs with specific ligands. These biomimetic characteristics can be useful to induce cell behaviors that better approximate *in vivo* conditions and will be essential for our future goal of developing an improved corneal prosthetic.

The Michael-type reaction was chosen for the incorporation of biochemistry into our hydrogel because its rapid reaction times and lack of undesirable by-products[33]. This technique is suitable for single molecules at low concentrations and short-time periods, such as those required by our study. For studies requiring longer temporal stability, our group is investigating other functionalization systems, such as the growth polymerization of acrylated peptides with well-defined spacer length where multiple peptides can be used at varied combinations and concentrations without change in the hydrogel properties[34].

According to our results, low relaxed swelling ratios are required in order to retain the nano and micro-scale topographic features on a hydrogel. The increase of the relaxed swelling at increasing molecular weight of the oligomer is due to the reduced crosslinking density, allowing for greater penetration of solvent. The swelling increased

while increasing the concentration of PEGDA because the pre-polymer is already in a solvated state, and the chemical potential of the PEG chains in the gel increases with concentration, leading to the increased penetration of solvent to equilibrate[35]. The molding of topographic features also depends on the crosslinking density of the hydrogels, and at very low concentrations (≤ 15%), the hydrogels did not retain the topographic features.

The different response in cell area and elongation ratio of HCECs on topographically patterned nano and micron-scaled surfaces when different media is used further demonstrates the effect of cytoactive soluble factors on the cellular response to the topography and suggests that soluble factors control these parameters on the response to topography more than protein adsorption. While HCECs cultured on NOA-81 surfaces showed a completely different response to topography when different media was used, cells cultured on RGD topographic surfaces showed a similar alignment profile, regardless of the media. This suggests that the alignment behavior depends on two non mutually-exclusive components: 1) protein adsorption from the media, which is inhibited on the RGD functionalized PEG surfaces, 2) the presence of surface-bound RGD that has a greater impact in the alignment response and overrides the influence of the soluble factors. In addition, we noted that contact guidance of HCECs on NOA-81 differs from previously reported studies of primary HCECs on silicon substrates[12]. HCECs cultured in Epilife® on NOA-81 surfaces exhibited perpendicular alignment on all topographies while on silicon substrates, cells preferentially aligned perpendicular to the topography below micron-sized features and parallel on features larger than one micrometer. This

disparity may be due to a difference in the profile of protein adsorption on silicon compared to NOA-81, or to small differences on the horizontal and vertical scales of the topographic features[12,13]. However, all of our results strengthen the argument that the HCEC response to the topographic cues is controlled by the interplay between topographic and soluble cues. The use of our functionalized hydrogel platform allows for discerning between the contribution of topography on cell behavior, and the confounding non-specific protein adsorption effect.

Differences in the media composition could potentially explain the alteration in the response to nano and micron-scale topographic cues. Previous work from our laboratory has demonstrated that the composition of the media regulates the topographic response of HCECs[13]. However, until now, it has been difficult to dissociate the contribution of the proteins adsorbing onto the surface from other soluble factors in the media. Through the use of materials that inhibit protein adsorption yet promote cell attachment through specific receptors, the influence of soluble constituents can be isolated. The alignment behavior of HCECs was substantially less context-dependent when cells were cultured on RGD-functionalized hydrogels, suggesting the influence of protein adsorption on contact guidance for the NOA-81 surfaces. Although there may be some effects from protein adsorption onto the hydrogel surfaces, we specifically selected a material that is resistant to protein adsorption. We believe that the differential response observed in cell area and elongation of HCECs when cultured in different media on RGD-functionalized hydrogel surfaces is due mainly to the effect of soluble cues on the topographic response.

Several differences between the two medias used could potentially explain the alteration in response to nano and micron scale topographic cues[12]: 1) The presence of serum in EP medium, 2) a 10-fold increase in epidermal growth factor (EGF) in EP medium with respect to Epilife®, and 3) a 10-fold increase in soluble Ca^{2+} in EP medium. Future studies will elucidate the role of these factors in downstream signaling that lead directly to changes in the orientation response to topography.

In summary, we fabricated non-fouling substrates that are moldable with nanotopography and that can be functionalized with specific biochemical motifs to promote HCEC attachment. Besides RGD, our topographic hydrogel substrates can allow for the incorporation of different adhesive peptides found in fibronectin or laminin that promote the binding and signaling of other receptors, such as syndecans or the $\alpha_6\beta_4$ integrin, which have been established as key components in corneal epithelial wound healing[36,37]. These substrates have the potential to mimic certain characteristics of the ECM and improve *in vitro* and *in vivo* applications.

3.5 Conclusions

This study demonstrates that soft materials such as PEGDA hydrogels can be used to engineer substrates incorporating relevant cellular cues, such as controlled biochemistry and topography. The choice of PEGDA molecular weight and concentration has to be balanced to minimize the deformation of the topographic features and inhibit non-specific binding. This study provides further evidence that nanoscale topography is a fundamental biomimetic cue impacting cell phenotype, and not only an indirect effect

due to the formation of chemical patterns through non-specific protein adsorption. In addition, we successfully isolated the confounding influence of non-specific protein adsorption onto the surfaces from other soluble factors to investigate the effect of nano and microscale topography on HCEC behavior. The use of our hydrogel materials will provide controlled biochemical and topographical cues to HCECs to form an intact epithelial layer and improve corneal prosthetics, and can be used to investigate the behavior of cells *in vitro*.

3.6 Figures

Hydrogel Names	Molecular weight of PEGDA pre-polymer	Mass fraction (w/w) in solution
P-700/10	700 g/mol	10%
P-700/15	700 g/mol	15%
P-700/20	700 g/mol	20%
P-700/25	700 g/mol	25%
P-700/40	700 g/mol	40%
P-3400/10	3400 g/mol	10%
P-3400/15	3400 g/mol	15%
P-3400/20	3400 g/mol	20%
P-3400/25	3400 g/mol	25%
P-8000/10	8000 g/mol	10%
P-8000/15	8000 g/mol	15%
P-8000/20	8000 g/mol	20%
P-8000/25	8000 g/mol	25%

Table 3.I: Molecular weight and mass fraction of the pre-polymer in the precursor solutions

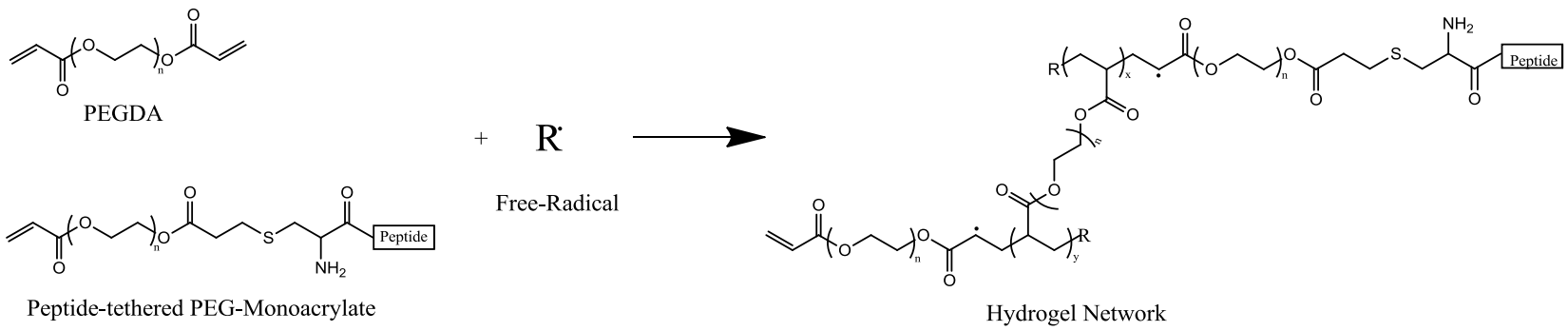

Scheme 3.1.- Free radical polymerization of PEGDA for the formation of hydrogels.

X and Y relate to the size of the poly(acrylate) domains. N relates to the size of the PEG domains.

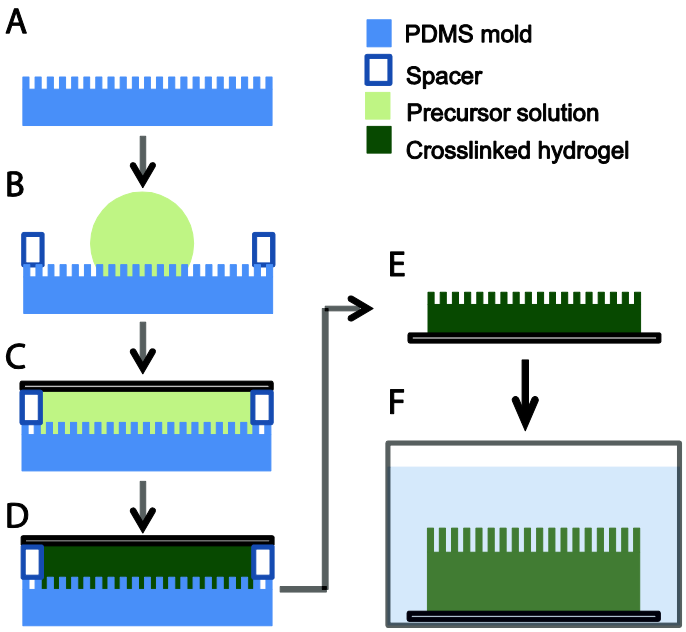

Figure 3.1: Schematic representation of the technique used to mold PEGDA hydrogels with topographic features:

A) Degassed PDMS mold with topographic features. B) A drop of precursor solution is placed on top of the PDMS mold. C) The precursor solution is covered with a glass coverslip previously treated with TPM. D) The hydrogel is UV-polymerized. F) The PDMS mold is removed. G) The hydrogel is soaked until it reaches equilibrium swelling.

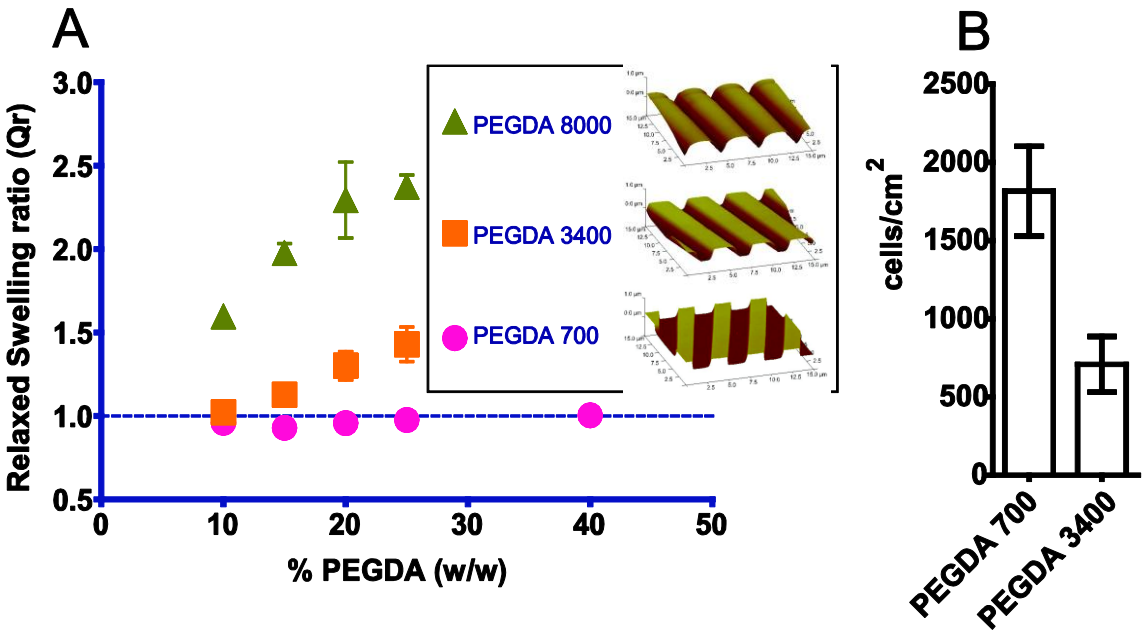

Figure 3.2: Increasing molecular weight increases the swelling response of PEGDA hydrogels and decreases cell attachment.

Relaxed swelling ratio of PEGDA hydrogels with different molecular weight at different macromer concentrations in the initial solution. Swelling ratio increases with increasing molecular weight and increasing macromer concentration. No swelling is indicated by the dashed line, where Q_R = 1.0. Insert: AFM images of 4000 nm pitch topography showing the deformation of the topographic features in hydrogels due to swelling.

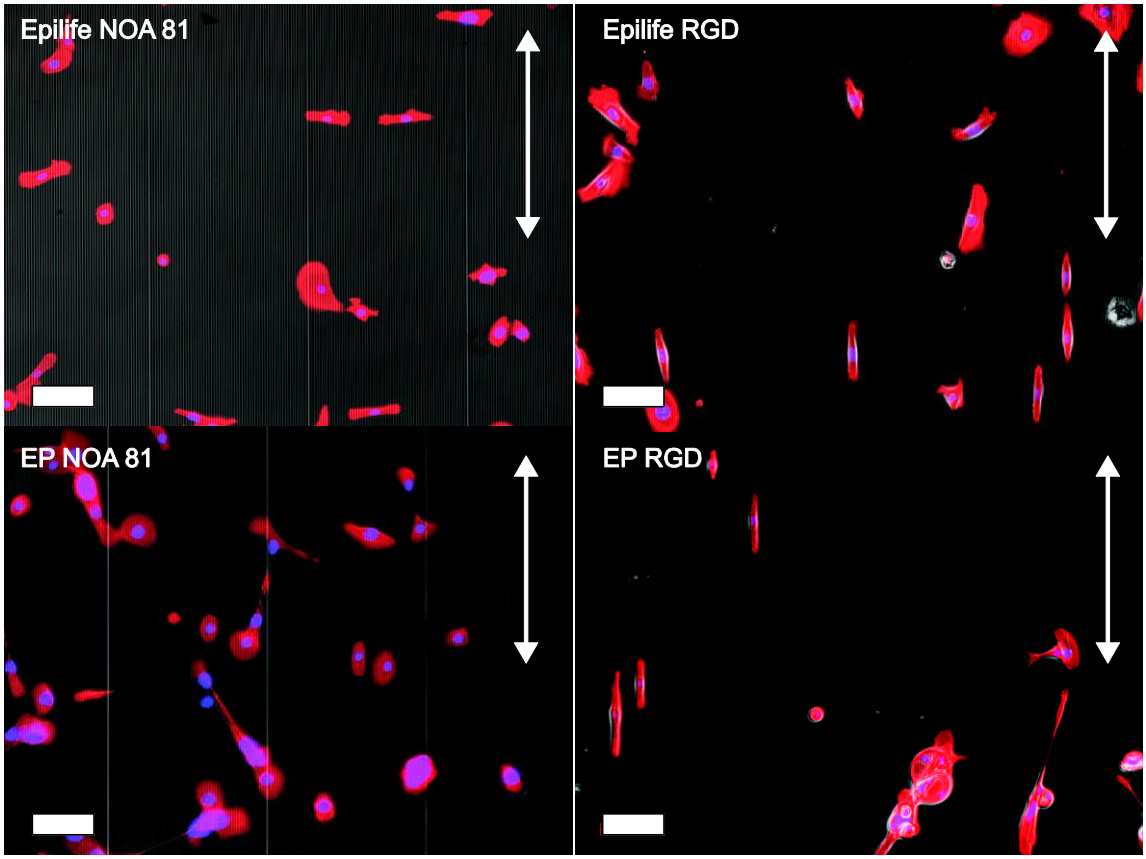

Figure 3.3.- HCECs cultured on 4000 nm pitch topography,

using NOA-81 surfaces showed an alignment perpendicular to the topographic features in Epilife® medium, but perpendicular to the topography when cultured in EP medium. On RGD-functionalized hydrogels, the alignment is parallel to the topographic features regardless of media type. Arrows indicate the direction of the topographic features. Scale bar: 100 μm.

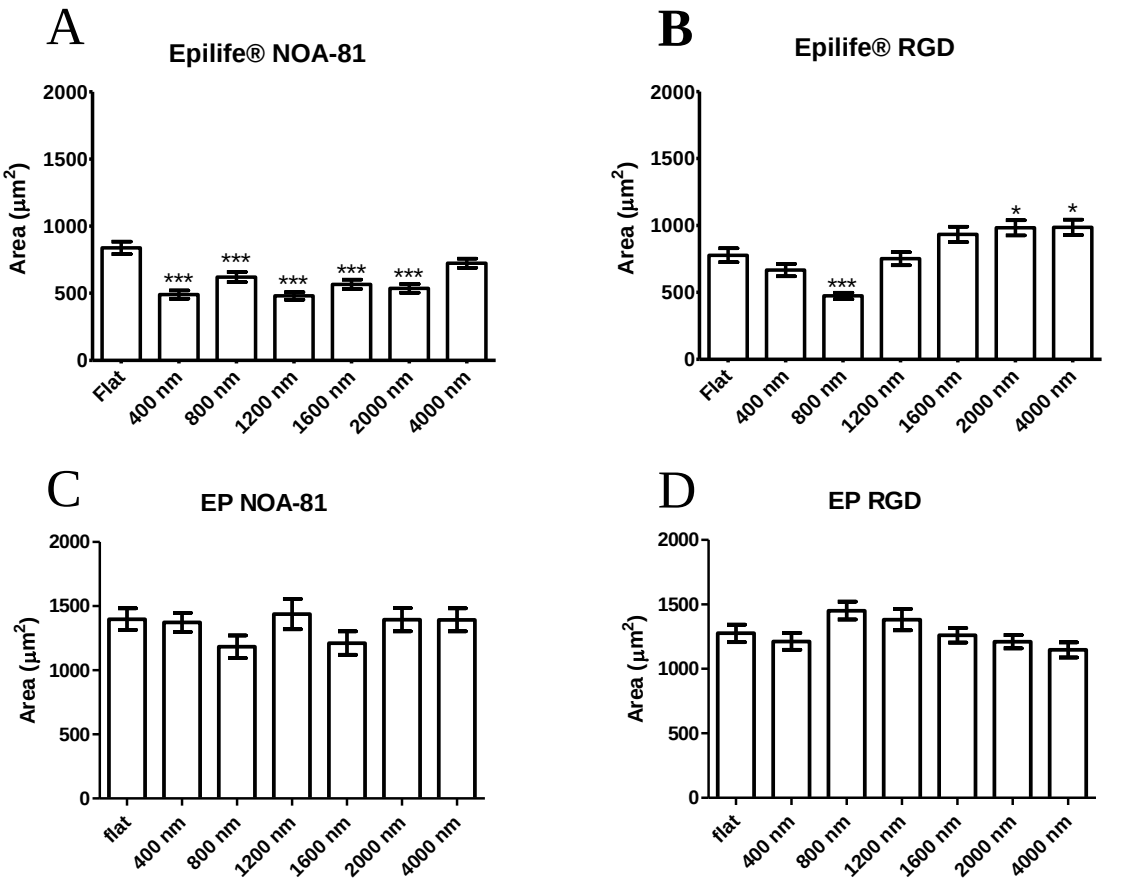

Figure 3.4.- HCECs in Epilife® on NOA-81 were significantly smaller on the topographic surfaces than on flat surfaces,

while HCECs in Epilife® on RGD hydrogels showed an increasing size with increasing topography. In EP medium, there was no significant difference for any type of substrate. A) Cells in Epilife® on NOA-81, B) Cells in Epilife® on RGD hydrogels, C) Cells in EP medium on NOA-81, D) Cells in EP medium on RGD hydrogels. Error bars: SEM (*** $P \leq 0.001$; ** $0.001 < P \leq 0.01$; * $0.01 < P \leq 0.05$).

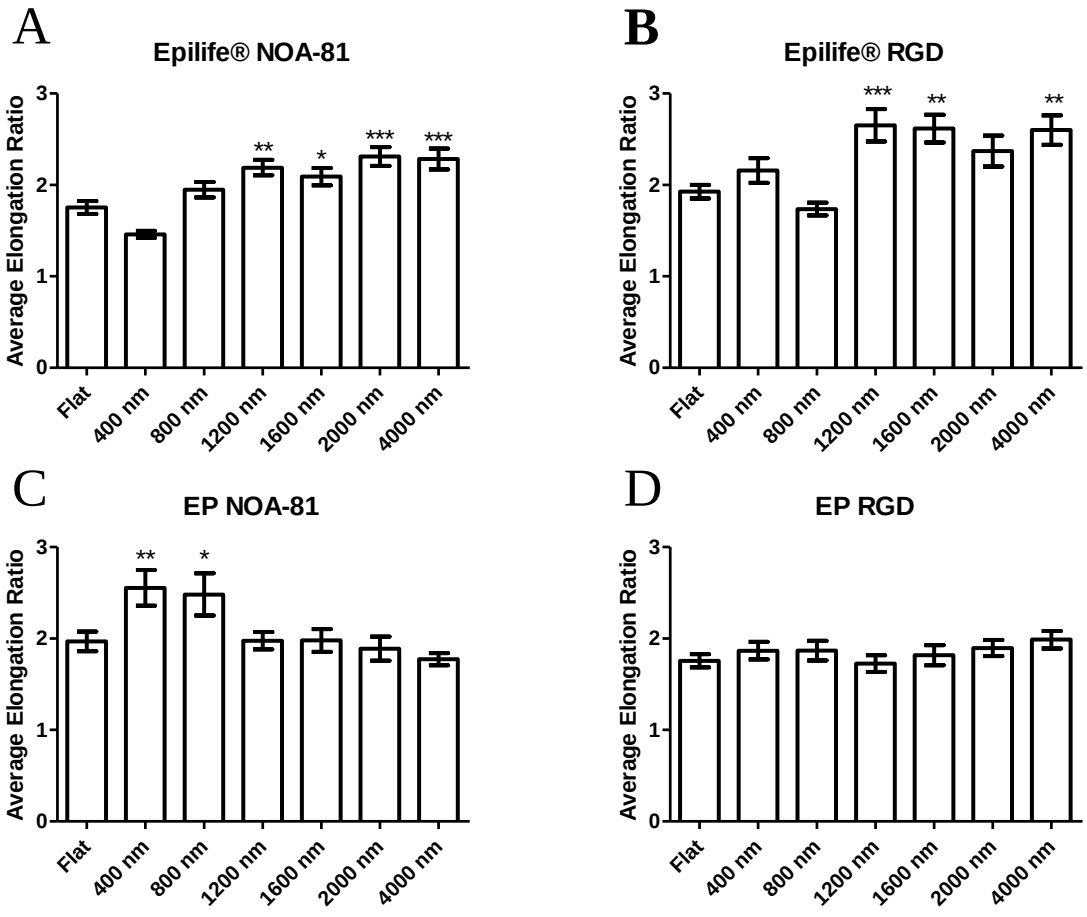

Figure 3.5.- HCECs in Epilife® on large-pitch topographic features (1200-4000 nm) showed a higher elongation ratio compared to flat surfaces on both types of substrates,

NOA-81 and RGD hydrogels. HCECs in EP media showed no difference in elongation ratio with respect to planar on topographic features greater than 1200 nm. A) Cells in Epilife® on NOA-81, B) Cells in Epilife® on RGD hydrogels, C) Cells in EP medium on NOA-81, D) Cells in EP medium on RGD hydrogels. Error bars: SEM (*** $P \leq 0.001$; ** $0.001 < P \leq 0.01$; * $0.01 < P \leq 0.05$).

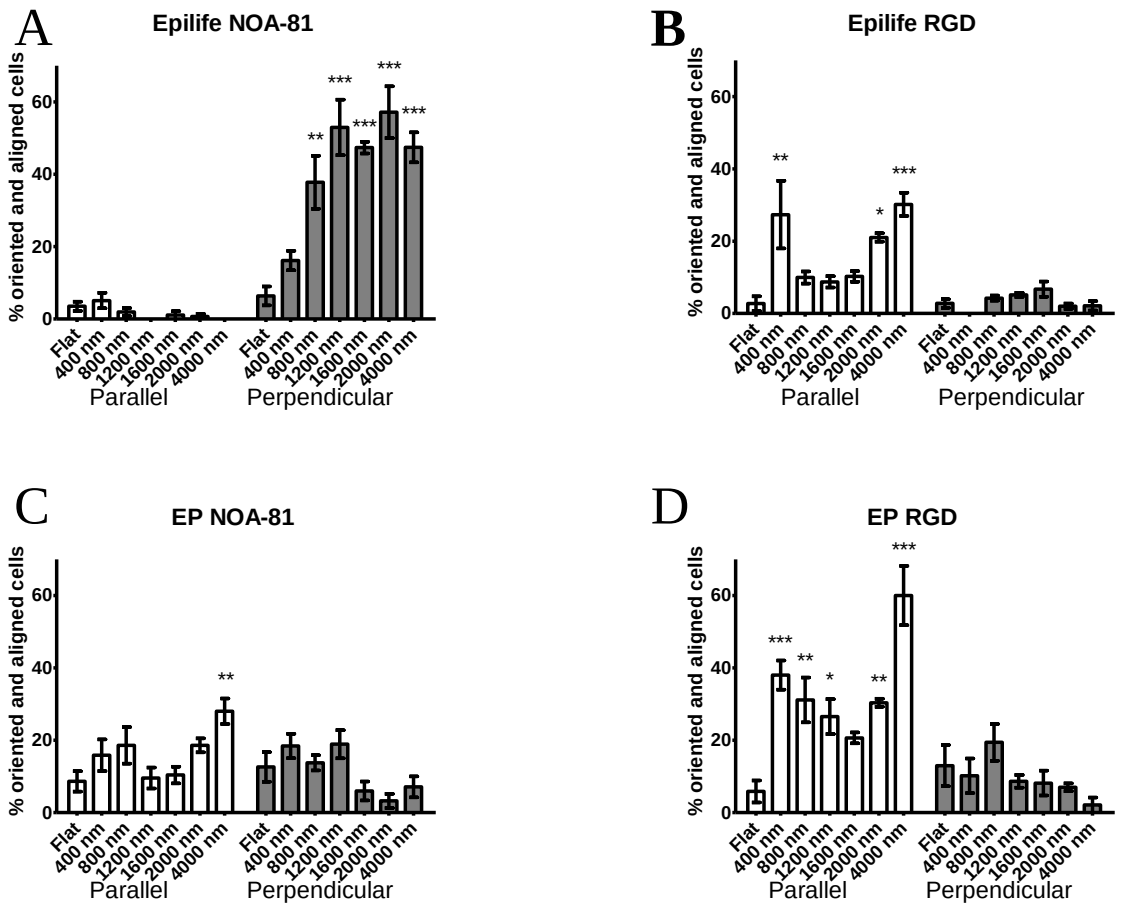

Figure 3.6.- HCECs on NOA-81 surfaces showed an alignment behavior fundamentally different for the different media types.

HCECs on RGD substrates showed the same alignment behavior for both media types. A) Cells in Epilife® on NOA-81, B) Cells in Epilife® on RGD hydrogels, C) Cells in EP medium on NOA-81, D) Cells in EP medium on RGD hydrogels. Error bars: SEM (*** $P \leq 0.001$; ** $0.001 < P \leq 0.01$; * $0.01 < P \leq 0.05$).

3.7 References

1. Whitcher JP, Srinivasan M, Upadhyay MP. Corneal blindness: a global perspective. Bulletin of the World Health Organization 2001;79:214-221.

2. Hicks CR, Fitton JH, Chirila TV, Crawford GJ, Constable IJ. Keratoprostheses: advancing toward a true artificial cornea. Survey of ophthalmology 1997;42(2):175-189.

3. Aiken-O'Neill P, Mannis MJ. Summary of corneal transplant activity: Eye Bank Association of America. Cornea 2002;21(1):1.

4. Flemming RG, Murphy CJ, Abrams GA, Goodman SL, Nealey PF. Effects of synthetic micro-and nano-structured surfaces on cell behavior. Biomaterials 1999;20(6):573-588.

5. Aquavella JV, Qian Y, McCormick GJ, Palakuru JR. Keratoprosthesis: current techniques. Cornea 2006;25(6):656.

6. Abrams GA, Schaus SS, Goodman SL, Nealey PF, Murphy CJ. Nanoscale topography of the corneal epithelial basement membrane and Descemet's membrane of the human. Cornea 2000;19(1):57.

7. Karuri NW, Liliensiek S, Teixeira AI, Abrams G, Campbell S, Nealey PF, Murphy CJ. Biological length scale topography enhances cell-substratum adhesion of human corneal epithelial cells. Journal of cell science 2004;117(Pt 15):3153.

8. Teixeira AI, Abrams GA, Bertics PJ, Murphy CJ, Nealey PF. Epithelial contact guidance on well-defined micro- and nanostructured substrates. Journal of Cell Science 2003;116(Pt 10):1881-1892.

9. Teixeira AI, Abrams GA, Murphy CJ, Nealey PF. Cell behavior on lithographically defined nanostructured substrates. Journal of Vacuum Science & Technology B: Microelectronics and Nanometer Structures 2003;21:683.

10. Diehl KA, Foley JD, Nealey PF, Murphy CJ. Nanoscale topography modulates corneal epithelial cell migration. Journal of Biomedical Materials Research Part A 2005;75(3):603-611.

11. Liliensiek SJ, Campbell S, Nealey PF, Murphy CJ. The scale of substratum topographic features modulates proliferation of corneal epithelial cells and corneal fibroblasts. Journal of Biomedical Materials Research Part A 2006;79(1):185-192.

12. Teixeira AI, McKie GA, Foley JD, Bertics PJ, Nealey PF, Murphy CJ. The effect of environmental factors on the response of human corneal epithelial cells to nanoscale substrate topography. Biomaterials 2006;27(21):3945-3954.

13. Fraser SA, Ting YH, Mallon KS, Wendt AE, Murphy CJ, Nealey PF. Sub micron and nanoscale feature depth modulates alignment of stromal fibroblasts and corneal epithelial cells in serum rich and serum free media. Journal of Biomedical Materials Research Part A 2008;86(3):725-735.

14. Tocce EJ, Smirnov VK, Kibalov DS, Liliensiek SJ, Murphy CJ, Nealey PF. The ability of corneal epithelial cells to recognize high aspect ratio nanostructures. Biomaterials 2010;31(14):4064-4072.

15. Curtis A, Wilkinson C. Topographical control of cells. Biomaterials 1997;18(24):1573-1583.

16. Lee KY, Mooney DJ. Hydrogels for tissue engineering. Chem. Rev 2001;101(7):1869-1880.

17. Drury JL, Mooney DJ. Hydrogels for tissue engineering: scaffold design variables and applications. Biomaterials 2003;24(24):4337-4351.

18. Perlin L, MacNeil S, Rimmer S. Production and performance of biomaterials containing RGD peptides. Soft Matter 2008;4(12):2331-2349.

19. Metters AT, Anseth KS, Bowman CN. Fundamental studies of a novel, biodegradable PEG-b-PLA hydrogel. Polymer 2000;41(11):3993-4004.

20. Mann BK, Gobin AS, Tsai AT, Schmedlen RH, West JL. Smooth muscle cell growth in photopolymerized hydrogels with cell adhesive and proteolytically degradable domains: synthetic ECM analogs for tissue engineering. Biomaterials 2001;22(22):3045-3051.

21. Suh KY, Seong J, Khademhosseini A, Laibinis PE, Langer R. A simple soft lithographic route to fabrication of poly (ethylene glycol) microstructures for protein and cell patterning. Biomaterials 2004;25(3):557-563.

22. Revzin A, Russell RJ, Yadavalli VK, Koh WG, Deister C, Hile DD, Mellott MB, Pishko MV. Fabrication of poly (ethylene glycol) hydrogel microstructures using photolithography. Langmuir 2001;17(18):5440-5447.

23. Ruoslahti E. RGD and other recognition sequences for integrins. Annual review of cell and developmental biology 1996;12(1):697-715.

24. Lauweryns B vdOJ, Volpes R, Foets B, Missotten, L. Distribution of very late activation integrins in the human cornea. Investigative ophthalmology & visual science 1991;32:2079-2085.

25. Jain S, Azar DT. Extracellular matrix and growth factors in corneal wound healing. Current Opinion in Ophthalmology 1994;5(4):3.

26. Carter RT. The role of integrins in corneal wound healing. Veterinary Ophthalmology 2009;12:2-9.

27. Fong E, Tzlil S, Tirrell DA. Boundary crossing in epithelial wound healing. Proceedings of the National Academy of Sciences;107(45):19302.

28. Lin CC, Metters AT. Metal-chelating affinity hydrogels for sustained protein release. Journal of Biomedical Materials Research Part A 2007;83(4):954-964.

29. Xia Y, Whitesides GM. Soft lithography. Annual Review of Materials Science 1998;28(1):153-184.

30. Allen-Hoffmann BL, Rheinwald JG. Polycyclic aromatic hydrocarbon mutagenesis of human epidermal keratinocytes in culture. Proceedings of the National Academy of Sciences of the United States of America 1984;81:7802-7806.

31. Sabatini LM, Allen-Hoffmann BL, Warner TF, Azen EA. Serial Cultivation of Epithelial Cells from Human and Macaque Salivary Glands. In Vitro Cellular & Developmental Biology 1991;27A(12):939-948.

32. Teixeira AI, Nealey PF, Murphy CJ. Responses of human keratocytes to micro and nanostructured substrates. Journal of Biomedical Materials Research Part A 2004;71(3):369-376.

33. Elbert DL, Hubbell JA. Conjugate addition reactions combined with free-radical cross-linking for the design of materials for tissue engineering. Biomacromolecules 2001;2(2):430-441.

34. Wilson M, Liliensiek, SJ., Murphy, CJ., Murphy, WL., Nealey, PF. Hydrogels with well-defined peptide-hydrogel spacing and concentration: impact on epithelial cell behavior. Soft Matter 2012;8(2):390-398.

35. Bray JC, Merrill EW. Poly (vinyl alcohol) hydrogels. Formation by electron beam irradiation of aqueous solutions and subsequent crystallization. Journal of Applied Polymer Science 1973;17(12):3779-3794.

36. Stepp MA, Gibson HE, Gala PH, StaIglesia DD, Pajoohesh-Ganji A, Pal-Ghosh S, Brown M, Aquino C, Schwartz AM, Goldberger O. Defects in keratinocyte activation during wound healing in the syndecan-1-deficient mouse. Journal of cell science 2002;115(23):4517-4532.

37. Jones JCR. The 3 laminin subunit, 6 4 and 3 1 integrin coordinately regulate wound healing in cultured epithelial cells and in the skin. Journal of Cell Science 1999;112:2615-2629.

CHAPTER 4: THE MIGRATION OF THE BORDER OF CORNEAL EPITHELIAL WOUNDS IS INFLUENCED BY THE TOPOGRAPHY OF THE SUBSTRATE.

4.1. Introduction

Worldwide, the insufficient supply of corneal donor tissue[1] motivates the use of artificial corneas as a therapy for corneal disorders that cause visual impairment[2]. The artificial corneas currently available focus mainly on the replacement and biointegration of the device into the stromal component, with less emphasis on the epithelial portion. Due to the exclusive effort on the stromal integration, problems including epithelial downgrowth[3], infection[4] and extrusion due to stromal melting[5] have been demonstrated to occur. It has been suggested that in order to reduce the aforementioned problems, the ideal artificial cornea should support the normal processes that allow the formation and maintenance of a stratified epithelium over the implant[6]. We hypothesize that the incorporation of biochemical and biophysical cues that have been characterized and quantified from the corneal epithelial basement membrane may promote wound healing and the formation of a fully functional anterior corneal epithelium.

The wound healing of the epithelium of the cornea is a highly organized series of events, where the basement membrane has many functions to help maintain a normal stratified epithelium[7-12]. There are several phases during the corneal epithelial wound healing process, including a lag phase (between wounding and initiation of cell

migration) where cells alter their metabolic status; a migration phase to cover the bare surface; a proliferation phase and a differentiation phase, where cells stratify and re-establish a differentiated multi-layer of cells[8,12,13]. In addition to morphological and behavioral alterations, specific signaling components involved in the reformation of the BM have been reported. Several molecules have been shown to be upregulated in corneal epithelial cells when wounded, including fibronectin[14], collagen[15], and laminin-332 (LN332)[16]. These molecules all serve as potential markers to determine whether biophysical and biochemical cues influence the wound healing process.

Previous research from our group as well as others has demonstrated that mimicking chemical and physical aspects of the basement membrane (BM) of the cornea[17] influenced behaviors essential to the wound healing process in the corneal epithelium, such as adhesion[18], proliferation[19] and migration[20]. These behaviors suggest that topography will have an effect on important phases of the corneal epithelial wound process, translating into an improved rate of wound healing, stratification and maintenance of a healthy epithelium.

Our approach is the use topographically and biochemically controlled poly(ethylene glycol) diacrylate (PEGDA) hydrogel substrates as an artificial BM to improve the wound healing and sustainment of a corneal epithelium. Topographically-molded PEGDA hydrogels functionalized with the adhesive peptide RGD, a sequence found in BM components when the corneal epithelium is wounded, such as fibronectin and collagen[21], have been demonstrated to provide specific biochemical and biophysical cues inspired by the BM to human corneal epithelial cells (HCECs)[22].

4.2. Materials and methods

4.2.1. Fabrication of biochemically functionalized PEGDA hydrogel substrates with topographic features

Precursor solutions of 20% (w/w) PEGDA were prepared by dissolving PEGDA 3400 in 10 mM 4-(2-hydroxyethyl)-1-piperazineethanesulfonic acid (HEPES) buffer at pH 8.0, with 0.067% (w/v) Lithium phenyl-2,4,6-trimethylbenzoylphosphinate (LAP) as the photoinitiator. RGD peptide (Cys-Gly-Gly-Arg-Gly-Asp-Ser-Pro) (UW-Madison Biotechnology Center, WI) was added to the precursor solutions to reach a final concentration of 10 mM. The hydrogel substrates were molded with groove-and-ridges with topographic features of different ranges (400 nm, 1400 nm and 4000 nm pitch) or with flat surfaces using a replica-molding technique, as previously reported[22]. Briefly, in a nitrogen atmosphere, a 30μL drop of the precursor solution was placed on top of a degassed PDMS stamp containing the desired topography with 0.5 mm PDMS spacers. The precursor solution was then covered by a glass coverslip previously treated with 3-(trichlorosilyl) propyl methacrylate (TPM, Sigma-Aldrich, UK) to ensure adhesion of the gels to the surface. The construct was polymerized under UV-light (364 nm for 900 s at 7.0 mW/cm^2) and the PDMS stamps were peeled off, transferring the pattern to the surface of the hydrogel. Hydrogel substrates were sterilized for 24 hours by soaking in 5% isopropyl alcohol (IPA) in 1X phosphate buffered saline (PBS, pH 7.2), rinsed for 24

hours in 1X PBS and pre-incubated for two hours in cell culture media for full equilibration.

4.2.2. AFM imaging of molded hydrogels

To ensure the incorporation of topographic cues, molded hydrogels containing topographic features were imaged by atomic force microscopy (AFM), using a Nanoscope IIIa Multimode scanning probe microscope (Veeco Instruments Inc., CA). Samples were hydrated in 1X PBS for at least 48 h at room temperature, and scanned in a fluid cell in contact mode using a SNL-10 silicon nitride cantilever with a silicon tip (Veeco Probes, CA).

4.2.3. HCEC culture

HCECs were harvested from human cadaver corneas graciously provided by the Lions Eye Bank of Wisconsin, Madison or the Missouri Lions Eye Bank (Columbia, MO) as previously reported[23]. Cells from two to four corneas were centrifuged and re-suspended in epithelial medium (EP medium). EP medium is composed of a 3:2 ratio of Ham's F12:Dulbeco's Modified Eagles medium (DMEM) (Invitrogen, CA), supplemented with 2.5% (v/v) fetal bovine serum (FBS), 0.4 μg/mL hydrocortisone, 8.4 ng/mL cholera toxin, 5 μg/mL insulin, 24 μg/lM adenine, 10 ng/mL epidermal growth factor, 100 units penicillin and 100 μg/mL streptomycin[24]. All HCECs were incubated on plates seeded with a feeder layer of mytomycin-treated swiss mouse 3T3 fibroblasts at

37 °C and 5% CO_2 until they reached approximately 70% confluence. HCECs were used between passages 1 and 4.

4.2.4 Wound healing assay.

HCECs at 60-70% confluence were exposed to 0.01% EDTA in 1X PBS for 1 minute to allow detachment of feeder cells. For the live fluorescence staining, cells were incubated with a 6 μM live dye solution of CellTracker green CMFDA (5-Chloromethylfluorescein diacetate, Life Technologies, NY) in Dulbecco's Modified Eagle Medium (DMEM) for 45 minutes at 37 °C and 5% CO_2 as recommended by the manufacturer. The dye solution was then replaced with fresh EP medium, and cells were incubated for another 45 minutes at 37 °C and 5% CO_2. After live staining, cells were harvested using 0.025% Trypsin/0.01% EDTA, centrifuged and resuspended in EP medium, and plated at a density of 150,000 cells/cm^2 on hydrogel surfaces around a 5 mm diameter cloning cylinder to act as an 'exclusion zone' (figure 4.1). After incubation for 24 h, the cloning cylinders were removed and the fluorescently labeled cells on the hydrogel samples were imaged at 0 h, 24 h, 48 h and 72 h using a Stemi SV11 dissecting microscope (Zeiss, NY) with a 1.2X objective lens. The area of the wound was measured using Axio Vision software (Zeiss, NY). The size of the wound was defined as the radius (R) of the circle of the measured area (A), using the equation: $\overline{\quad}$, and the wound closure was defined as the difference of the radius from the radius of the starting point ($\Delta R = R_O - R$). From the wound closure data, a linear regression was performed, and the slope was reported as the wound healing rate in mm/hour. An experimental set

consisted of at least four replicates of each hydrogel substrate. Each experimental set was repeated in triplicate.

4.2.5. Proliferation assay

The assessment of cell proliferation was measured through the incorporation of 5-ethynyl-2'-deoxyuridine (EdU) with the Click-iT EdU Cell Proliferation Assay Kit (Invitrogen, CA). HCECs were plated using the wound healing method described above. For the starting time point, cells were incubated in 10 μM EdU for 12 hours before removal of the cloning cylinders. For subsequent time points (12 h, 24 h and 36 h), the cloning cylinders were removed and HCECs were incubated for 12 hours in 10 μM EdU prior to the corresponding time point. At each corresponding time point, cells were fixed and permeabilized and the EdU was stained according to the manufacturer's protocol. The nuclei of cells that replicated in the 12 hour period of incubation with EdU were labeled in red. Cells were then stained with 0.1 μg/mL 4',6-Diamidino-2- phenylindole (DAPI) (Invitrogen, CA) in 1X PBS for 30 minutes, to label the nucleus of non-proliferating cells (blue).

The proportion of proliferating cells was determined by fluorescence microscopy. The cells that incorporated EdU into their DNA (proliferating cells) were counted, as well as non-proliferating cells. The results show the percentage of cells that incorporated EdU in the 12-hour incubation period with respect to the total number of cells. The area of the confluent layer was measured, and the cell density was reported as the total number of

cells/area. At least three images were analyzed for each topography in each experiment, and the experiments were repeated in triplicate.

4.2.6. Immunocytochemistry and analysis of LN332 expression and location

For the purpose of evaluating the migratory status of cells upon epithelial wounding, we analyzed the expression and location of LN332 in HCECs. Following each time point, cells were fixed with a 1% paraformaldehyde solution in 1X PBS at room temperature for 20 minutes. Cells were then permeabilized with 0.1% (w/v) Triton X-100 (Sigma–Aldrich, St Louis, MO) in 1X PBS for 7 minutes, followed by exposure to a solution of 1% (w/v) bovine serum albumin (Sigma–Aldrich, St Louis, MO) and 1% goat serum (Sigma–Aldrich, St Louis, MO) in 1X PBS for 20 min to block non-specific binding. Cells were then incubated with 5 μg/mL of mouse anti-laminin-5 IgG clone P3H9-2 (Millipore, MA) for 1 hour, rinsed in 1X PBS and incubated in 2 μg/mL of AlexaFluor 488 labeled goat anti-mouse IgG (Invitrogen, CA) for 1 hour to label laminin-5 (green). Cells were rinsed with 1X PBS and incubated in 0.1 μg/mL DAPI in 1X PBS for 30 minutes, to label the nucleus (blue). To demonstrate the specificity of the staining, experiments with secondary antibody alone served as the negative control. Images of fluorescently stained cells on the corneal epithelial edge of the wound were obtained for each substrate using a 10X objective lens. On each topographic substrate at least four images were taken. Image analysis was performed using AxioVision software (Zeiss, NY). The border of the wound was defined as the area 50 μm thick from the edge of the wound. The fluorescence density of that area was measured and divided by the number

of cells in that area. This was normalized to the fluorescence level per cell of the flat surface at the starting time point to obtain the relative expression of laminin-5 per cell in the wound border. At least three substrates for each topography were analyzed for each experiment, and experiments were repeated in triplicate.

4.2.7. Real time-Polymerase Chain Reaction (RT-PCR)

Total RNA was extracted from three replicates for each topographic substrate (flat, 400 nm, 1400 nm and 4000 nm pitch) at 0, 12, 24 and 36 hours following the Qiagen RNeasy Kit protocol (Qiagen, Germantown, MD). Briefly, cells were lysed in 350 µl Qiagen RLT buffer containing 10 µl/ml of 2-mercaptoethanol (Sigma-Aldrich, St Louis, MO). An equal amount of 70% ethanol was added to each sample, and mixed prior to loading onto Quiagen H-Bind columns. Colums were washed with Qiagen buffers RW1 and RPE and eluted with 30 µL of nuclease-free water. Sample concentrations were measured at OD 260 for total RNA using a NanoDrop 2000 spectrophotometer (Thermo Scientific, Wilmington, DE). The concentration of RNA was calculated using the equation: $C=(A*\varepsilon)/b$ where C is the nucleic acid concentration (ng/µL), A is the absorbance at 260 nm, ε is the extinction coefficient (40 ng·cm/µL for RNA) and b is the path length in cm. Samples were further diluted with nuclease-free water to a concentration of 75 ng/mL and stored at -20 °C.

Primers and probes were purchased from the pre-developed TaqMan assay reagents (PE Applied Biosystems, Carlsbad, CA). The reference numbers for the products are Laminin-α3: Hs00165042-m1 and Laminin-γ2: Hs01043711-m1. Gene expression

levels were normalized to 18S RNA (reference number Hs99999901-s1). RT-PCR was performed using TaqMan one-step Master Mix reagents (PE Applied Biosystems, Carlsbad, CA). The reaction mixture contained 5μL of TaqMan 2X-Universal PCR Master Mix, 0.25μL of 40X Multiscribe and RNase inhibitor mix, 3.25 μL of nuclease free water, 0.5 μL of the primers mixture, and 1μL of the samples containing 75ng/mL total RNA, for a total of 10 μL reaction volume per sample. The mixtures were added to MicroAmp Fast Optical 48-well reaction plates (PE Applied Biosystems, Carlsbad, CA) and centrifuged at 1000 rpm for 1 min. The real-time PCR was completed on a StepOne RT-PCR system (Applied Biosystems, Carlsbad, CA). Reaction conditions were as follows: 50°C for 20 min, 95°C for 10 min, and 40 cycles of 95°C for 15 s and 60°C for 1 min. The relative quantification of gene expression was performed using the $\Delta\Delta C_T$ method[25] using the StepOne Real-Time PCR software (Applied Biosystems, Carlsbad, CA). Blank controls were run to ensure the specificity of the amplifications.

4.2.8. Statistics

Experimental data were analyzed using analysis of variance (ANOVA). When variability was determined to be significant (α=0.05) the Bonferroni multiple comparison test was used to determine significance between flat surfaces and topographic surfaces. Significant results were further divided into "statistically significant" ($0.01 \leq P \leq 0.05$, *), "very significant" ($0.001 \leq P < 0.01$, **), and "extremely significant" ($P < 0.001$, ***).

4.3. Results

4.3.1. Molding of topographic features

To ensure the incorporation of topographic cues onto the substrates, PEG hydrogels functionalized with RGD peptide were fabricated by soft lithography using nano- and micro-patterned PDMS molds. The precursor solution consisted of a mixture of PEGDA previously reacted with a cysteine-ended peptide and photoinitiator. The hydrogels were syntesized with the presence of a UV source, creating a crosslinked network that retained the anisotropic ridge and groove pattern of the stamp, as exhibited with the AFM images in figure 4.2. The pitches used in our experiments were 400 nm, 1400 nm and 4000 nm, and the depth of the grooves ranged from 200 nm to 400.

4.3.2. The presence of topography improves the in vitro wound healing.

Fluorescently stained HCECs were cultured to confluence on hydrogel substrates functionalized with RGD peptide, using a 5 mm diameter cloning cylinder as an 'exclusion zone'. After 24 h, the cylinder was removed; creating a wound that was imaged at 0 h, 24 h, 48 h, 72 h and 96 h. The area of each wound at every time point was measured, and the wound advance rate was quantified as described above. The closure of the wounds is shown in figure 4.3, where we observed increased wound closure at earlier time points on the topographic surfaces, compared to the flat surfaces. Compared with flat surfaces with the same chemical characteristics, hydrogel substrates molded with topography (400 nm, 1400 nm and 4000 nm pitch) demonstrated significant increases in

the wound advance, starting after 24 hours of wounding, that was maintained up to 96 hours (figure 4.4A). The wound healing rate in all the topographic substrates was significantly increased compared to the flat substrates ($p < 0.001$), at 52%, 62% and 43% faster in the 400 nm, 1400 nm and 4000 nm pitch substrates respectively (figure 4.4B). Interestingly, we observed that although single cells usually present contact guidance to the topographic features, the wound border does not appear to have a preferential direction of closure. Based on this observation, we analyzed the cell alignment on the border of the wound at higher magnification (10X, figure 4.5). In topographic substrates, the isolated cells away from the wound border aligned to the topography, but cells contained within the border of the wound do not exhibit any alignment.

4.3.3. There is no significant difference in proliferation or spreading between the flat surfaces and the topographic substrates

Proliferation assays were performed on *in vitro* wounds by observing the incorporation of EdU into the DNA of replicating cells. After incubation in EdU for 12 hours, cells were fixed, EdU was labeled in red for proliferating cells and cell nuclei of non-proliferating cells were stained using DAPI (blue). The wound edge was then imaged. An example image is shown in figure 4.6A, where no qualitative differences between cells on topography vs. planar surfaces were observed. To verify, proliferating cells were counted, as well as non-proliferating cells. The percentage of proliferating cells was calculated at 0 h, 12 h, 24 h and 36 h for each one of the topographic substrates. Figure 4.6B shows the quantitative results, where a significant difference in proliferation

between different time points can be observed. However, there is no difference as a result of the topography. Cell density was also calculated by dividing the total number of cells on the surface by the area they covered. Again, in figure 4.6C, we observe significant differences in cell density between the time points, but no difference between the topographies. Upon closer examination of the images shown in Figure 4.6A, we noted that the cells on the edge of the wound are not proliferating, while their nuclei appear to be larger. This observation motivated the investigation of cell migration on the wound border.

4.3.4. Topographic features alter the expression of LN332 in the wound border, suggesting increased migration.

In vitro wound assays were performed using the previously described protocol. Cells were fixed at 0 h, 12 h, 24 h and 48 h after wounding and immunolabeling for LN332. Images of the wound border were performed using fluorescence microscopy. Representative images of the wound border are shown in figure 4.7. An increased expression of LN332 can be observed for the 48 h time point on all topographic substrates, as well as LN332 tracks following the cell migration path. The fluorescence of the area 50 μm next to the wound edge was measured, and the number of cells in that area was counted. Figure 4.8 shows the relative fluorescence per cell in the wound border. Compared to the flat surfaces, a very significant increase in the relative expression of LN332 per cell on the wound edge of topographic substrates can be clearly observed after 12 hours (66% for 400 nm, 83% for 1400 nm and 71% for 4000 nm); and

after 24 hours (142% for 400 nm, 129% for 1400 nm and 147% for 4000 nm). The relative expression/cell of LN333 on the flat substrates appears to remain constant throughout the experiment.

4.3.5. In flat surfaces, the overall RNA expression of LN332 subunits is increased with respect to topographic substrates

RT-PCR was performed on the entire population of HCECs for the α3 and the γ2 subunits of LN332 at 0 h, 12 h, 24 h and 48 h after wounding. The results of the relative expression of these LN332 subunits are shown in figure 4.9. For the flat substrates, we observed an increased expression of 3.3-fold for the α3 subunit and of 2.3-fold for the γ2 subunit during the first 24 hours. After this period the expression of both subunits returned to basal levels. The topographic substrates also presented a modest increase in expression of the subunits on the first 24 hours; however, the RNA expression of LN332 on the flat surfaces was significantly higher than in the topographic substrates for every time point.

4.4. Discussion

The healing and renewal of the corneal epithelium is a complex process highly dependent on a balance of cell behaviors, such as adhesion[18], proliferation[19], differentiation[13], migration[20] and cell death[12]. Those behaviors are regulated by an intricate coordination of signals that originate from the cellular environment, including cell-cell communication, soluble molecules, and interactions with the ECM[26]. Our group

has demonstrated that a subset of those cues, inspired from the topographic characterization of the ECM[17], unequivocally influence the wound healing related behaviors[18-20]. Based on our results, we hypothesize that the incorporation of topography onto artificial corneas may improve the formation and maintenance of a corneal epithelium. Other groups have also demonstrated the influence of topography in wound healing, as published by Parkinson, et. al. , where the size of nano-pores on aluminum oxide membranes influenced the rate of cell proliferation and migration *in vitro*[27] of another epithelial cell type, keratinocytes. In addition, the use of topographical membranes as dressings lead to less granulation tissue and a more mature epidermal layer in skin than control standard burn dressings *in vivo*[28].

Our results provide additional evidence that biophysical cues are essential, and that the topography of the surface effectively improves corneal epidermal wound healing. Although we anticipated a preferred directionality of the migration of the wound border parallel to the topographic features, the wound closure was mostly uniform. Previous research on topographic cues and cell migration conducted by our laboratory showed that single cells plated on SiO_2 topographic substrates migrated along the topography[20]. Colonies of cells also presented a preferential dispersion along the topographic features, although this effect is small, and migration perpendicular to the topography was always present[20]. Recent unpublished work conducted on PEGDA hydrogels also demonstrates less contact guided migration in epidermal confluent sheets compared to single cell studies[29,30]. These results suggest that, upon wounding, epithelial cells in a confluent

sheet respond to the presence of topographic cues, but do not exhibit the same degree of contact guided migration as single cells.

To elucidate the mechanisms leading to the increased wound closure when cells are in contact with topography, we investigated possible changes in proliferation, cell spreading and migration. The observation on the uniform cell-spreading on all the surfaces is consistent with previous reported results, using the same type of substrates and media compared to this work[22]. However, the constant proliferation of HCECs across our substrates is an unexpected result, because we have previously reported that the proliferation of an immortalized cell line (SV40-HCECs), as well as primary cells decreased in response to decreasing topographic features[19]. One potential explanation for this disagreement is the difference in experimental settings. In experiments using single cells, the topographic response is due exclusively to the influence of cell-substrate; while on sheets of cells the response is affected by the cell-substrate interactions, as well as the influence of other cells via cell-cell communication.

We also investigated the expression of LN332 on the wound border. LN332 is a major component in the corneal BM[7] that has been used as a migration marker [31]. The increased expression of intracellular LN332 in the wound border for topographic substrates suggests an enhanced rate of migration. However, this result contradicts the observation of the data generated by our RT-PCR experiments, where the overall RNA expression of both α3 and the γ2 subunits of LN332 on flat surfaces were significantly higher than in the topographic substrates. This apparent discrepancy can be explained by the dual function of LN332. LN332 can act both as a promoter of cell adhesion or

migration, depending on the status and processing stage of the molecule[7]. Human LN332 is initially synthesized as a protein containing a 190 kDa α3 chain, a 135 kDa β3 chain and a 150 kDa γ2 chain[32]. The molecule increases its adhesive activity upon cleavage of the α3 subunit to the 160 kDa isoform[33]. This mature form of LN332 supports the formation of hemidesmosomes, linking the ECM with the keratin cytoskeleton, via the integrin α6β4[34-36]. The mature LN332 can also support the formation of focal adhesions, binding to the integrin α3β1 , which links the ECM to the actin cytoskeleton[37]. The deposition of LN332 occurs on the rear of the cells, in a trail that follows the path of migration[38]. However, under pathological conditions, such as epidermal wounding, the γ2 subunit is cleaved to an isoform of 105 kDa, which increases cell motility and decreases cell adhesion[39]. The isoform containing the cleaved γ2 subunit is unable to assemble in the ECM[40], and this molecule works as a motility-inducing soluble factor[41]. It has been suggested that this motility is triggered by the binding of the cleaved γ2 subunit to the epidermal growth factor receptor (EGFR)[42]. Although the mechanism is not completely understood, it is believed that bone morphogenetic protein 1 (BMP-1) and mammalian tolloid metalloproteinase (mTLD) are responsible for the processing of the γ2 chain[43,44].

Thus the observed LN332 expression is consistent with a model originally proposed for the regulation of tumor cell migration[32]: Epithelial cells on planar surfaces interpret the lack of topographic cues as the absence of BM, and initiate expression and secretion of LN332 that is rapidly deposited under the cells as a means to create their own BM, a process which will inhibit cell migration. Cells on topographic substrates sense the

topography as the presence of BM and proceed to migrate and close the wound. HCECs on topographic substrates do not express much LN332 except on the wound border, where cells express and post-process the γ2-cleaved form of LN332, enhancing the migration of the cells, and polarizing the cells to move towards the center of the wound. This hypothesis is consistent with research performed by our laboratory, demonstrating that ECM proteins are uniformly downregulated on topographic substrates compared to planar controls[45].

In summary, we fabricated substrates with biomimetic characteristics of the BM of the cornea that enhanced the closure of epithelial wounds *in vitro*. These substrates can be incorporated into currently used keratoprosthesis to induce epithelialization and improve their outcomes. Future studies will further explore the role of important BM components, such as LN332, and the incorporation of our hydrogel platform onto artificial corneas for *in vivo* experiments, using animal models.

4.5. Conclusions

This study demonstrates that nano- and micro-scale topography is a fundamental parameter to be included in the engineering of biomimetic materials. Substrates made with PEGDA hydrogels functionalized with molecules that induce specific interactions with the HCECs showed improved rates of healing when topographic features were present. We determined that the enhanced rate of wound closure is due to increased migration of the wound border towards the center. In addition, we elucidated some

possible mechanisms of the cellular response upon wounding in the presence of topography involving the expression and processing of BM molecules.

4.6. Figures

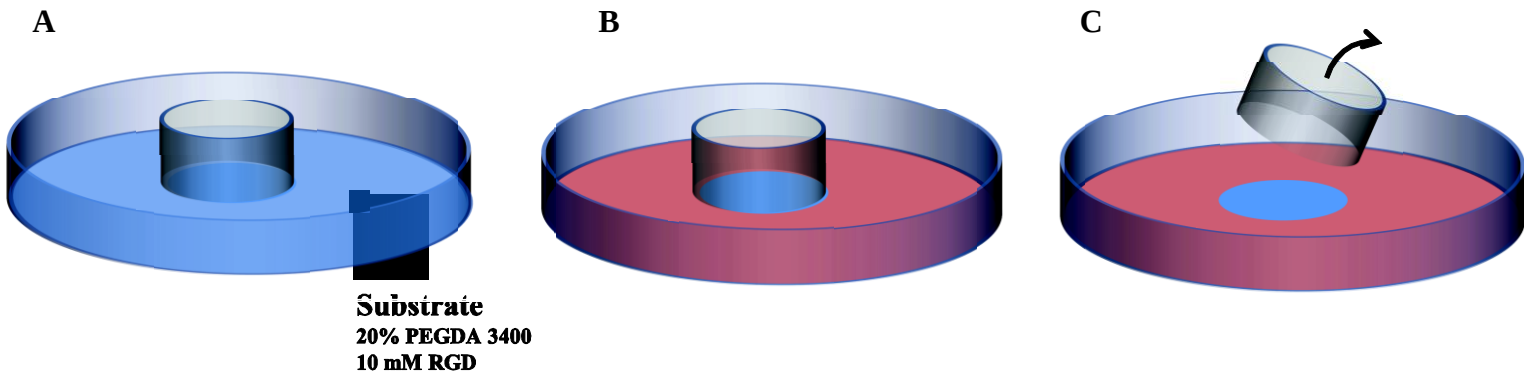

Figure 4.1.- Wound healing assay for the testing of topographic substrates.

A) The bottom of a culture dish is covered with the PEGDA substrates, containing topography. A cloning cylinder is placed on top to act as an exclusion zone. B) HCECs are cultured on the substrates, until confluent. C) The cloning cylinder is removed, creating a wound.

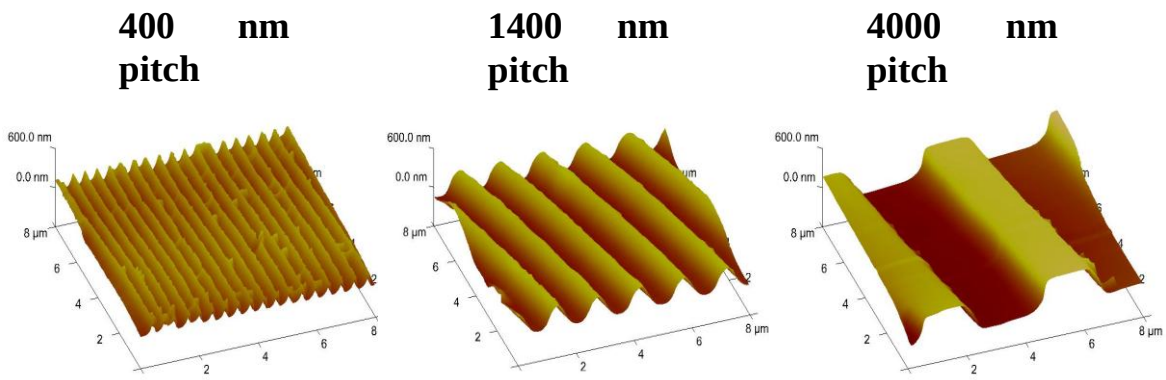

Figure 4.2.- AFM images of equilibrium-hydrated hydrogels,

showing the molding of the topographic features of 400 nm, 1400 nm and 4000 nm pitch.

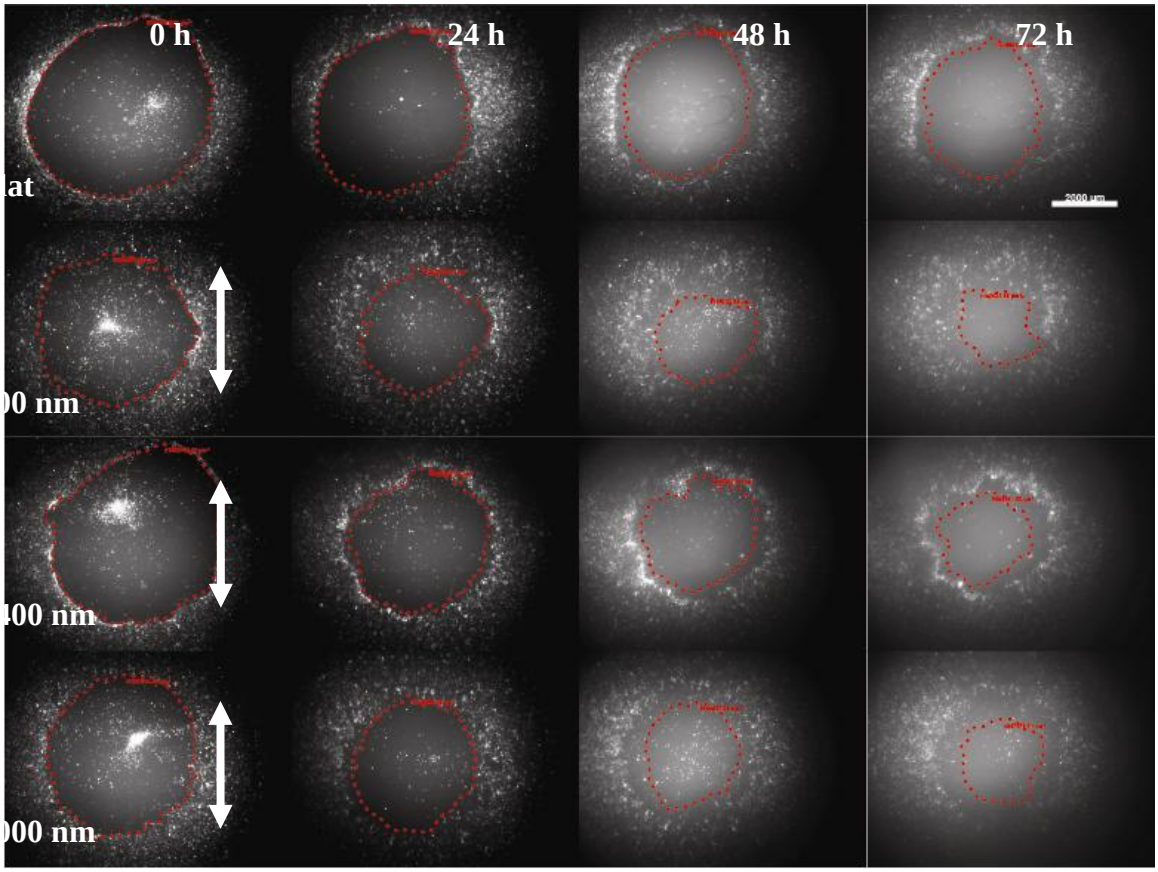

Figure 4.3.- Closure of the wounds on control flat surfaces, and on topographies of 400 nm, 1400 nm and 4000 nm pitch after 24 h, 48 h and 72 h.

Increased wound closures can be appreciated on topographic substrates. The arrows show the direction of the topographic features (grooves and ridges). The edge of the wound is marked by red dots. The closure of the wounds does not appear to be contact guided. Scale bar: 2 mm

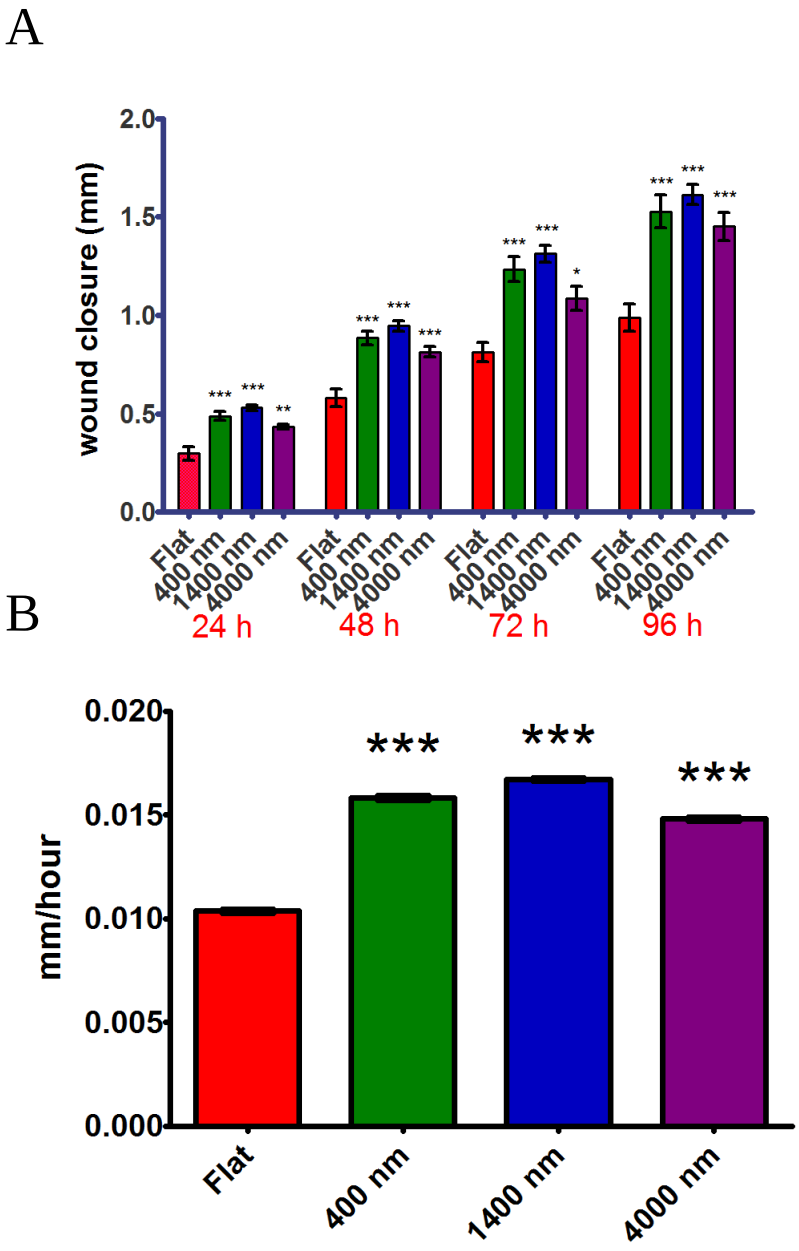

Figure 4.4.- The wound closure is increased on topographic substrates, compared to planar surfaces.

A) The wound advanced on topography faster than on flat surfaces, starting 24 hours after wounding. B) The wound closure rate is approximately 50% faster on topographic substrates. Error bars: SEM (*** $p \leq 0.001$; ** $0.001 < p \leq 0.01$; * $0.01 < p \leq 0.05$).

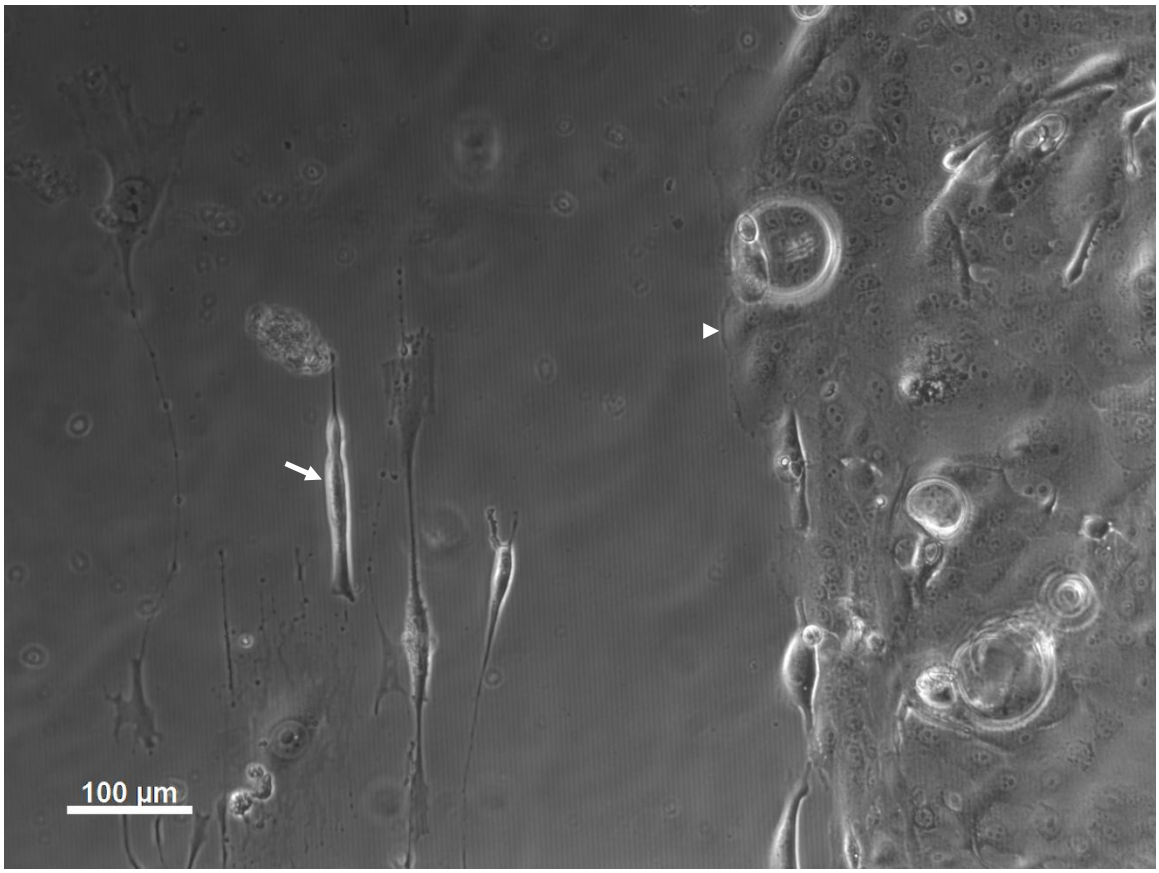

Figure 4.5.- Close up image (10X) of the wound border on 4000 nm pitch, 48 hours after wounding.

On single cells detached from the wound border, elongation and alignment of the cells can be observed (arrow). No contact guidance was observed for cells on the border of the wound (arrowhead).

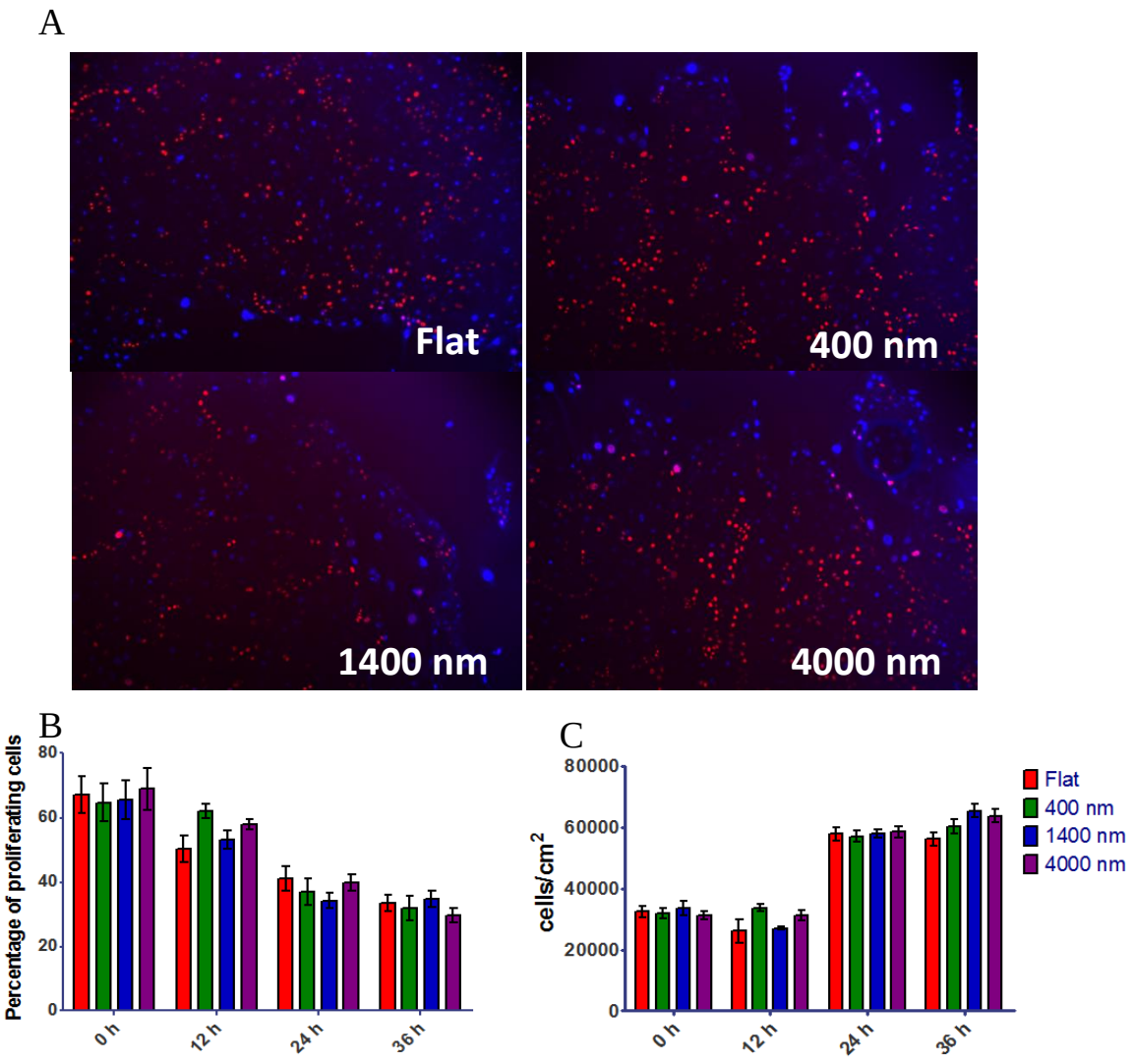

Figure 4.6.- EdU proliferation assay.

A) Images of the wound border on the different substrates. Cells proliferating are stained in red. Cells not proliferating are stained in blue. B) The percentage of proliferating cells at each time point is not significantly different for any of the substrates used. Proliferation is uniformly reduced after 36 hours. C) Cell density is not significantly different at each time point for our substrates. Error bars: SEM.

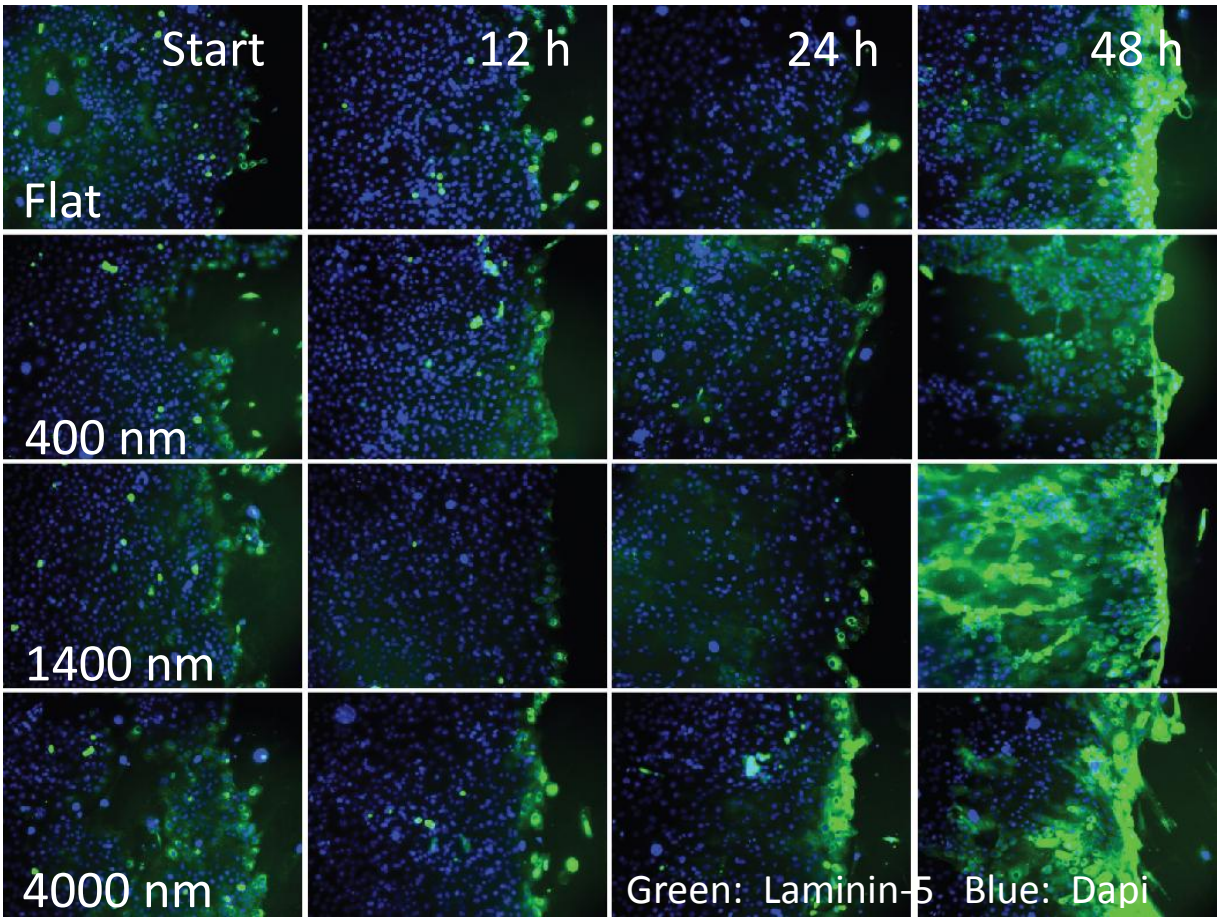

Figure 4.7.- Images of the wound border at 0, 12 h, 24 h and 48 h with LN332 stained in green.

Cell nuclei are stained in blue. The increase in expression on the border of the wound is apparent for the topographic features after 48 hours. Deposition of LN332 following the cellular track of migration can be clearly observed for 1400 nm at the 48 h timepoint.

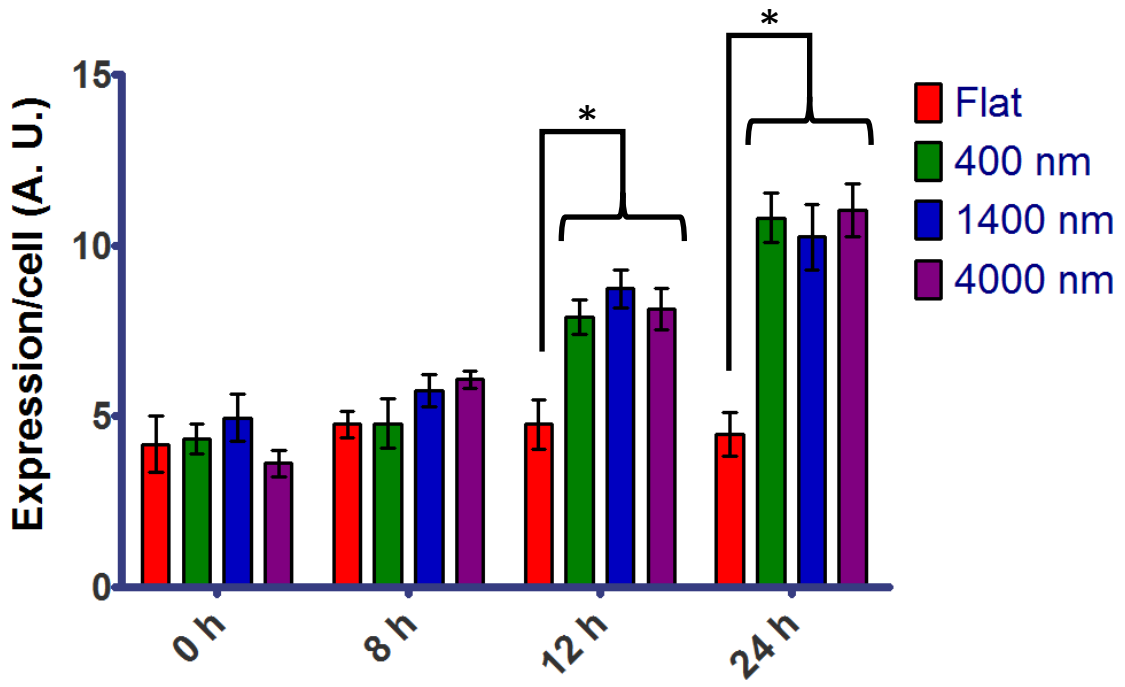

Figure 4.8.- Relative expression per cell of LN332 on the wound border.

After 12 h, cells on the wound border on topographic features presented an increased expression 1.5-fold vs. cells on flat surfaces. After 24 hours, the increased expression on topography was 2-fold. Error bars: SEM (*** $p \leq 0.001$).

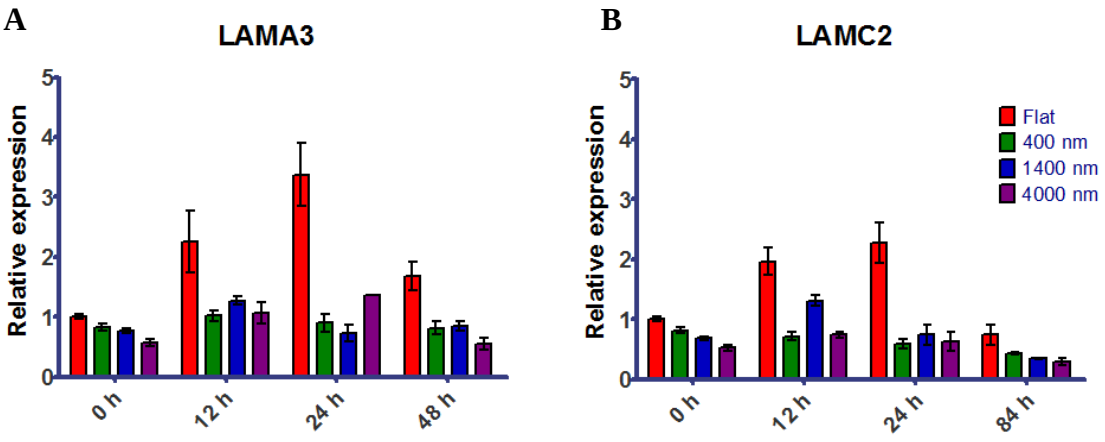

Figure 4.9.- RNA expression of LN332 subunits for the entire population of cells.

A) Expression profile for the LN332 α3 chain. B) Expression profile for the LN332 γ2 chain. LN332 chains have an increase of expression on flat surfaces after 12 hours, and return to base level after 48 hours. The expression of LN332 subunits on topographic surfaces is downregulated with respect to flat substrates at every time point.

4.7. References

1. Aiken-O'Neill P, Mannis MJ. Summary of corneal transplant activity: Eye Bank Association of America. Cornea 2002;21(1):1.

2. Whitcher JP, Srinivasan M, Upadhyay MP. Corneal blindness: a global perspective. Bulletin of the World Health Organization 2001;79:214-221.

3. Aldave AJ, Kamal KM, Vo RC, Yu F. The Boston type I keratoprosthesis: improving outcomes and expanding indications. Ophthalmology 2009;116(4):640.

4. Barnes SD, Dohlman CH, Durand ML. Fungal colonization and infection in Boston keratoprosthesis. Cornea 2007;26(1):9-15.

5. JirÃ¡skovÃ¡ N, Rozsival P, Burova M, Kalfertova M. AlphaCor artificial cornea: clinical outcome. Eye;25(9):1138-1146.

6. Hicks CR, Fitton JH, Chirila TV, Crawford GJ, Constable IJ. Keratoprostheses: advancing toward a true artificial cornea. Survey of ophthalmology 1997;42(2):175-189.

7. Ebihara N, Mizushima H, Miyazaki K, Watanabe Y, Ikawa S, Nakayasu K, Kanai A. The functions of exogenous and endogenous laminin-5 on corneal epithelial cells. Experimental eye research 2000;71(1):69.

8. Bentley E, Murphy CJ. Topical therapeutic agents that modulate corneal wound healing. VETERINARY CLINICS OF NORTH AMERICA SMALL ANIMAL PRACTICE 2004:623-638.

9. Germain L, Carrier P, Auger FA, Salesse C, GuÃ©rin SL. Can we produce a human corneal equivalent by tissue engineering? Progress in retinal and eye research 2000;19(5):497-527.

10. Myung D, Duhamel PE, Cochran JR, Noolandi J, Ta CN, Frank CW. Development of Hydrogel-Based Keratoprostheses: A Materials Perspective. Biotechnology progress 2008;24(3):735-741.

11. Reid B, Song B, McCaig CD, Zhao M. Wound healing in rat cornea: the role of electric currents. The FASEB journal 2005;19(3):379-386.

12. Lu L, Reinach PS, Kao WWY. Corneal epithelial wound healing. Experimental Biology and Medicine 2001;226(7):653-664.

13. Dalton BA, Evans MDM, McFarland GA, Steele JG. Modulation of corneal epithelial stratification by polymer surface topography. Journal of biomedical materials research 1999;45(4):384-394.

14. Nishida T, Awata T, Ohashi Y, Suda T, Inoue Y, Manabe R, Nakagawa S. Dynamics of fibronectin in corneal wound healing: Immunohistochemical study of experimental bullous keratopathy in rabbits. Cornea 1982;1(4):311.

15. Gipson IK, Spurr-Michaud SJ, Tisdale AS. Hemidesmosomes and anchoring fibril collagen appear synchronously during development and wound healing. Developmental biology 1988;126(2):253-262.

16. Nguyen BP, Ryan MC, Gil SG, Carter WG. Deposition of laminin 5 in epidermal wounds regulates integrin signaling and adhesion. Current opinion in cell biology 2000;12(5):554-562.

17. Abrams GA, Schaus SS, Goodman SL, Nealey PF, Murphy CJ. Nanoscale topography of the corneal epithelial basement membrane and Descemet's membrane of the human. Cornea 2000;19(1):57.

18. Karuri NW, Liliensiek S, Teixeira AI, Abrams G, Campbell S, Nealey PF, Murphy CJ. Biological length scale topography enhances cell-substratum adhesion of human corneal epithelial cells. Journal of cell science 2004;117(Pt 15):3153.

19. Liliensiek SJ, Campbell S, Nealey PF, Murphy CJ. The scale of substratum topographic features modulates proliferation of corneal epithelial cells and corneal fibroblasts. Journal of Biomedical Materials Research Part A 2006;79(1):185-192.

20. Diehl KA, Foley JD, Nealey PF, Murphy CJ. Nanoscale topography modulates corneal epithelial cell migration. Journal of Biomedical Materials Research Part A 2005;75(3):603-611.

21. Tuori A, Uusitalo H, Burgeson RE, Terttunen J, Virtanen I. The immunohistochemical composition of the human corneal basement membrane. Cornea 1996;15(3):286.

22. Yanez-Soto B, Liliensiek SJ, Murphy CJ, Nealey PF. Biochemically and topographically engineered poly(ethylene glycol) diacrylate hydrogels with biomimetic characteristics as substrates for human corneal epithelial cells. Journal of Biomedical Materials Research Part A 2012.

23. Teixeira AI, Abrams GA, Bertics PJ, Murphy CJ, Nealey PF. Epithelial contact guidance on well-defined micro- and nanostructured substrates. Journal of Cell Science 2003;116(Pt 10):1881-1892.

24. Allen-Hoffmann BL, Rheinwald JG. Polycyclic aromatic hydrocarbon mutagenesis of human epidermal keratinocytes in culture. Proceedings of the National Academy of Sciences of the United States of America 1984;81:7802-7806.

25. Livak KJ, Schmittgen TD. Analysis of Relative Gene Expression Data Using Real-Time Quantitative PCR and the 2^(-ΔΔCt) Method. methods 2001;25(4):402-408.

26. Lutolf MP, Hubbell JA. Synthetic biomaterials as instructive extracellular microenvironments for morphogenesis in tissue engineering. Nature biotechnology 2005;23(1):47-55.

27. Parkinson LG, Giles NL, Adcroft KF, Fear MW, Wood FM, Poinern GE. The potential of nanoporous anodic aluminium oxide membranes to influence skin wound repair. Tissue Engineering Part A 2009;15(12):3753-3763.

28. Parkinson LG, Rea SM, Stevenson AW, Wood FM, Fear MW. The Effect of Nano-Scale Topography on Keratinocyte Phenotype and Wound Healing Following Burn Injury. Tissue Engineering Part A 2012;18(7-8):703-714.

29. Wilson MJ, Jiang Y, Yanez-Soto B, Liliensiek S, Murphy WL, Nealey PF. Arrays of topographically and peptide-functionalized hydrogels for analysis of biomimetic extracellular matrix properties. Journal of Vacuum Science & Technology B: Microelectronics and Nanometer Structures 2012;30(6):06F903-06F903-7.

30. Wilson MJ. Personal communication. 2012.

31. Daniels JT, Geerling G, Alexander RA, Murphy G, Khaw PT, Saarialho-Kere U. Temporal and spatial expression of matrix metalloproteinases during wound healing of human corneal tissue. Experimental eye research 2003;77(6):653-664.

32. Miyazaki K. Laminin-5 (laminin-332): Unique biological activity and role in tumor growth and invasion. Cancer science 2006;97(2):91-98.

33. Tsubota Y, Yasuda C, Kariya Y, Ogawa T, Hirosaki T, Mizushima H, Miyazaki K. Regulation of biological activity and matrix assembly of laminin-5 by COOH-terminal, LG4â€“5 domain of Î±3 chain. Journal of Biological Chemistry 2005;280(15):14370-14377.

34. Hamill KJ, Paller AS, Jones JCR. Adhesion and Migration, the Diverse Functions of the Laminin [alpha] 3 Subunit. Dermatologic clinics 2010;28(1):79-87.

35. Mercurio AM, Rabinovitz I, Shaw LM. The α6β4 integrin and epithelial cell migration. Current opinion in cell biology 2001;13(5):541-545.

36. Goldfinger LE, Stack MS, Jones JCR. Processing of laminin-5 and its functional consequences: role of plasmin and tissue-type plasminogen activator. The Journal of cell biology 1998;141(1):255-265.

37. Margadant C, Raymond K, Kreft M, Sachs N, Janssen H, Sonnenberg A. Integrin α3β1 inhibits directional migration and wound re-epithelialization in the skin. Journal of cell science 2009;122(2):278-288.

38. Frank DE, Carter WG. Laminin 5 deposition regulates keratinocyte polarization and persistent migration. Journal of cell science 2004;117(8):1351-1363.

39. Ogawa T, Tsubota Y, Maeda M, Kariya Y, Miyazaki K. Regulation of biological activity of laminin-5 by proteolytic processing of γαμμα−2 chain. Journal of cellular biochemistry 2004;92(4):701-714.

40. Gagnoux-Palacios L, Allegra M, Spirito F, Pommeret O, Romero C, Ortonne J, Meneguzzi G. The short arm of the laminin γ2 chain plays a pivotal role in the incorporation of laminin 5 into the extracellular matrix and in cell adhesion. The Journal of cell biology 2001;153(4):835-850.

41. Kariya Y, Miyazaki K. The basement membrane protein laminin-5 acts as a soluble cell motility factor. Experimental cell research 2004;297(2):508-520.

42. Schenk S, Hintermann E, Bilban M, Koshikawa N, Hojilla C, Khokha R, Quaranta V. Binding to EGF receptor of a laminin-5 EGF-like fragment liberated during MMP-dependent mammary gland involution. The Journal of cell biology 2003;161(1):197-209.

43. Amano S, Scott IC, Takahara K, Koch M, Champliaud MF, Gerecke DR, Keene DR, Hudson DL, Nishiyama T, Lee S. Bone morphogenetic protein 1 is an extracellular processing enzyme of the laminin 5 γ2 chain. Journal of Biological Chemistry 2000;275(30):22728-22735.

44. Veitch DP, Nokelainen P, McGowan KA, Nguyen TT, Nguyen NE, Stephenson R, Pappano WN, Keene DR, Spong SM, Greenspan DS. Mammalian tolloid metalloproteinase, and not matrix metalloprotease 2 or membrane type 1 metalloprotease, processes laminin-5 in keratinocytes and skin. Journal of Biological Chemistry 2003;278(18):15661-15668.

45. Gasiorowski JZ, Liliensiek SJ, Russell P, Stephan DA, Nealey PF, Murphy CJ. Alterations in gene expression of human vascular endothelial cells associated with nanotopographic cues. Biomaterials 2010;31(34):8882-8888.

CHAPTER 5: CONCLUSIONS AND FUTURE WORK

5.1 Significance of results

The focus of this dissertation has involved the design and engineering of a synthetic basement membrane (BM) with biomimetic characteristics inspired by the native BM of the cornea. Throughout our research, we developed soft materials capable of presenting uniform and controllable biochemical and biophysical motifs to the cells, based on moldable and functionalizable poly(ethylene glycol) diacrylate (PEGDA) hydrogels. We demonstrated that our PEGDA hydrogels interact with the cells through the binding of specific cellular receptors. Through the use of these materials we were able to distinguish the contribution of the topography on human corneal epithelial cell (HCEC) behavior from the confounding nonspecific protein adsorption effect. In addition, we provided further evidence that nanoscale topography is a fundamental cue impacting the cell phenotype. Our substrates also allowed us to investigate the influence of cytoactive soluble factors in the media on the cellular response to topography.

In addition, we progressed from single cell studies to the study of the full epithelial tissue response to topographic cues. To explore this, we developed an *in vitro* wound healing protocol for testing of our soft substrates as an artificial BM mimic, and demonstrated that the topography of the substrate contributes to the wound healing of the corneal epithelium. We selected several cellular behaviors essential to the wound healing of the cornea, including proliferation, spreading and migration, to determine how the topography contributes to the observed enhanced healing rate. We also identified the migration of the cells next to the wound edge as the most affected observable factor. Upon observation of the increased expression of laminin-332 (LN332) in the

wound border on topographic features, we investigated the total RNA expression of this particular marker. Interestingly, the overall expression of LN332 is significantly increased on flat substrates compared to topographic surfaces during the epithelial healing process. Our results led us to suggest a model where cells interpret the flatness of the substrate as the absence of BM, resulting in the HCEC overexpression and deposition of BM components, such as LN332; while cells on topographic surfaces concentrate their efforts in enhancing the migration and closure of the wound border by expressing the soluble and migration-inducing form of LN332.

All these results are important for the advancement towards the use of a biomimetic artificial basement membrane of the cornea to promote the formation and maintenance of a healthy corneal epithelium. These results also provide a foundation from which future studies can be developed, such as the evaluation of the conditions needed for the epithelialization of artificial substrates, and the incorporation of those features into artificial corneas.

5.2 Future work

5.2.1 Use of isotropic topography in would healing assays

Previous results from our group demonstrated that single cells presented epithelial contact guidance on topographic substrates[1-6], and migration along the patterns in anisotropic topographies[7]. However, our recent results show that cells migrating on the border of an epithelial sheet at the edge of the wound do not advance preferentially in the direction of the topography, suggesting that full tissues respond to the presence of topographic cues rather than

being guided by the contact with the topography. Despite this observation, to test the cellular response to isotropic topographies, we developed an easy protocol to fabricate isotropic topography using a modified nanosphere lithographic method[8], described in Appendix A. This method allows the rapid fabrication of isotropic topography with varied sizes, depending on the diameter of the polystyrene spheres used. Images of a sample of the resulting substrates, with topography in the range between 190 nm and 2000 nm are shown in Figure 5.1. We performed preliminary wound healing tests as described in Chapter 4 using those substrates, and analyzed the results. We observed the same trend as in anisotropic substrates, where the wound closure on topographic substrates is increased with respect to the flat surfaces (Figure 5.2), strengthening the evidence that topographic cues enhance corneal epithelial wound healing.

5.2.2 Use of synergistic peptides

Our investigation involved the use of the integrin-specific RGD peptide, which is found in important extracellular matrix (ECM) components in the corneal BM, such as fibronectin, laminin, collagen, vitronectin or fibrinogen[9-12], to induce cell attachment to our substrates. However, our laboratory has investigated other ECM peptides that are present on the basement membrane and play a role in behaviors relevant to the wound healing of the corneal epithelium[7]. Our goal is to find the minimal combination of peptides that can provide the coverage and maintenance of the epithelium before HCECs produce their own BM. Some examples are the syndecan 1 and 4-binding peptide AG73 (Arg-Lys-Arg-Leu-Gln-Val-Gln-Leu-Ser-Ile-Arg-Thr), a sequence that contributes to cell differentiation[13,14] and act synergistically with integrin-binding

motifs to accelerate cell adhesion and spreading[15,16]; or CAG (Cys-Ala-Gly), found in collagen IV, that selectively controls cell adhesion[17].

To test the synergistic effect of the combination of peptides, our group has developed a platform to control the presentation, concentration and accessibility of peptides[18]. This platform allows the functionalization of PEGDA hydrogels with multiple biological molecules at controlled concentrations. Since the simultaneous presentation of a combination of peptides and topography require the use of high-throughput testing, we have also developed arrays for the analysis of these biomimetic characteristics[7]. These techniques will help elucidate the biochemical and biophysical characteristics that will optimize the epithelialization of an artificial BM.

5.2.3 Studies on the expression/knockdown of ECM components involved in the wound healing of the cornea, such as LN332 and LN511

Our results show that after epithelial wounding, cells on the border of the wound express LN331 intracellularly. This expression is increased when cells are in presence of topographic features. LN332 has been used as a marker for cellular migration[19], but recent studies have demonstrated that two different levels of processing of LN332 are associated with increased cellular migration or with increased adhesion respectively[20-22]. Furthermore, when we performed real-time PCR in the overall culture, we observed an increase in the RNA expression of LN332 subunits in the flat surfaces, compared to the topographic substrates. We hypothesize that cells cultured on flat surfaces increase the expression and deposition of the unprocessed LN332 to increase their adhesion; while cells on topographic substrates do not express LN332, except the

migration-inducing form on the border of the wound. Our hypothesis can be tested by measuring the expression of other proteins involved in the cleavage of LN332[23], the identification of the LM332 isoform by the use of specific antibodies, and the knockdown of LN332 subunits with small interfering RNA, which has been proved to reduce the migration rate during wound healing[24].

5.2.4 Influence of topographic cues on differentiation and stratification of the corneal epithelium

One of the most important characteristics of a healthy epithelium is the formation and maintenance of a stratified layer of cells[25]. In healthy epithelia, cells in contact with the BM express keratin 14 (related to low level of differentiation)[26], while cells in the stratified squamous layer express 14-3-3σ (indicating a higher level of differentiation)[27]. Preliminary results from our group using real time PCR have verified the influence of topography on HCEC differentiation, because cells plated on nanoscale topography upregulate the expression of keratin 14 and downregulate the expression of 14-3-3σ. For this reason, we hypothesize that the incorporation of topographic cues to an artificial BM will mimic the differentiation and stratification of a native corneal epithelium. To test this hypothesis, airlifted 3D organotypic cultures can be used (Figure 5.3)[28]. In this type of culture, the desired substrate to test is placed on an insert over a polycarbonate membrane. HCEC are plated in the insert and submerged in media for four days. At this time point, the construct is lifted to the air-liquid interface to induce stratification. This type of culture can be performed with or without the inclusion of corneal fibroblasts. Possible experimental end points are: the analysis of RNA, protein levels and localization of specific markers of HCEC differentiation, such as keratin 3 and 12[29]; the

evaluation of BM formation through the staining of collagen IV, and the analysis of histological features.

5.2.5 Incorporation of a synthetic basement membrane onto artificial corneas as a laminated structure

Our approach of engineering an artificial BM is suitable for their incorporation onto currently used keratoprosthesis, such as AlphaCor[30], or the Eyegenix™ cornea, currently in phase 1 clinical study[31]. The goal of this device is to engineer a physiologically functional tissue substitute that re-epithelializes as well as induces nerve growth into the stroma to maintain corneal health[32]. Unfortunately, the Eyegenix™ cornea presents a flat surface, thus limiting the resulting re-epithelialization. For that purpose, we propose a procedure to resurface the lenticules using laminated structures, depicted in figure 5.4. Recent investigations have reported the combination of two separate layers to provide extracellular cues to the stroma or the epithelium, such as the addition of growth factors in a bioresponsive polymer[33]. However, this approach does not consider the incorporation of biophysical cues such as topography. Our method involves the use of a mold that contains the topographic features. PEGDA pre-polymer supplemented with adhesion promoters is applied to the surface and the lenticule is pressed onto the mold. The PEGDA prepolymer is then photocrosslinked and the lenticule is released with a thin layer of PEGDA hydrogel attached.

The molds containing the topography inspired by the BM must match the curvature of the lenticule. A procedure to fabricate curved molds with nanotopographic features on the concave surface is described in appendix B. The advantages of this method include the possibility of

using currently tested topographies, the use of elastomers to facilitate the release of the lenticules and the molding of large areas. An example of a mold presenting curved surfaces and a lenticule fabricated, confirming the transfer of the topography to the lenticule is shown in figure 5.5.

5.2.6 Ex vivo and In vivo wound healing studies

The natural next step for the evaluation of our PEGDA hydrogels as substrates for the corneal epithelium is the use of *ex-vivo* organ cultures. In these studies, the cornea and sclera of commercially available rabbit eyes can be excised and mounted on a perfusion chamber[34,35]. The cornea is trephined to remove the epithelium, the basement membrane and a portion of the anterior stroma. The biosynthetic membranes incorporating the biochemical and biophysical cues can be overlaid onto the wounded area and the rate of wound closure evaluated, as well as RNA expression, protein expression, localization and histology.

Dogs have the appropriate corneal diameter, thickness and curvature to employ Eyegenix™ corneas functionalized with our artificial BM. *In vivo* studies using canine models can be performed. The biosynthetic corneas are implanted using anterior lamellar keratoplasty[36], and all dogs receive a general physical exam and detailed ophthalmic exam pre- and post-operatory, and at appropriate time points. The ophthalmic exam includes: slit lamp examination, spectral domain OCT evaluation, confocal slit lamp imaging of all corneal layers, Schirmer tear test, intraocular pressures and Cochet-Bonnet aesthesiometry. After 16 weeks, dogs will be humanely euthanized and corneas from both eyes collected for histopathology, immunohistochemistry, and transmission electron microscopy (TEM) for verification of stratification, expression of

differentiation markers (using canine specific antibodies), and the presence of intact basement membrane.

These future experiments represent a comprehensive strategy to achieve the goal of engineering substrates as a biomimetic basement membrane of the corneal epithelium, and will provide a key step in the translation of our research from the bench to the clinic. Those materials will be able to provide an environment to promote the epithelialization of artificial corneas and improve their biointegration into the eye.

5.4 Figures

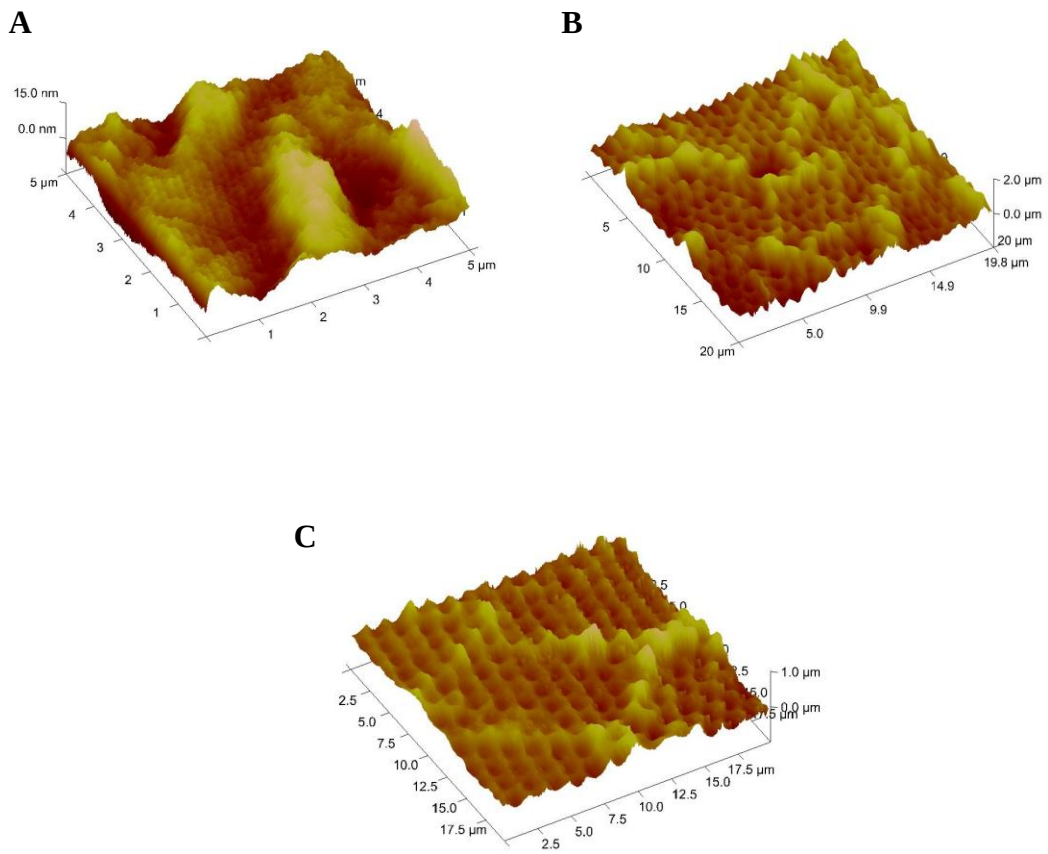

Figure 5.1: AFM images of hydrated PEGDA hydrogels molded using nanosphere lithography containing isotropic topography in different scales.

A) Topography obtained with nanospheres of 190 nm in diameter. B) Topography obtained with nanospheres of 1260 nm in diameter. C) Topography obtained with nanospheres of 2000 nm in diameter.

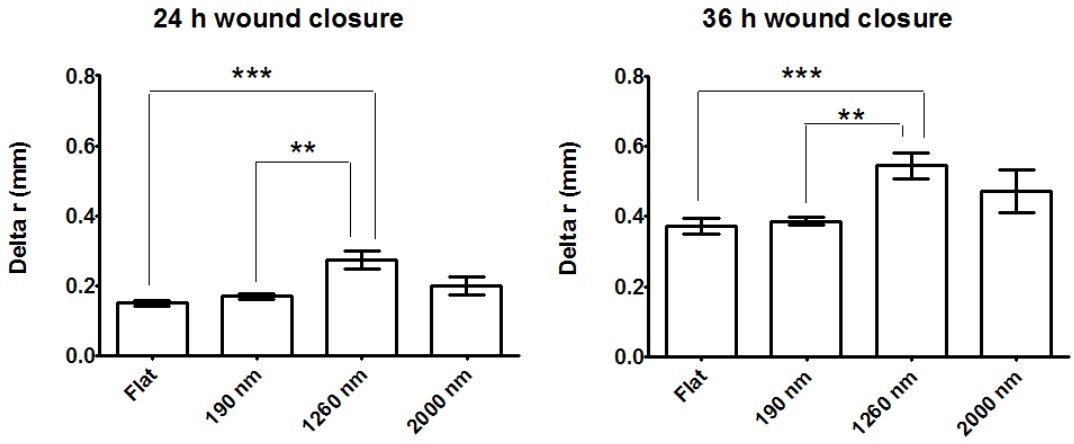

Figure 5.2: Evaluation of the wound closure in substrates molded with anisotropic topography.

A) Wound closure after 24 hours. B) Wound closure after 36 hours. Error bars: SEM. (*** $p \leq 0.001$; ** $0.001 < p \leq 0.01$.)

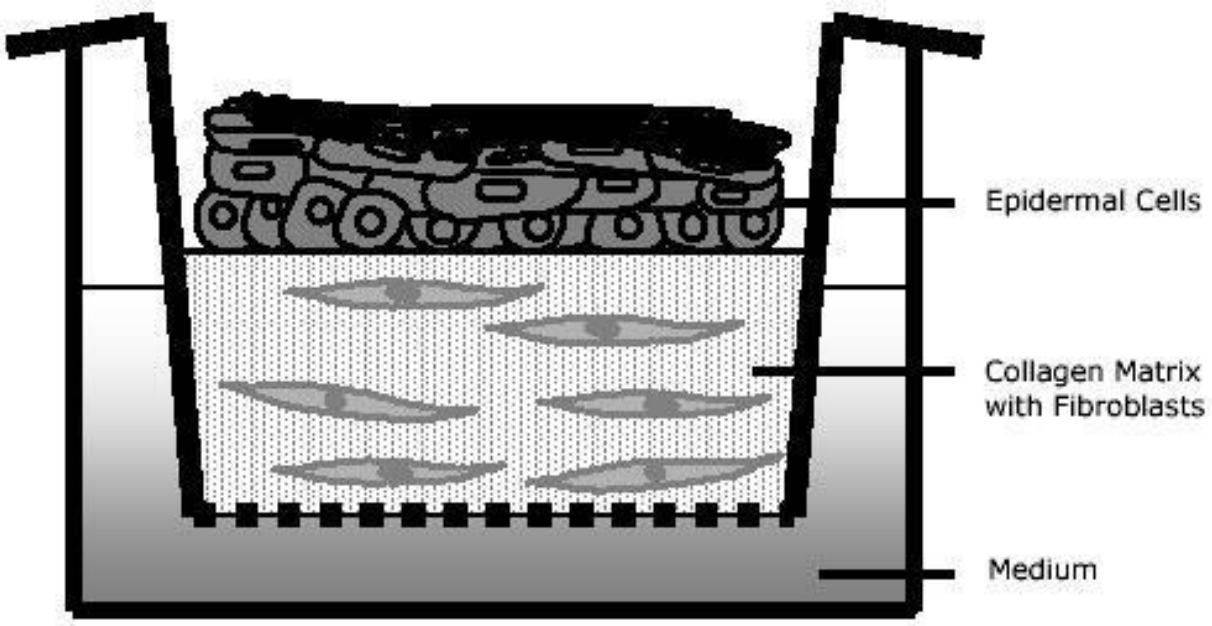

Figure 5.3: Lift-off technique for the differentiation of cells (organotypic co-culture).

From Stark H, et. al. (2006) *Biol Proced Online* 6(1), 55-60 (reference 28). A hydrogel engineered with biochemical and biophysical cues is placed in an insert containing a polycarbonate membrane. Fibroblasts can be incorporated into the hydrogel or cultured directly on the membrane. Corneal epithelial cells are cultured on the hydrogel and submerged in the media for 7 days. After that, the developing culture is raised to the air-liquid interface.

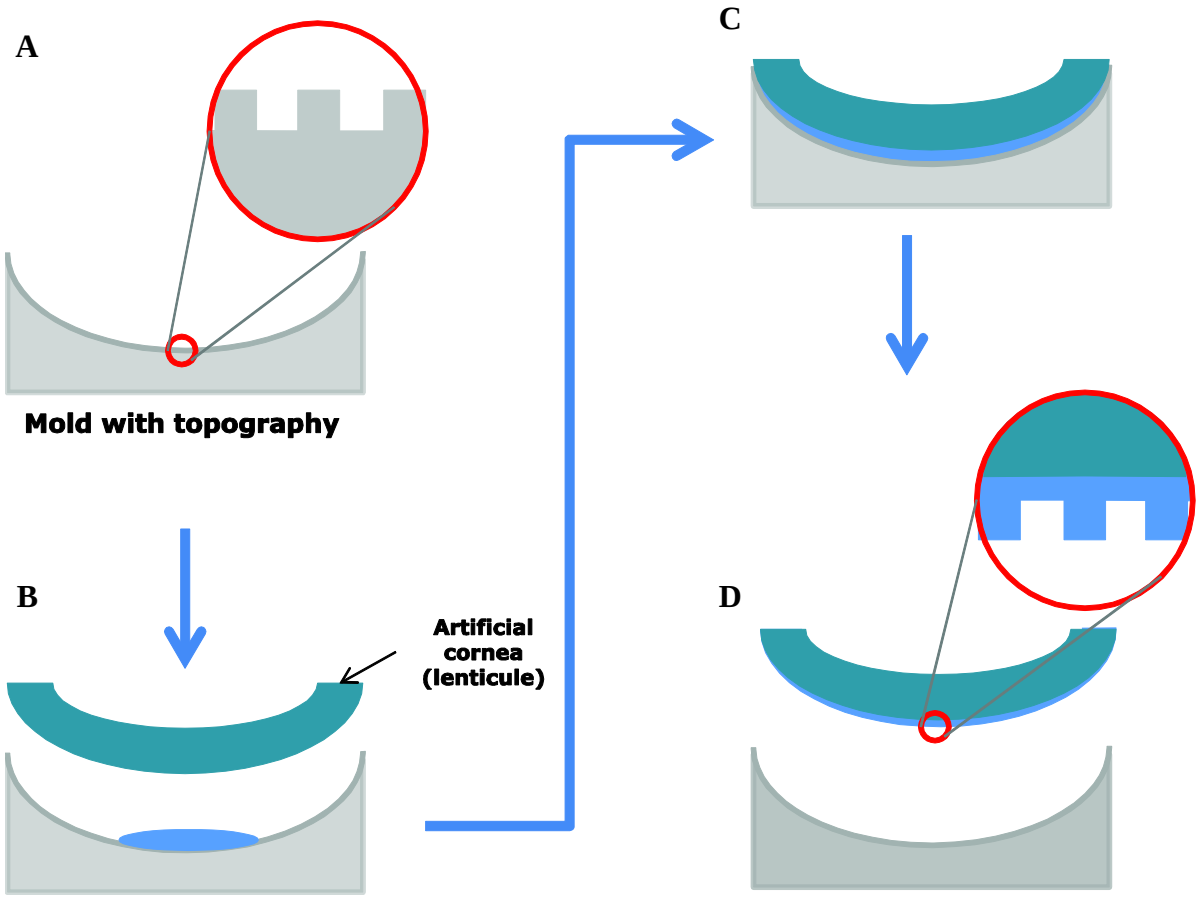

Figure 5.4: Incorporation of a synthetic basement membrane onto artificial corneas as a laminated structure.

A) Mold replicating the curvature of the lenticule, containing topographic features onto the concave surface. B) PEGDA pre-polymer is placed onto the concave surface of the mold and the lenticule is pressed on top. C) The PEGDA is crosslinked under UV light. D) The lenticule with a layer of PEGDA hydrogel is removed from the mold.

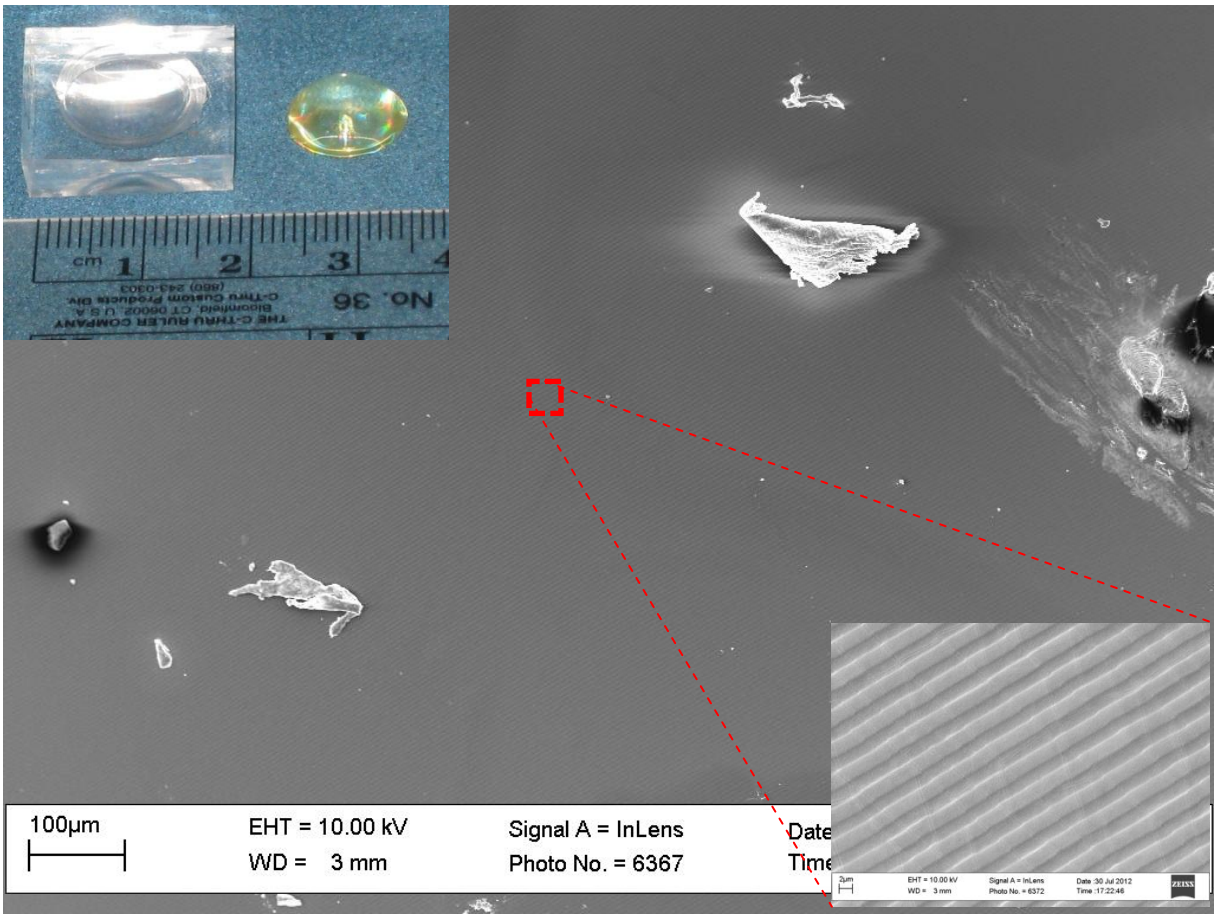

Figure 5.5.- Topographic features molded into curved surfaces.

The image shows a scanning electronic micrograph a polyurethane lenticule, fabricated in a curved mold with groove-and-ridges topography with 4000 nm pitch, showing the capability to mold large surfaces with topography. The top inset shows the PDMS mold containing the topography on the concave surface, and the polyurethane lenticule obtained. The inset on the bottom shows a higher magnification of the surface.

5.4 References

1. Teixeira AI, Abrams GA, Bertics PJ, Murphy CJ, Nealey PF. Epithelial contact guidance on well-defined micro- and nanostructured substrates. Journal of Cell Science 2003;116(Pt 10):1881-1892.

2. Teixeira AI, Abrams GA, Murphy CJ, Nealey PF. Cell behavior on lithographically defined nanostructured substrates. Journal of Vacuum Science & Technology B: Microelectronics and Nanometer Structures 2003;21:683.

3. Fraser SA, Ting YH, Mallon KS, Wendt AE, Murphy CJ, Nealey PF. Sub micron and nanoscale feature depth modulates alignment of stromal fibroblasts and corneal epithelial cells in serum rich and serum free media. Journal of Biomedical Materials Research Part A 2008;86(3):725-735.

4. Tocce EJ, Liliensiek SJ, Broderick AH, Jiang Y, Murphy KC, Murphy CJ, Lynn DM, Nealey PF. The influence of biomimetic topographic features and the extracellular matrix peptide RGD on human corneal epithelial contact guidance. Acta Biomaterialia 2012.

5. Tocce EJ, Smirnov VK, Kibalov DS, Liliensiek SJ, Murphy CJ, Nealey PF. The ability of corneal epithelial cells to recognize high aspect ratio nanostructures. Biomaterials 2010;31(14):4064-4072.

6. Yanez-Soto B, Liliensiek SJ, Murphy CJ, Nealey PF. Biochemically and topographically engineered poly(ethylene glycol) diacrylate hydrogels with biomimetic characteristics as substrates for human corneal epithelial cells. Journal of Biomedical Materials Research Part A 2012.

7. Wilson MJ, Jiang Y, Yanez-Soto B, Liliensiek S, Murphy WL, Nealey PF. Arrays of topographically and peptide-functionalized hydrogels for analysis of biomimetic extracellular matrix properties. Journal of Vacuum Science & Technology B: Microelectronics and Nanometer Structures 2012;30(6):06F903-06F903-7.

8. Haynes CL, Van Duyne RP. Nanosphere lithography: A versatile nanofabrication tool for studies of size-dependent nanoparticle optics. The Journal of Physical Chemistry B 2001;105(24):5599-5611.

9. Gipson IK, Spurr-Michaud SJ, Tisdale AS. Hemidesmosomes and anchoring fibril collagen appear synchronously during development and wound healing. Developmental biology 1988;126(2):253-262.

10. Nguyen BP, Ryan MC, Gil SG, Carter WG. Deposition of laminin 5 in epidermal wounds regulates integrin signaling and adhesion. Current opinion in cell biology 2000;12(5):554-562.

11. Nishida T, Awata T, Ohashi Y, Suda T, Inoue Y, Manabe R, Nakagawa S. Dynamics of fibronectin in corneal wound healing: Immunohistochemical study of experimental bullous keratopathy in rabbits. Cornea 1982;1(4):311.

12. Tuori A, Uusitalo H, Burgeson RE, Terttunen J, Virtanen I. The immunohistochemical composition of the human corneal basement membrane. Cornea 1996;15(3):286.

13. Hoffman MP, Nomizu M, Roque E, Lee S, Jung DW, Yamada Y, Kleinman HK. Laminin-1 and laminin-2 G-domain synthetic peptides bind syndecan-1 and are involved in acinar formation of a human submandibular gland cell line. Journal of Biological Chemistry 1998;273(44):28633-28641.

14. Yamada Y, Hozumi K, Aso A, Hotta A, Toma K, Katagiri F, Kikkawa Y, Nomizu M. Laminin active peptide/agarose matrices as multifunctional biomaterials for tissue engineering. Biomaterials 2012.

15. Hozumi K, Kobayashi K, Katagiri F, Kikkawa Y, Kadoya Y, Nomizu M. Syndecan-and integrin-binding peptides synergistically accelerate cell adhesion. FEBS letters 2010;584(15):3381-3385.

16. Yamada Y, Katagiri F, Hozumi K, Kikkawa Y, Nomizu M. Cell behavior on protein matrices containing laminin Î±1 peptide AG73. Biomaterials 2011;32(19):4327-4335.

17. Kanie K, Narita Y, Zhao Y, Kuwabara F, Satake M, Honda S, Kaneko H, Yoshioka T, Okochi M, Honda H. Collagen type IV-specific tripeptides for selective adhesion of endothelial and smooth muscle cells. Biotechnology and bioengineering 2012.

18. Wilson M, Liliensiek, SJ., Murphy, CJ., Murphy, WL., Nealey, PF. Hydrogels with well-defined peptide-hydrogel spacing and concentration: impact on epithelial cell behavior. Soft Matter 2012;8(2):390-398.

19. Daniels JT, Geerling G, Alexander RA, Murphy G, Khaw PT, Saarialho-Kere U. Temporal and spatial expression of matrix metalloproteinases during wound healing of human corneal tissue. Experimental eye research 2003;77(6):653-664.

20. Ebihara N, Mizushima H, Miyazaki K, Watanabe Y, Ikawa S, Nakayasu K, Kanai A. The functions of exogenous and endogenous laminin-5 on corneal epithelial cells. Experimental eye research 2000;71(1):69.

21. Goldfinger LE, Stack MS, Jones JCR. Processing of laminin-5 and its functional consequences: role of plasmin and tissue-type plasminogen activator. The Journal of cell biology 1998;141(1):255-265.

22. Hamill KJ, Paller AS, Jones JCR. Adhesion and Migration, the Diverse Functions of the Laminin [alpha] 3 Subunit. Dermatologic clinics 2010;28(1):79-87.

23. Greciano PG, Moyano JV, Buschmann MM, Tang J, Lu Y, Rudnicki J, Manninen A, Matlin KS. Laminin 511 partners with laminin 332 to mediate directional migration of Madinâ€“Darby canine kidney epithelial cells. Molecular Biology of the Cell 2012;23(1):121-136.

24. Mak GZ, Kavanaugh GM, Buschmann MM, Stickley SM, Koch M, Goss KH, Waechter H, Zuk A, Matlin KS. Regulated synthesis and functions of laminin 5 in polarized Madin-Darby canine kidney epithelial cells. Molecular biology of the cell 2006;17(8):3664-3677.

25. Lu L, Reinach PS, Kao WWY. Corneal epithelial wound healing. Experimental Biology and Medicine 2001;226(7):653-664.

26. Kurpakus MA, Maniaci MT, Esco M. Expression of keratins K12, K4 and K14 during development of ocular surface epithelium. Current eye research 1994;13(11):805-814.

27. Lu Q, Xin Y, Ye F, Foulks G, Li Q. 14-3-3Ï*f* controls corneal epithelium homeostasis and wound healing. Investigative Ophthalmology & Visual Science;52(5):2389-2396.

28. Stark HJ, Szabowski A, Fusenig NE, Maas-Szabowski N. Organotypic cocultures as skin equivalents: A complex and sophisticated in vitro system. Biological procedures online 2004;6(1):55-60.

29. Sun TT, Eichner R, Nelson WG, Tseng SCG, Weiss RA, Jarvinen M, Woodcock-Mitchell J. Keratin classes: molecular markers for different types of epithelial differentiation. Journal of Investigative Dermatology 1983;81:109s-115s.

30. Hicks CR, Crawford GJ, Lou X, Tan DT, Snibson GR, Sutton G, Downie N, Werner L, Chirila TV, Constable IJ. Corneal replacement using a synthetic hydrogel cornea, AlphaCorâ„¢: device, preliminary outcomes and complications. Eye 2003;17(3):385-392.

31. Fagerholm P, Lagali NS, Merrett K, Jackson WB, Munger R, Liu Y, Polarek JW, Soderqvist M, Griffith M. A biosynthetic alternative to human donor tissue for inducing corneal regeneration: 24-month follow-up of a phase 1 clinical study. Science translational medicine;2(46):46ra61-46ra61.

32. Li F, Carlsson D, Lohmann C, Suuronen E, Vascotto S, Kobuch K, Sheardown H, Munger R, Nakamura M, Griffith M. Cellular and nerve regeneration within a biosynthetic extracellular matrix for corneal transplantation. Proceedings of the National Academy of Sciences 2003;100(26):15346-15351.

33. Hardwicke J, Song B, Moseley R, Thomas DW. Investigation of the potential of polymer therapeutics in corneal re-epithelialisation. British Journal of Ophthalmology;94(12):1566-1570.

34. Cameron JD, Waterfield RR, Steffes MW, Furcht LT. Quantification of corneal organ culture migration: central and peripheral epithelium. Investigative ophthalmology & visual science 1989;30(11):2407-2413.

35. Tanelian DL, Bisla K. A new in vitro corneal preparation to study epithelial wound healing. Investigative ophthalmology & visual science 1992;33(11):3024-3028.

36. Bentley E, Murphy CJ, Li F, Carlsson DJ, Griffith M. Biosynthetic corneal substitute implantation in dogs. Cornea 2010;29(8):910-916.

APPENDIX A.- MOLDING OF POLY(ETHYLENE GLYCOL) DIACRYLATE (PEGDA) HYDROGELS WITH ISOTROPIC TOPOGRAPHY, USING NANOSPHERE LITHOGRAPHY

The fabrication of PEGDA hydrogels with isotropic topography was completed following the protocol shown in figure A.1. A silicon wafer was cleaned with O2 plasma (300 sec, 250 W, O_2 flow rate of 50 cc/min). The surface was spin-coated with a thin layer (50-200 nm) of poly(isobutyl methacrylate) (PiBMA, MW 300,000, Acros, NJ). The surface was covered with a poly(dimethyl siloxane) (PDMS, Sylgard® 184, Dow Corning, MI) stencil with a void space of 1 cm in diameter. The covered wafer was O_2 plasma-treated (20 sec, 100 W, O_2 flow rate of 8 cc/min) to render the surface of the exposed PiBMA hydrophilic. The amount of nanospheres required to cover the exposed area of the wafer in a monolayer was calculated as , where N is the number of spheres, A is the area of the wafer exposed to the O_2 plasma and D is the diameter of the nanosphere. Suspensions of polystyrene nanospheres with diameters of 190, 1260 and 2000 nm were purchased from Bangs Laboratories (Fishers, IN). The suspensions were centrifuged and the supernatant liquid was replaced by a mixture of 40% methanol in water, containing 1/1000 concentration of Triton-X 100 (Sigma-Aldrich, MO) as a dispersant, to enhance the coverage of the exposed surface of the wafer. The PiBMA-coated wafer was placed on a slight angle in a covered crystallizing dish, saturated with methanol to control evaporation of the liquid. The nanosphere suspension was applied on one side and the liquid covered the whole exposed surface. Upon evaporation, a monolayer of nanospheres was formed. Next, the nanospheres on the PiBMA surface were annealed by heating the wafer to 70

°C (a temperature between 47 °C and 100 °C; the glass transition points of the PiBMA and polystyrene, respectively) for four hours. After annealing, the wafers were transferred to a nitrogen atmosphere. A 30 μL drop of a solution containing 20% (w/w) poly(ethylene glycol) diacrylate (PEGDA) MW 3400, 10 mM RGD peptide and 0.067% w/v lithium phenyl-2,4,6-trimethylbenzoylphosphinate (LAP) was placed on top and covered with a glass coverslip previously treated with 3-(trichlorosilyl) propyl methacrylate (TPM, Sigma-Aldrich, UK). The hydrogel was crosslinked under UV (364 nm for 900 s at 7.0 mW/cm2), and the coverslip was carefully removed from the wafer using a razor blade. The coverslip was then submerged in chloroform and sonicated for 12 hours, to dissolve the polystryrene nanospheres. The coverslip containing the topographic gel was dried overnight and sterilized for 24 hours by soaking in 5% isopropyl alcohol in 1X phosphate buffer saline (PBS, pH 7.2), rinsed for 24 hours in 1X PBS and pre-incubated for 12 hours in cell culture media for full equilibration before cell plating.

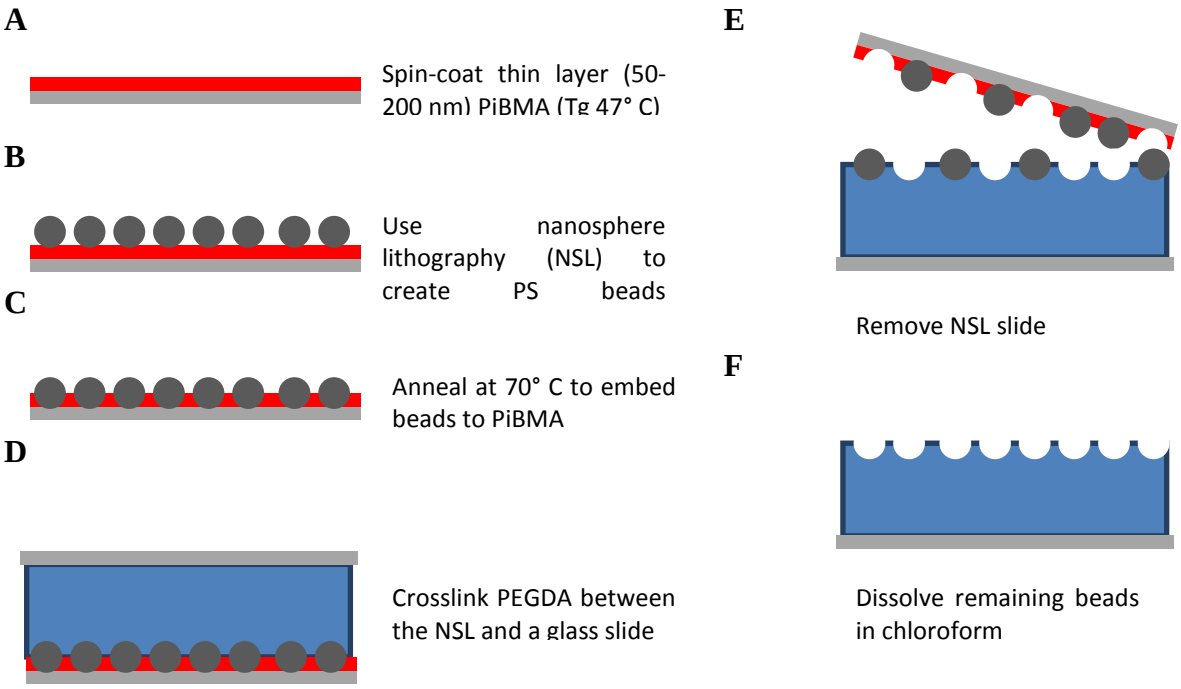

Figure A.1: Modified nanosphere lithographic method to fabricate PEGDA hydrogels with isotropic topography.

A) A silicon wafer is spin-coated with PiBMA and plasma-etched, to render the surface of the polymer hydrophilic. B) A monolayer is created by applying a suspension of polystyrene spheres to the surface. C) The monolayer is annealed at 70 °C to embed the spheres into the PiBMA. D) PEGDA pre-polymer is applied to the surface, covered with a TPM-treated cover slip and UV-crosslinked. E) The cover slip is carefully removed from the silicon wafer. F) The polystyrene spheres are dissolved in chloroform, leaving their imprint on the surface of the hydrogel.

APPENDIX B.- FABRICATION OF CURVED MOLDS WITH TOPOGRAPHIC FEATURES

B.1. Fabrication of thin Poly(dimethyl siloxane) (PDMS) membranes with topographic features

Thin PDMS membranes (thickness of approximately 500 μm) were fabricated according to the protocol shown in figure B.1. Briefly, silicon masters patterned with grooves and ridges with a pitch of 4000 nm and depth of 300 nm were placed on the bottom of a polystyrene culture dish to be used as molds to create thin polymeric stamps by soft lithography. The amount of PDMS (Sylgard® 184, Dow Corning, MI) needed to form a thin membrane (500 μm thick) on top of the silicon master was calculated. The PDMS was prepared by mixing Sylgard® 184 prepolymer and curing agent 10:1 by volume. The mixture was poured over the silicon master, degassed in vacuum for 20 min and cured for two hours at 60 °C. A thick slab of PDMS (5 mm thick) was O_2 plasma treated (20 sec, 100 W, O_2 flow rate of 8 cc/min), and exposed to trichloro (1H,1H,2H,2H-perfluorooctyl) silane (Sigma-Aldrich, St. Louis, MO) vapor for one hour in an inert atmosphere under vacuum conditions. The treated slab was placed on top of the silicon wafer with the thin layer of PDMS. PDMS prepolymer was poured over the construct until complete coverage, degassed under vacuum for 20 min and cured for another two hours at 60 °C. After that, the whole PDMS composite was carefully peeled from the master, and the slab was manually separated from the PDMS membrane. The membrane was then trimmed for subsequent processing.

B.2.- Fabrication of PDMS curved molds with topographic features

Curved PDMS molds molded with topographic features were fabricated following the procedure depicted in figure B.2. Briefly, the PDMS membrane prepared in the previous step was O_2 plasma treated (20 sec, 100 W, O_2 flow rate of 8 cc/min) and exposed to trichloro (1H,1H,2H,2H-perfluorooctyl) silane vapor for one hour in a nitrogen atmosphere under vacuum conditions. A 1 cm hole was drilled on the bottom of a 35 mm polystyrene culture dish. The fluorinated PDMS membrane was placed under this culture dish, with the topographic surface facing up. The bottom end of a 5 mL polystyrene Falcon test tube (BD labware, Franklin Lakes, NJ) was cut. The dome was glued concave-side down to the center of the culture dish lid, using acrylic glue (Loctite® 326, Henkel, Germany), and placed under the culture dish, pushing the membrane through the hole. PDMS prepolymer was poured inside the culture dish, degassed under vacuum for 20 minutes and cured at 60 °C for two hours. The PDMS mold was carefully separated from the membrane, leaving the original topography from the silicon master molded onto the concave surface.

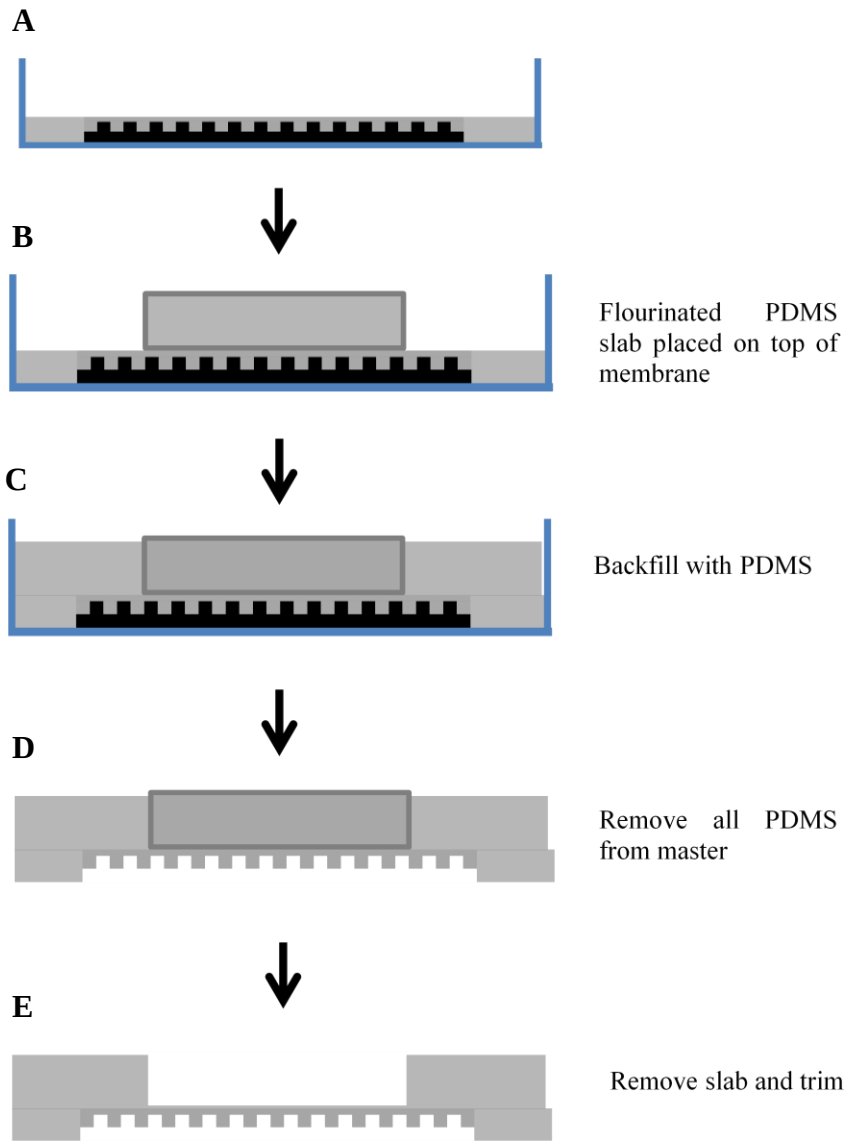

Figure B.1: Fabrication of PDMS membranes with topographic features.

A) A thin layer of PDMS prepolymer to form a thin membrane is poured and cured over a silicon master containing topographic features. B) A fluorinated PDMS slab is placed on top of the membrane. C) The construct is covered with PDMS prepolymer and cured. D) All the composite is peeled from the silicon master. E) The PDMS slab is removed and the membrane is trimmed.

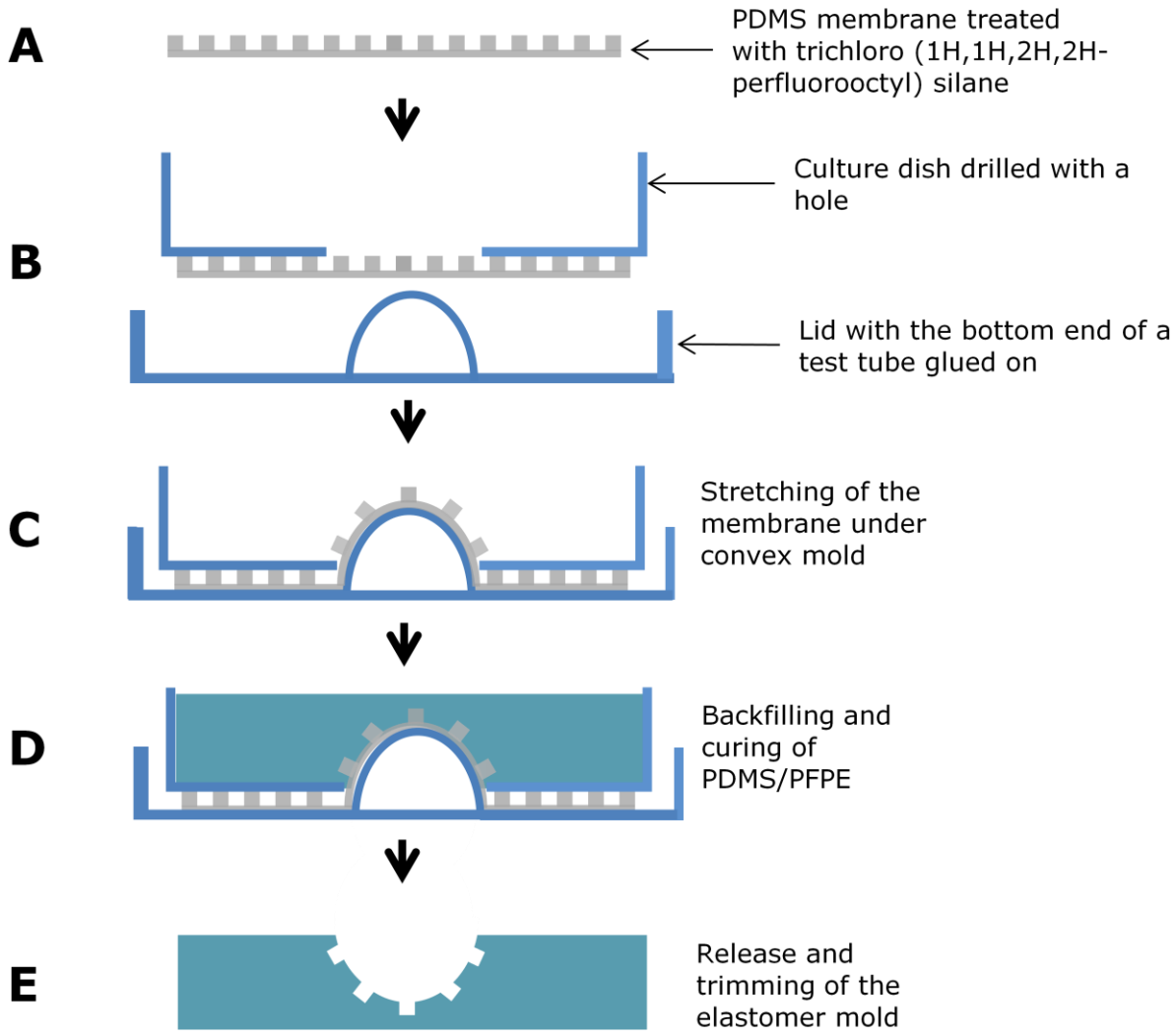

Figure B.2: Fabrication of PDMS molds with topographic features.

A) The PDMS membrane is treated with trichloro (1H,1H,2H,2H-perfluorooctyl) silane. B) The membrane is placed with the topography facing-up under a culture dish with a hole drilled on the bottom. C) A convex mold is pushed through the membrane, to stretch it. D) The culture dish is filled with PDMS prepolymer and cured . E) The PDMS is released from the construct and trimmed.